ADVANCED MATERIALS
www.advmat.de

Recent Progress in Biomimetic Additive Manufacturing Technology: From Materials to Functional Structures

*Yang Yang, Xuan Song, Xiangjia Li, Zeyu Chen, Chi Zhou, Qifa Zhou, and Yong Chen**

Nature has developed high-performance materials and structures over millions of years of evolution and provides valuable sources of inspiration for the design of next-generation structural materials, given the variety of excellent mechanical, hydrodynamic, optical, and electrical properties. Biomimicry, by learning from nature's concepts and design principles, is driving a paradigm shift in modern materials science and technology. However, the complicated structural architectures in nature far exceed the capability of traditional design and fabrication technologies, which hinders the progress of biomimetic study and its usage in engineering systems. Additive manufacturing (three-dimensional (3D) printing) has created new opportunities for manipulating and mimicking the intrinsically multiscale, multimaterial, and multifunctional structures in nature. Here, an overview of recent developments in 3D printing of biomimetic reinforced mechanics, shape changing, and hydrodynamic structures, as well as optical and electrical devices is provided. The inspirations are from various creatures such as nacre, lobster claw, pine cone, flowers, octopus, butterfly wing, fly eye, etc., and various 3D-printing technologies are discussed. Future opportunities for the development of biomimetic 3D-printing technology to fabricate next-generation functional materials and structures in mechanical, electrical, optical, and biomedical engineering are also outlined.

Dr. Y. Yang, X. Li, Prof. Y. Chen
Epstein Department of Industrial and Systems Engineering
Viterbi School of Engineering
University of Southern California
3715 McClintock Ave, Los Angeles, CA 90089-0192, USA
E-mail: yongchen@usc.edu
Prof. X. Song
Department of Mechanical and Industrial Engineering
University of Iowa
Iowa City, IA 52242, USA
Prof. X. Song
Center for Computer-Aided Design
University of Iowa
Iowa City, IA 52242, USA
Dr. Z. Chen, Prof. Q. Zhou
Department of Biomedical Engineering
Viterbi School of Engineering
University of Southern California
3650 McClintock Ave, Los Angeles, CA 90089, USA
Prof. C. Zhou
Department of Industrial and Systems Engineering
University at Buffalo
The State University of New York
Buffalo, NY 14260, USA

DOI: 10.1002/adma.201706539

1. Introduction

Living organisms are composed of natural materials built by hard and soft phases arranged in complex hierarchical architectures with dimensions spanning from the nanoscale to the macroscale.[1,2] The developed multiscale structures of biological materials exhibit inherent multifunctional integration.[3]The creatures in nature possess almost perfect structures and functions after millions of years of evolution.[4,5] For example, the Arapaima gigas fish scale is a natural body armor possessing excellent mechanical properties as well as superior flexibility.[6] Spider silk, nacre, and the Bouligand-type collagen fiber found in shrimp claws all demonstrate structures exhibiting excellent impact strength.[7–9] Various plants (Bauhinia pods, flowers) and animals also exhibit remarkable shape-changing properties to survival and reproduction (**Figure 1**).[10,11] In addition to mechanical properties, other physical properties are critical to survival for numerous species. For example, from a hydrodynamic perspective, the microstructure of shark skin significantly reduces the drag force in water,[12–14] whereas the eggbeater microstructure of the surface of Salvinia Molesta, an aquatic fern native to south-eastern Brazil, achieves a degree of superhydrophobicity allowing this free-floating plant to remain buoyant in water (Figure 1).[15–18] Vascular systems in animals comprise efficient multiscale networks of blood vessels providing tissues with oxygen and nutrients as well as removing CO_2 and wastes products.[19–21] Biological multiscale structures and multifunctional materials also yield an astounding array of specialized sensory capabilities in living organisms. For example, with respect to visual sense organs, compound eyes of insects provide wraparound vision that allows them to simultaneously see in all directions,[22–24] whereas the eyesight of an eagle is four to eight times more acute than that of the average human (Figure 1).[25] From an electrochemical (galvanic) response perspective, the human epidermis demonstrates excellent motion, temperature, and humidity sensitivity. An example of specialized acoustics/hearing ultrasound generation and detection in bats presents an extraordinarily accurate prey/environment echolocation capability.[26–29] These biological skills and attributes represent capabilities that are far beyond conventional

 © 2018 WILEY-VCH Verlag GmbH & Co. KGaA, Weinheim

engineering systems.[30–32] As a consequence, scientists began to ask an important question: how can biological designs be reproduced/reformulated as engineered systems using bioinspired advanced materials and structures that are structurally and functionally optimized, and that are capable of self-generation, self-repair, and evolution?[33–35]

Biological constructs comprise a significant source of inspiration for the design of next-generation structural materials, given the variety of excellent mechanical, hydrodynamic, optical, and electrical properties to be found in especially evolved organic structures.[36–39] Of particular interest, biomaterials and biostructures exhibiting unexpected properties have been studied with several inspirational examples that have fueled a recent escalation of interest in smart biological structures, based on the study of several notable examples.[40,41] However, rather than simply duplicating natural materials and structures, a great challenge is to understand the design principles and physical/chemical mechanisms that determine optimized structural organization in biological systems and its relationship to function. Moreover, the optimal solution of an engineering problem may lead to a quite different material from the biological material due to different boundary conditions and constraints presented in biological environment from engineering systems.[26,42,43] In addition to material and structural research, another important consideration is what are the pathways for the synthesis and manufacturing of biomimetic materials and structures based on the identified physical/chemical principles?

The complicated architectures in nature far exceed the capability of traditional design and fabrication technologies, which hinders the progress of biomimetic study and its use in engineering systems. Additive manufacturing (3D printing) has created new opportunities for manipulating and mimicking the intrinsically multiscale, multimaterial and multifunctional structures. 3D printing has been demonstrated as an effective pathway to fabricate customized products with complicated 3D structures for wide applications in industry, academia, and daily usages.[46,47] During the past 30 years, many novel additive manufacturing (AM) processes have been successfully developed.[48–50] The AM processes are generally flexible in fabricating a computer-aided design (CAD) model with good control on the resulting geometric shape. Recent advances in material, process, and machine developments have enabled AM processes to evolve from prototyping (rapid prototyping) to manufacturing (rapid manufacturing).[51,52] From craftsmanship to mass production, many believe the future of manufacturing lies in mass customization to which AM may present an effective solution.[46,53,54] According to the American Society for Testing and Materials (ISO/ASTM 52900:2015) there are over 50 different AM technologies that can be classified into seven different categories: binder jetting, material jetting, material extrusion, vat photo-polymerization, powder bed fusion, energy deposition, and sheet lamination.[55,56] Other ways to distinguish these technologies are to group them by the physical state of raw materials (i.e., liquid, solid, or powder form) and by the methods that are used to fuse the raw materials together (e.g., thermal, ultraviolet (UV) light, laser, or electron beam).[57] A number of mature AM technologies have been successfully commercialized such as fused deposition modeling (FDM), direct ink writing (DIW), selective laser sintering,

Yang Yang is a Postdoctoral Research Associate in the Epstein Department of Industrial and Systems Engineering and Center for Advanced Manufacturing at the University of Southern California. He received his Ph.D. degree in condensed matter physics from the School of Physics and Technology, Wuhan University, in 2015. His research work focuses on the development of novel 3D-printing process, 3D printing of bioinspired structures, high-dielectric-polymer-based nanocomposites, multiscale and multimaterials 3D printing, 3D printing of capacitors and piezoelectric transducers, 4D printing, bioinspired superhydrophobic surface, and wearable sensors.

Xuan Song is an Assistant Professor at the Department of Mechanical and Industrial Engineering at the University of Iowa. He obtained his Ph.D. degree in industrial and systems engineering from the University of Southern California in 2016. His research interests are additive manufacturing process development and optimization as well as novel applications of AM technologies in various areas, including biomedical imaging, tissue engineering, energy harvest, robotics, etc. At UIowa, his research focuses on the development of next-generation additive manufacturing processes with multimaterial, multiscale, or multidirectional capabilities.

Yong Chen is an Associate Professor in the Epstein Department of Industrial and Systems Engineering and Department of Aerospace and Mechanical Engineering at the University of Southern California. He received his Ph.D. degree in mechanical engineering from Georgia Institute of Technology in 2001. Prior to joining USC in 2006, he was a Senior Research and Development Engineer at 3D Systems Inc. His research focuses on additive manufacturing (3D printing) in micro- and mesoscales, especially the modeling, analysis, synthesis, and optimization of digital design and manufacturing.

© 2018 WILEY-VCH Verlag GmbH & Co. KGaA, Weinheim

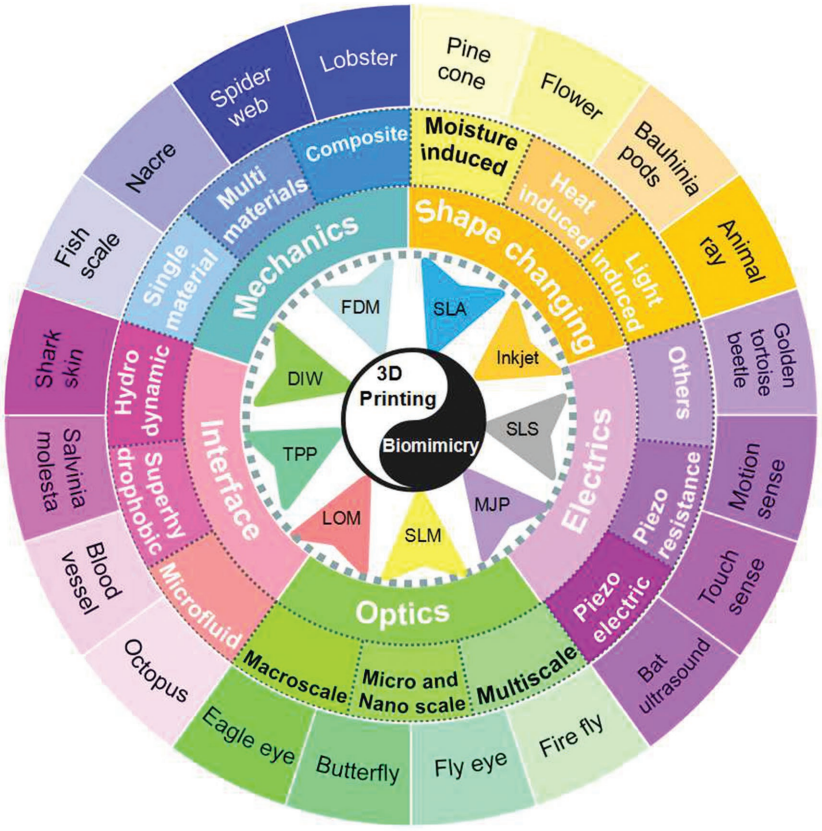

Figure 1. Integration of 3D printing with biomimicry, and the inset shows the categories of 3D-printing technology. 1) 3D printing of bioinspired mechanics reinforced structures inspired by fish scales, nacre, spider webs, lobster claws, and fabricated by single material, multimaterials, and composites (Section 2); 2) 3D printing of bioinspired shape-changing structures inspired by pine cones, flowers, Bauhinia pods, rays (e.g., manta rays, stingrays), and induced by moisture, heat, and light (Section 3); 3) 3D printing of bioinspired interface structures inspired by shark skin, *Salvinia molesta*, blood vessels, octopuses, with enhanced hydrodynamic, superhydrophobic properties, and microfluidic structures (Section 4); 4) 3D printing of bioinspired optics devices on the nano-, micro-, and macroscale, and multiscale levels inspired by eagle eyes, butterfly wings, fly eyes, and fireflies (Section 5); 5) 3D printing of bioinspired electrical devices based on piezoresistive, piezoelectric, and other materials inspired by bats and human skin (Section 6).

stereolithography (SLA), powder bed inkjet 3D printing (inkjet 3D), two-photon polymerization, laminated object manufacturing,[58] and their variants such as multijet printing (MJP)[59] and selective laser melting[60,61] (Figure 1). However, how well can these AM processes be used in fabricating biomimetic materials and structures and what is the current status of AM technology development to address the fabrication challenges of biomimetic materials and structures?

Here, we provide an overview of recent developments in 3D printing of biomimetic materials and structures to fabricate reinforced mechanics, shape changing, and hydrodynamic structures as well as optical and electrical devices. The main part of the review is organized into two sections: (1) bioinspired mechanics reinforced and shape-changing structures. Inspired by creatures such as fish scale, nacre, and lobster claw, bioinspired reinforced structures were fabricated by 3D printing using single material, multimaterials, and composites (Section 2). Also based on mechanical properties but inspired by pine cone and flower, objects with shape-changing properties were fabricated by 3D printing that can be triggered by moisture, heat, and light (Section 3). (2) Bioinspired materials and structures for other physical properties including interface (Section 4), optics (Section 5), and electrics (Section 6). A number of 3D-printed structures inspired by the shark skin, blood vessel, fly eyes, and human skins have been developed to study their hydrodynamic, optical, and electrical functionalities. Discussions based on the design and fabrication requirements of bioinspired materials and structures and the current status of 3D-printing technology are presented in each section. Finally, current challenges, perspectives, and future work toward improved biomimetic additive manufacturing are discussed.

2. Bioinspired Mechanics Reinforced Structures by 3D Printing

Human body armor has come a long way from the steel-plated suits in the Middle Ages to nowadays bulletproof vest. In comparison, the protective animal structures such as shells and fish scales still beat the most sophisticated man-made gears in terms of mobility and rigidity.[62–64] Examples of tough biological structures including fish scales, lobster claws, antler bones, abalone nacre, and silica sponge enhance toughness by the mechanisms such as interrupting crack propagation, deflecting cracks, or bridging gaps created by cracks. The distinct commonality of animal armors is that they are composed of rigid plates connected to the body and to themselves by collagen fibers/mussels.[62] Nature provides insights into the design of reinforced mechanics for flexible body armor.[65–67] However, the fabrication of bioinspired flexible armors, for a long time, is restricted due to the limited capability of the traditional fabrication technology. The recent development of 3D-printing technology allows researchers to build models of complicated bioinspired structures.[68–70] Consequently, the 3D-printed mechanics reinforced structures can be designed based on the mechanics of the natural biological systems. The discussion of the recent 3D-printing technology developments to fabricate bioinspired structures is classified into three categories: single material, multimaterials, and composites. The related bioinspired structures are to mimic various kinds of creatures including fish scale, nacre, lobster claw, etc.

2.1. Single Material

The single material used in 3D-printed bioinspired structures includes polymer, metal, graphene, etc. Besides the mechanical

© 2018 WILEY-VCH Verlag GmbH & Co. KGaA, Weinheim

property of the material itself, the bioinspired structures play an important role in the enhancement of its mechanical strength. (1) In the nanoscale, biomimetic nanostructures inspired from butterfly wings were fabricated by the two-beam superresolution lithography. These artificial structures are shown to have size, controllability, and uniformity that are superior to those of their biological counterparts. In particular, the elastic Young's modulus of the fabricated nanowires is enhanced by 20%. This fabrication technique provides a unique tool for extracting 3D designs from nature (**Figure 2**a).[71] (2) In the microscale, an aerosol jet 3D printer was developed to build lattice structures that are inspired from natural materials such as wood and bone due to their high strength-to-weight ratio. The building materials were first crushed into nanoparticles and mixed with a solvent (ethylene glycol) to form an ink. The droplet was then deposited by the printer into precise locations to build the designed 3D structures. The resulting tiny structures are tested to be very strong while being porous to offer a large surface area. So far, the researches have built shapes such as microscaffolds with trusses, donut-shaped pillars, spirals, and accordion-like electronic connections (Figure 2f).[74] (3) In the macroscale, 3D-printed armor inspired by fish scale was studied due to its flexibility and high impact resistance. One of the reports was carried out by Song et al. to mimic the three-spine stickleback (Figure 2b),[72] a kind of fish covered by thick bony plates for protection as well as body mobility through peg-and-socket joints. Macroscopic scaled-up (ten times) prototypes were fabricated via 3D printing (using ZPrinter 310 Plus from ZCorp) based on the CAD models that were created from microcomputed tomography data of the stickleback armor. The results show that the porous, sandwich like cross section is beneficial for bending stiffness and strength at minimum weight. The fish scale replicas were used not only for protection, but also for enabling multiple degrees of freedom (translational and rotational). In addition to the design of bioinspired fish scales, the effects of interactions between neighboring scales were studied. 3D printing was used to fabricate arrays of scales with increasingly complex geometries and arrangements, from simple squares with no overlap to complex ganoid scales with overlaps and interlocking features. As shown in Figure 2c, the interactions between the scales can significantly increase the resistance to puncture, and these interactions can be maximized by tuning the geometry and arrangement of the scales. Interestingly, the designs that offer the best combinations of puncture resistance and flexural compliance are similar to the geometry and arrangement of natural teleost and ganoid scales, demonstrating that natural evolution has shaped these systems to maximize flexible protection.[68]

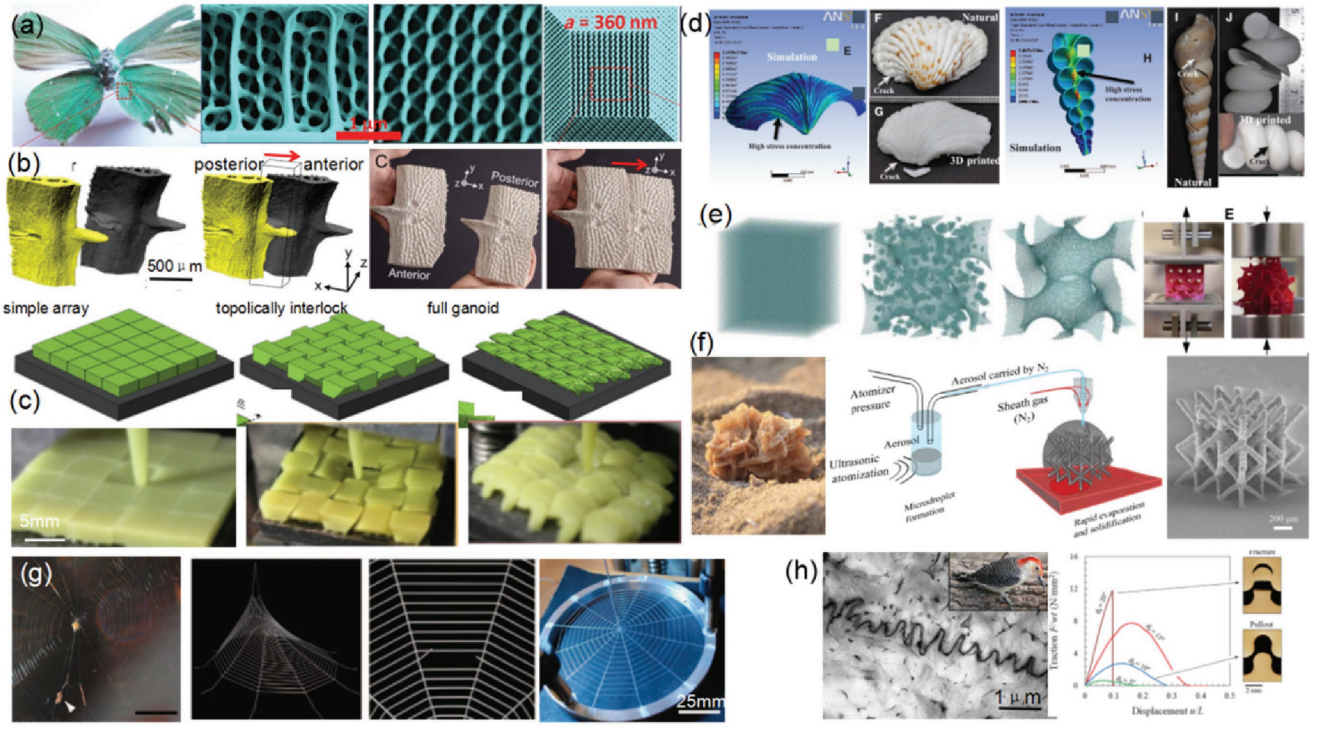

Figure 2. Bioinspired mechanics reinforced 3D-printing structures with single material. a) Butterfly wings inspired strong gyroid nanostructures with high modulus. Reproduced with permission.[71] Copyright 2016, American Association for the Advancement of Science. b) 3D-printed prototypes of two lateral plates. Reproduced with permission.[72] Copyright 2015, Elsevier. c) Schematics of different scaled skin designs and their puncture performances. Reproduced with permission.[68] Copyright 2017, Elsevier. d) Digital images and stress distribution of natural and 3D-printed patelliform shell and Turritella shell. Reproduced with permission.[8] Copyright 2015, American Association for the Advancement of Science. e) Different atomistic and 3D-printed models of gyroid geometry for mechanical tests. Reproduced with permission.[73] Copyright 2017, American Association for the Advancement of Science. f) Desert Rose and the 3D buildup of nanoparticles by pointwise printing to realize microarchitectures. Reproduced with permission.[74] Copyright 2017, American Association for the Advancement of Science. g) Spider web in nature and 3D-printed web. Reproduced with permission.[75] Copyright 2014, Nature Publishing Group. h) Examples of sutured interfaces in red-bellied woodpecker and experiments on the jigsaw interlocked tabs. Reproduced with permission.[76] Copyright 2017, Elsevier.

© 2018 WILEY-VCH Verlag GmbH & Co. KGaA, Weinheim

The shape selectivity by nature plays an important role in the evolution of the marine species. For example, two natural shapes of seashells demonstrate the evolution for the protection of soft body. One is the diametrically converging localization of stresses (Bivalves) and another is a helicoidally concentric localization of stresses (Terebridae) (Figure 2d).[8] The models of seashells were first generated by a software system and then fabricated by an FDM printer. These results show that the complex shapes can sustain loads that are nearly twice as high as those based on their respective counterpart simple shapes. Finite element analysis (FEA) reveals that stress is managed at the hinge point, and then the mechanical load travels from the center to the top. This research also highlights interesting possibilities in achieving a new design of structures with bioinspired optimization objectives. Another unusual geometrical configuration was designed to translate 2D strength graphene into 3D structures. The results show that by compressing and fusing flakes of graphene with a density of just 5%, the strength of ten times that of steel can be achieved. The new finding shows that the crucial aspect of 3D forms relates more with their unusual geometrical configuration than with the material itself. This suggests that similar strong, lightweight materials could be made from a variety of engineering materials by creating similar geometric features (Figure 2e).[73]

Inspired by spider web due to its high strength, elasticity, and graceful failure, computational modeling and microscale 3D printing based on DIW were developed to investigate the mechanical response of elastomeric webs under multiple loading conditions (Figure 2g).[75] The results show that a homogeneous distribution is better for localized loading, while stronger radial threads with weaker spiral threads are better for distributed loading. Another inspiration is from red-bellied woodpecker (*Melanerpes carolinus*) beak as sutured interfaces in nature (Figure 2h).[76] In natural suture lines, the interfaces have complex geometries and re-entrant features. A high-resolution 3D printer based on the digital light processing (DLP) technology was used for its fabrication and FEA is used to provide design guidelines. The results show that pullout strength and energy absorption for the 3D-printed jigsaw-puzzle-like structure increase with higher interlocking angles and higher coefficients of friction.

2.2. Multimaterials

Biological materials fall into two broad structural categories: "soft" structures, which are nonmineralized, and "hard" structures, which are composites of minerals and fibrous organic biopolymers. In order to fully mimic the biological materials and structures, single material is usually not sufficient and multimaterials have been studied. Multimaterials such as soft (TangoPlus) and hard (VeroWhite) polymers were used in the MJP-based 3D printing. Several parameters, such as plate stiffness, scale aspect ratio, spatial overlap, and angle of inclination, were modified to study the effect on the protection and flexibility of armors. The 3D-printed replicas of ganoid fish scales were fabricated by using a multimaterial 3D printer (Objet Connex500) for their potential usages as body armor (**Figure 3**a).[77] The model was designed according to the size of the joints of the ganoid scales.[62] A novel hierarchical computational model, MetaMesh, was proposed to adapt a segmented fish scale armor system to fit complex host surfaces with different curvatures, e.g., human arm, shoulder, and body. Inspired by the overlapping fish scales, prototypes of mixing stiff plate and soft matrix were built using Objet Connex500 3D printer (Figure 3b).[63] Indentation and bending tests show that both protection and flexibility are highly tunable by the geometrical parameters of the microstructure. The penetration resistance can be amplified by a factor of 40, while flexibility decreases in less than five times. Another study by the same research group showed that the actuation angle monotonically increases with an increase in indentation depth for all cases (Figure 3c).[78] Composites with large lamination angles (close to 90°) exhibit higher actuation angles as a response to a localized loading at a decreasing slope. These researches provide guidelines for developing material architectures that are flexible and at the same time strong, and can be tuned for specific applications.

Another way to mimic overlapping fish scales is by gluing rigid scales on soft substrates (Figure 3d,e). Browning et al. fabricated elasmoid fish scale inspired structures by FDM and then cast them into a silicon rubber acting as a flexible base (Figure 3e).[80] Three configurations were investigated and the results showed that this network of armor serves to distribute the load of a predatory attack over a large area to mitigate stress concentrations. Similarly, overlapped scales were 3D-printed (polyjet) by Ghosh et al. and glued onto a flexible silicon base (Figure 3d).[79,87] The existence of three distinct kinematic phases of operation has been proved: spanning linear, nonlinear, and rigid behavior driven by kinematic interactions of scales. The comparison of two different bending configurations (convex and concave) shows that there is a significant enhancement in bending resistance of the beam with biomimetic scales.

The brick-and-mortar architecture found in bone and mollusk shells was studied using 3D-printing technology. Combined experiments and computer simulations on the fracture behavior of a multimaterial printed bone-like plate (Figure 3f)[81] reveal that toughness in this bioinspired architecture emerges from the synergetic effects of a load-bearing stiff anisotropic phase (bricks) and a soft and ductile polymer matrix (mortar). The results confirm that specific topological arrangements of soft and stiff phases as a design mechanism can significantly enhance the structures' mechanical behavior. Besides the layer structure, the mineral bridges are also studied which contribute to the high strength and toughness in nacre and nacre-inspired materials.[88] In addition, it is possible to tune the composite properties by changing sizes and content of structural features in the heterogeneous material (Figure 3h).[83] In the above research, 2D structures inspired from nacre are actually scaled up in order to be 3D printed. A fully 3D hierarchical structure was fabricated with nacre-mimetic composite made of aluminum tablets and vinylester adhesive to test the resistance against blast-induced transverse impulsive loading (Figure 3g).[82] A novel mapping algorithm is developed to design complex structures of nacre-like composites readily to be fabricated by the dual-material 3D-printing technology. The results show that the cohesive and adhesive layers help to mitigate and absorb the imparted energy from the shock wave and minimize the plastic damages to the composite tablets. Similarly, parametric modeling and

© 2018 WILEY-VCH Verlag GmbH & Co. KGaA, Weinheim

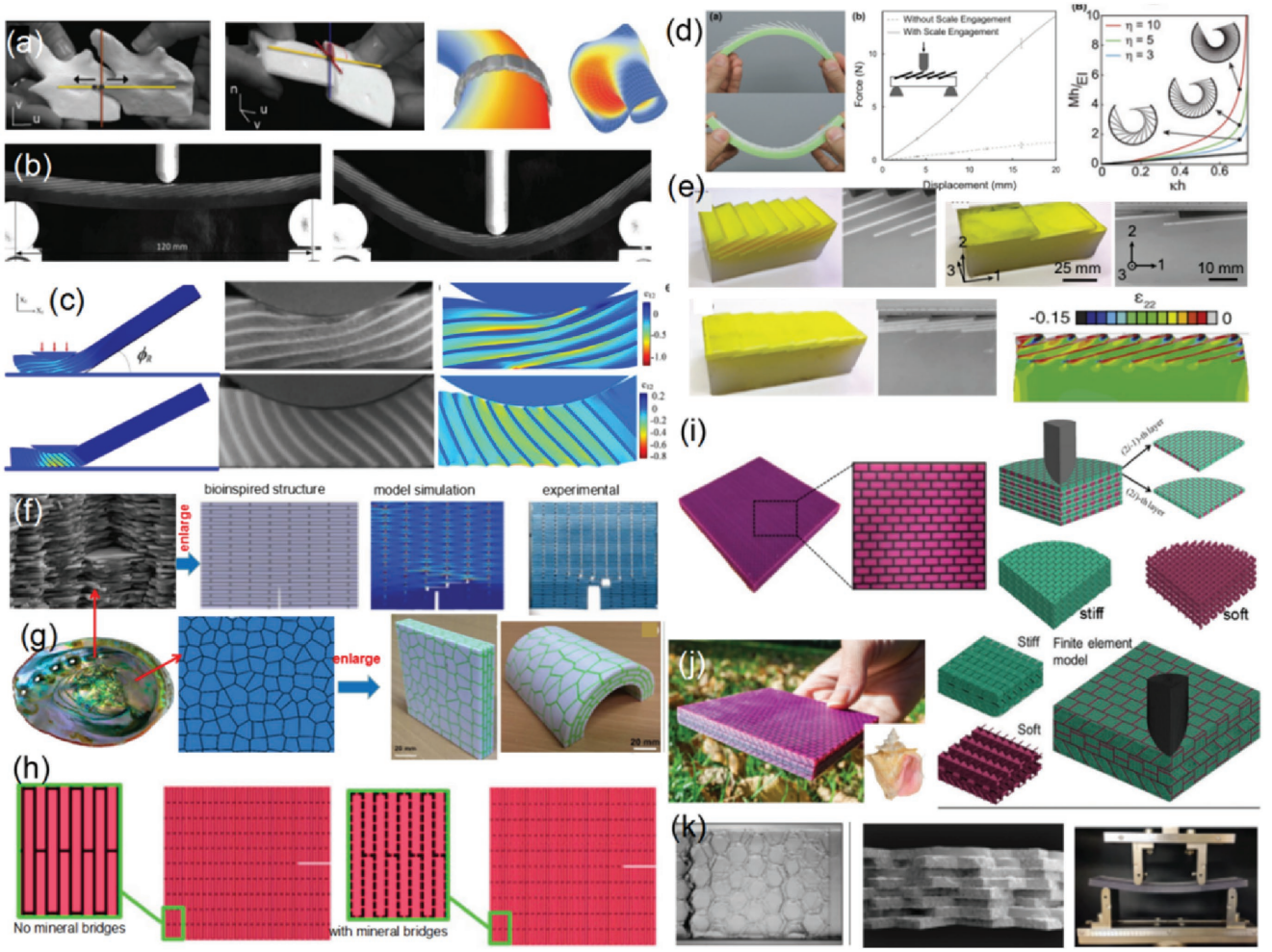

Figure 3. Bioinspired mechanics reinforced 3D-printing structures with multimaterials. a) Allowable motions between 3D-printed adjacent scales and the printed armor on human body. Reproduced with permission.[77] Copyright 2015, Elsevier. b) Fish scale inspired 3D-printed specimen at initial bending and finite bending. Reproduced with permission.[63] Copyright 2015, Royal Society of Chemistry. c) 3D-printed actuated composites with different lamination angles and shear strain distributions with FE simulations. Reproduced with permission.[78] Copyright 2014, Wiley-VCH. d) An illustration of the 3D-printed biomimetic system deformation under bending in two opposite directions and curvature response with various overlap ratios. Reproduced with permission.[79] Copyright 2016, IOP Publishing. e) Macroscale 3D-printed and molded synthetic fish scale. Reproduced with permission.[80] Copyright 2013, Elsevier. f) Bioinspired composites with 3D printing and proceed to test the synthesized specimens. Reproduced with permission.[81] Copyright 2013, Wiley-VCH. g) 3D-printed nacre-like composite prototypes of different shapes. Reproduced with permission.[82] Copyright 2017, Elsevier. h) Comparison of Crack propagation of printed samples with and without mineral bridges. Reproduced with permission.[83] Copyright 2017, Elsevier. i) 3D-printed nacre inspired sample and quarter geometry of the nacre-like design in simulation. Reproduced with permission.[84] Copyright 2016, Elsevier. j) Conch-shell-inspired structure fabricated via multimaterial 3D printing. Reproduced with permission.[85] Copyright 2017, Wiley-VCH. k) Nacre-inspired sample fabricated by multimaterial 3D printing and under mechanical test. Reproduced with permission.[86] Copyright 2017, Wiley-VCH.

multimaterial 3D printing were used to investigate the scaled-up bioinspired brick and mortar-like architecture design from mollusk nacre (Figure 3k).[86] Several parameters such as tablet width, organic layer thickness, and tablet voronosity were adjusted to study their effects on the structure's mechanical property. Gu et al. used a multimaterial 3D-printing machine (an Objet 500 3D printer) to replicate the innate toughness of the nacre and a conch shell. In the nacre-like designs, two base materials that are vastly different in properties are assembled in a ply with an architecture that is similar to nacre. These plies are then stacked with orientation angles of 0° and 90° to generate a laminate construct by multimaterial 3D printing (Figure 3i).[84] And the 3D-printed structure is up to 85% stronger by mimicking the criss-crossed layers typically found in the shell (Figure 3j).[85] The enhanced toughness is attributed to cracks forming in the inner layer that are difficult to reach the middle layer due to their arrest at the rotated interface.[89] These developments will allow for studies, where not only structural parameter spaces can be probed, but also where design principles can be effectively tested at different length scales and with materials that are different from biology.

2.3. Composites Using Field-Assisted 3D Printing

Mineralized composites play an important role in biological structures for strong mechanical properties. These composites consist

© 2018 WILEY-VCH Verlag GmbH & Co. KGaA, Weinheim

of a mineral reinforcement phase, such as hydroxyapatite, calcium carbonate, or silica, embedded in a biopolymer matrix, such as collagen or chitin. With the inspiration, additive manufacturing is evolving from single material and multimaterials for structural purpose to composites and multifunctional 3D printing. The addition of microfillers (e.g., ceramic platelets and microfibers) and nanofillers (e.g., carbon nanotubes, graphene, etc.) have been developed to reinforce the 3D-printed structures.[90,91] In order to mimic biological structures, the combination of shear force, electrical-field, and magnetic-field-assisted methods with 3D printing have been developed to get the anisotropic mechanical properties by controlled filler alignment. We define these as 'field-assisted 3D printing' and will discuss them in the following sections.

2.3.1. Shear-Force-Assisted Bioinspired 3D Printing

Two key structural features in nature are the low-weight cellular architecture of the overall object reinforced with stiff fibers and the low weight of balsa by the honeycomb-type porous structure.[90] In order to mimic these structures, the shear-force-assisted direct ink writing process was developed to get the aligned silicon carbide whiskers and carbon fibers in polymer resins (**Figure 4**a).[90] Reinforced walls of the printed cellular structures were accomplished through the force alignment due to the shear stress during the extrusion. Similarly, a class of aligned carbon fiber reinforced composite was fabricated by the DIW technology. Carbon fibers were aligned in epoxy or aromatic thermoset resin via controlled microextrusion and the extruded mixture is subsequently cured into complex geometries.[98] The composites with carbon fiber alignment outperform equivalently filled composites with randomly oriented fibers[92] (Figure 4b). In the developed FDM of continuous fiber-reinforced thermoplastics (Figure 4d),[94] polylactic acid and carbon fibers (or natural jute fibers) were separately supplied to the FDM printer head, and the fibers were impregnated with the filament within the heated nozzle immediately before printing. Those parts with aligned carbon fiber showed

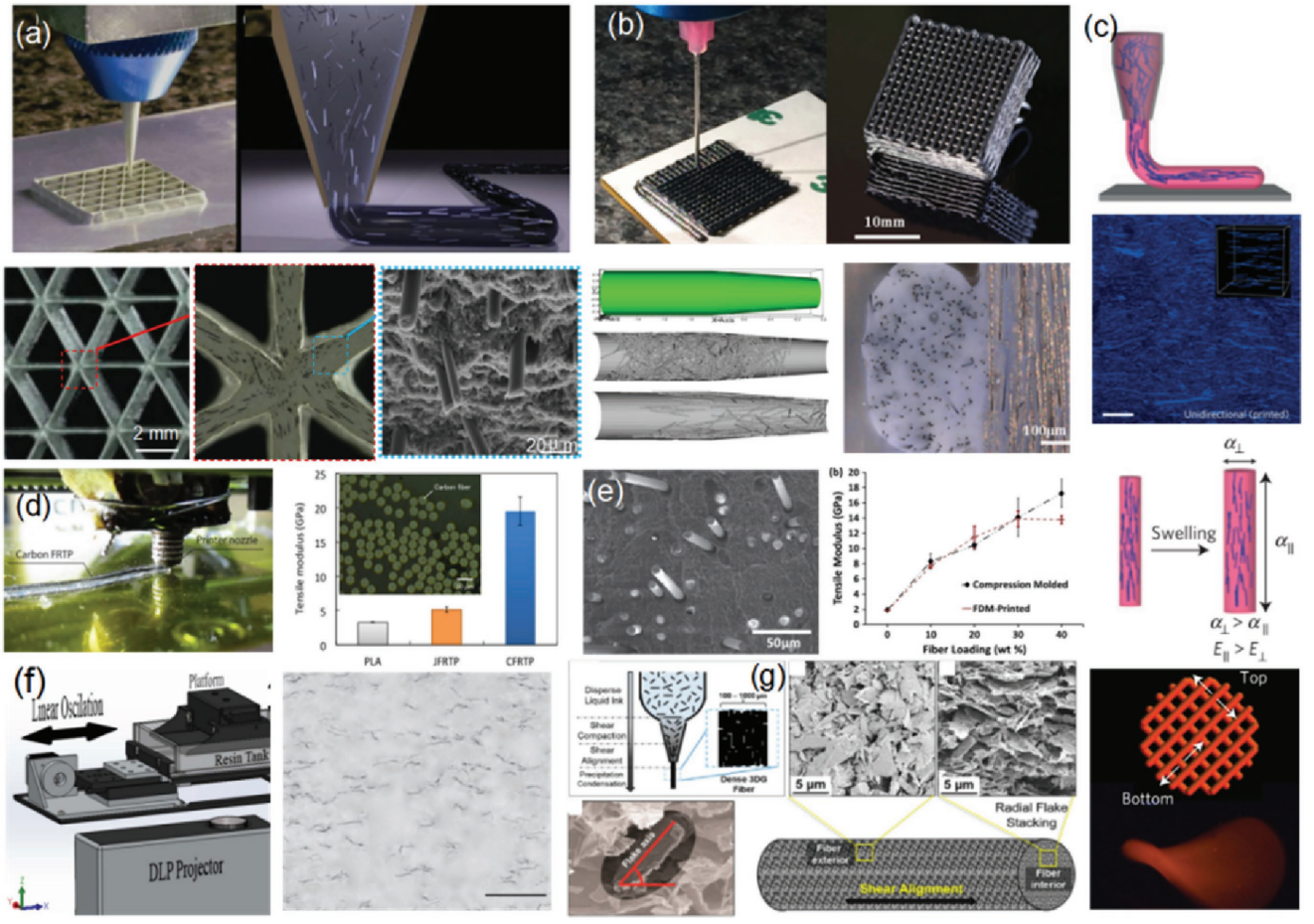

Figure 4. Shear-force-assisted 3D-printing technology. a) Optical image of 3D printing of a triangular honeycomb composite aligned SiC/C-fiber. Reproduced with permission.[90] Copyright 2014, Wiley-VCH. b) Microextrusion of carbon fiber loaded bisphenol-F resin and microscopic images of cross sections of printed parts. Reproduced with permission.[92] Copyright 2017, Nature Publishing Group. c) Schematic of the shear-induced alignment of cellulose fibrils and subsequent effects on anisotropic stiffness and swelling strain. Reproduced with permission.[93] Copyright 2016, Nature Publishing Group. d) Photograph of the 3D printing of carbon fiber reinforced thermoplastic composites. Reproduced with permission.[94] Copyright 2016, Nature Publishing Group. e) Fracture surface SEM microscopic images of ABS/carbon fiber composites. Reproduced with permission.[95] Copyright 2014, Elsevier. f) Aluminum oxide nanowires aligned in photocurable resins. Reproduced with permission.[96] Copyright 2016, IOP Publishing. g) Shear-force-induced graphene flake alignment. Reproduced with permission.[97] Copyright 2015, ACS Publication.

© 2018 WILEY-VCH Verlag GmbH & Co. KGaA, Weinheim

reinforced mechanical properties superior to those of both the jute-reinforced and unreinforced thermoplastics. Carbon fiber was aligned in acrylonitrile–butadiene–styrene (ABS) by FDM with high fiber orientation (up to 91.5%) compared with the traditional compression modeling process. They both exhibited comparable tensile strength and modulus (Figure 4e)[95]; however, further research is needed to reduce the high porosity observed in the 3D-printed composite parts.

Special biomimetic structures with shape-changing properties were 3D printed by aligning cellulose fibrils in hydrogel through shear force (Figure 4c).[93] As a result, anisotropic modulus was produced, i.e., the filament expands easily in the radial direction (40%) but not in the longitudinal direction (10%) when immersed in water. The different expansion rates lead to the programmable folding behavior of designed artificial flowers (as discussed in detail in Figure 10h). Direct ink writing was also used to fabricate reinforced polymer composites consisting of shear-force-aligned graphene flakes and aluminum oxide nanowires. The graphene/polylactide-*co*-glycolide composite is mechanically stable and versatile, which enables thinner printed structures to be rolled, folded, and even fused together (Figure 4g).[97] Another 3D-printing process with shear force alignment is through the stereolithography process. Aluminum oxide nanowires were aligned by the shear flow generated by the lateral oscillation and the image patterned SLA printing (Figure 4f).[96] The tensile strength was enhanced by 28% with 5 wt% of aligned aluminum oxide nanowires. Shear-force-assisted 3D printing of composite materials offers an opportunity to combine the desired anisotropic mechanical, electrical, and thermal properties with the shape flexibility of 3D printing.[97] This helps engineers to optimize their designs where composition and stiffness in a 3D structure need to be digitally adjusted.

2.3.2. Magnetic-Field-Assisted Bioinspired 3D Printing

Magnetic field has been widely used in manufacturing processes because of its flexibility in controlling the alignment of fillers in polymer resins. For example, the fabrication of high-performance Li-ion battery electrodes via magnetic templating[106] and magnetically aligned graphite electrodes.[107] The magnetic-field-assisted freeze casting process can control the alignments to achieve enhanced strength and stiffness by two times[108] as well as the rotated alignments to fabricate bioinspired spiraling ceramics.[109] The combination of magnetic field with 3D printing was developed as 3D magnetic printing, which was successfully used to build bioinspired architectures inspired by bone, mollusk shells and mantis shrimp (**Figure 5**a).[7] The alignments of magnetic response particles (decorated with superparamagnetic iron oxide nanoparticles) in the reactive resin were controlled by magnetic field.[110,111] The particle orientation can either be strengthened or weakened in individual voxels depending on whether the alignment is parallel (local hardening) or perpendicular (crack steering) to the loading direction. These 3D-printed objects also show new mechanical properties such as programmable fracture toughness, that is not accessible using the homogeneous monoliths or conventional fabrication technology.[7] Pan et al. fabricated the 3D-printed magnetic field-responsive smart polymer composite, which creates a wide range of potential applications such as sensing and actuation in soft robotics, biomedical devices, and autonomous systems (Figure 5h).[104] In the multimaterial magnetic-assisted 3D (MM-3D) printing, multiple materials can be printed by simply loading distinct syringes with inks containing different monomer compositions and ultrahigh magnetic response (UHMR) particle concentrations, which are aligned by a magnet or electromagnetic coils (Figure 5b).[99] The magnetic alignment of 15wt% (4.4 vol%) platelets in the tensile loading direction increases the strength and elastic modulus by 49% and 52%, respectively. Compared with the shear-induced alignment method that has limited alignment directions, the magnetic alignment method can ensure deliberate texture control to eliminate the local swelling response.[90,101]

Magnetically assisted slip casting (MASC) is developed to deposit particles in an additive layer-based slip casting process (Figure 5c)[100], in which an advanced magnetically assisted technology is used to control the orientation of fillers during deposition.[110] Bioinspired synthetic tooth was fabricated containing an outer enamel layer made by silica nanoparticles and magnetically aligned alumina platelets to replicate the orientation design of natural tooth. The results show that the presence of silica and the perpendicularly aligned alumina platelets lead to synthetic enamel that is significantly denser and harder than the inner dentin layer. A robust and universal casting method assisted by magnetic field was presented to fabricate bioinspired composites that can replicate the shape-changing structures in nature. The controlled alignments result in anisotropic mechanical property and related swellable/shrinkable properties. Based on the design, Studart and co-workers studied two kinds of polymer composites. One is the controllable alignment of aluminum oxide platelets in hydrogels, which results in various folding behaviors to mimic conifer pinecone, wheat awn and orchid tree seedpod (Figure 5e).[45] The other is the bioinspired shape-changing ceramics by the alignment of magnetized alumina platelets using the rotating magnetic field (Figure 5f).[102] Thus bending, twisting or combinations of these two basic movements can be successfully programmed to obtain a myriad of complex shapes.

Besides the SLA and slip casting processes, the combination of magnetic field with direct writing was also studied. First, In order to overcome the shear force generated from the nozzle, the fiber length needs to be small and a high magnetic field is required, or the system needs to be operated at low shear rates (Figure 5d).[101] Magnetic fields were used to actively control the orientation of reinforcing fillers (i.e., calcium phosphate microrods and alumina microplatelets) in epoxy during printing the fiber reinforced composites (Figure 5g).[103] The magnetic field was applied by the three orthogonal iron-core solenoids around the syringe tip. This technology offers a promising route forward in making high-resolution, optimally reinforced composite materials with 3D printing. Magnetic films with and without particle alignment were printed, and their magnetic properties were compared.[105] The linear alignment field was also applied in the *X* direction during the printing process as shown in Figure 5i in the square sample and the substrate was rotated to get the radial alignment. An increase in high frequency permeability and a decrease in hysteresis

© 2018 WILEY-VCH Verlag GmbH & Co. KGaA, Weinheim

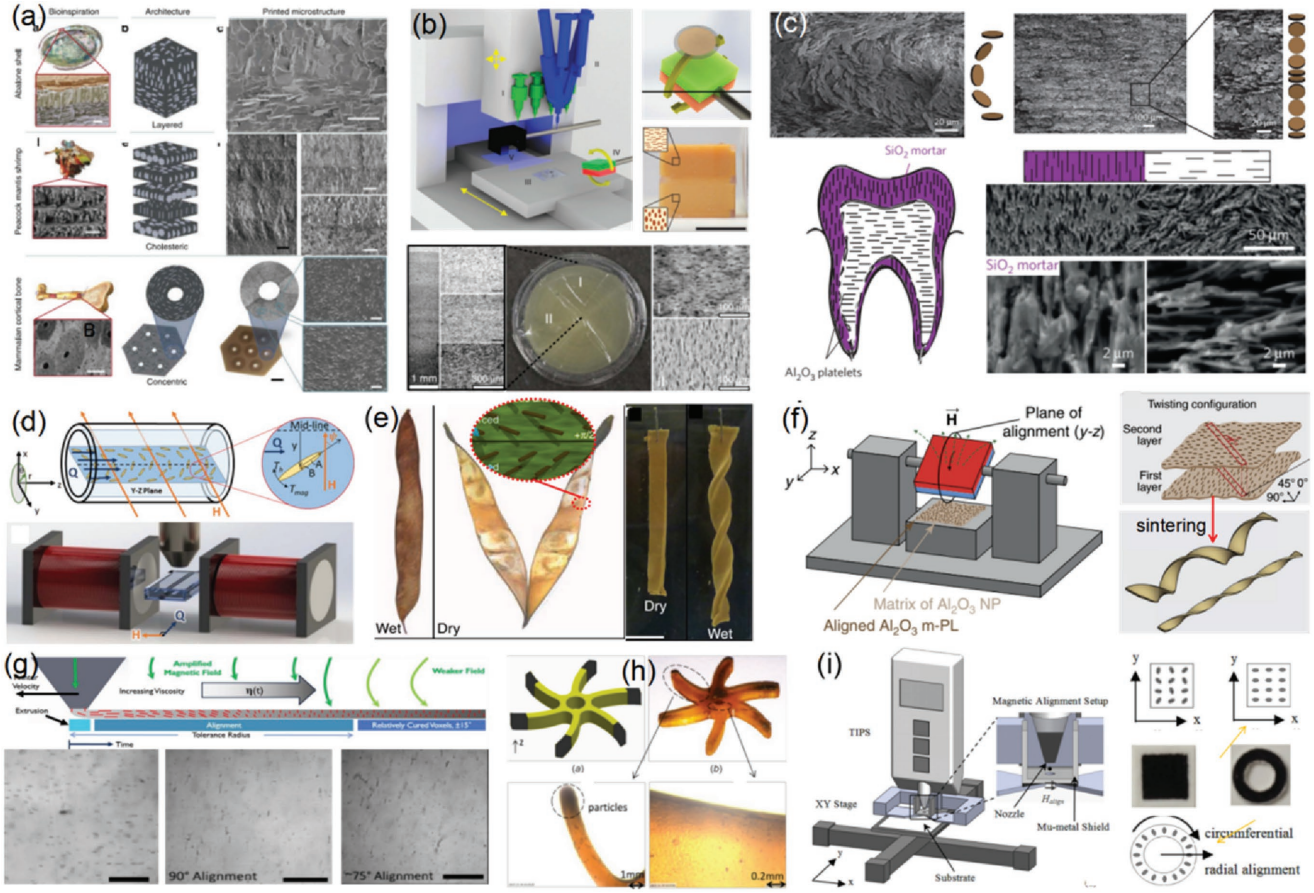

Figure 5. Magnetic-field-assisted 3D-printing technology. a) Bioinspired composites with microstructured architectures created by 3D magnetic printing, the inspiration from Abalone shell, peacock mantis shrimp, and Mammalian cortical bone, respectively. Reproduced with permission.[7] Copyright 2015, Nature Publishing Group. b) Schematics of the multimaterial magnetic 3D printing of heterogeneous composites. Reproduced with permission.[99] Copyright 2015, Nature Publishing Group. c) Bioinspired artificial tooth by the magnetic-assisted slip casting method. Reproduced with permission.[100] Copyright 2015, Nature Publishing Group. d) Schematics of extrusion setup with magnetic field. Reproduced with permission.[101] Copyright 2015, Royal Society of Chemistry. e) Magnetic-field-assisted synthetic chiral seedpods. Reproduced with permission.[45] Copyright 2013, Nature Publishing Group. f) Magnetically aligned platelet and self-shape ceramic. Reproduced with permission.[102] Copyright 2016, Nature Publishing Group. g) Overview image of the real-time orientation requirements of magnetically active reinforcing particles in a curing epoxy matrix. Reproduced with permission.[103] Copyright 2017, SPIE. h) Pictures of the fabricated impeller using the developed magnetic-field-assisted projection stereolithography process. Reproduced with permission.[104] Copyright 2017, The American Society of Mechanical Engineers. i) Schematic of inkjet printing and magnetic alignment setup. Reproduced with permission.[105] Copyright 2014, AIP Publishing.

losses are observed in the alignment direction. This technology enables prototyping and development of novel magnetic composite materials and the related components for inductor and antennae applications.

2.3.3. Electric-Field and Acoustic-Wave-Assisted Bioinspired 3D Printing

Dielectrophoresis has been used to align fillers including ceramic (PZT short fiber), carbon nanotubes, graphite, and glass fibers in polymer resins using both AC and DC fields.[120] The electric field can be applied to produce composites with uniform oriented structure or locally modified surfaces in selected areas. Bioinspired reinforced structure by controlling different alignments of multiwalled carbon nanotubes (MWCNT) using electric field during 3D printing was presented by Yang et al. The 3D-printed Bouligand MWCNT reinforced composites provide insight into understanding the toughening mechanism in nature and reveal guidelines for the design of high impact resistant structures. In addition, this work provides a feasible method for printing artificial meniscus with enhanced mechanical performance, which may find wide applications in the repair of meniscal defects and other fibrous tissues (**Figure 6**a).[112] Another electric-field-assisted Laminar composite additive manufacturing process was developed to align microsized alumina particles into chain-like structures within ultraviolet photopolymer matrix by using electric field (Figure 6b).[113] Polymer/alumina particle composites are deposited on the surface layer and the sample is then fabricated layer by layer. The electric field can be controlled to accommodate a variety of particulate materials and geometries.

The combination of electric field with inkjet printing leads to the electrohydrodynamic jet (E-jet) 3D-printing technology.

© 2018 WILEY-VCH Verlag GmbH & Co. KGaA, Weinheim

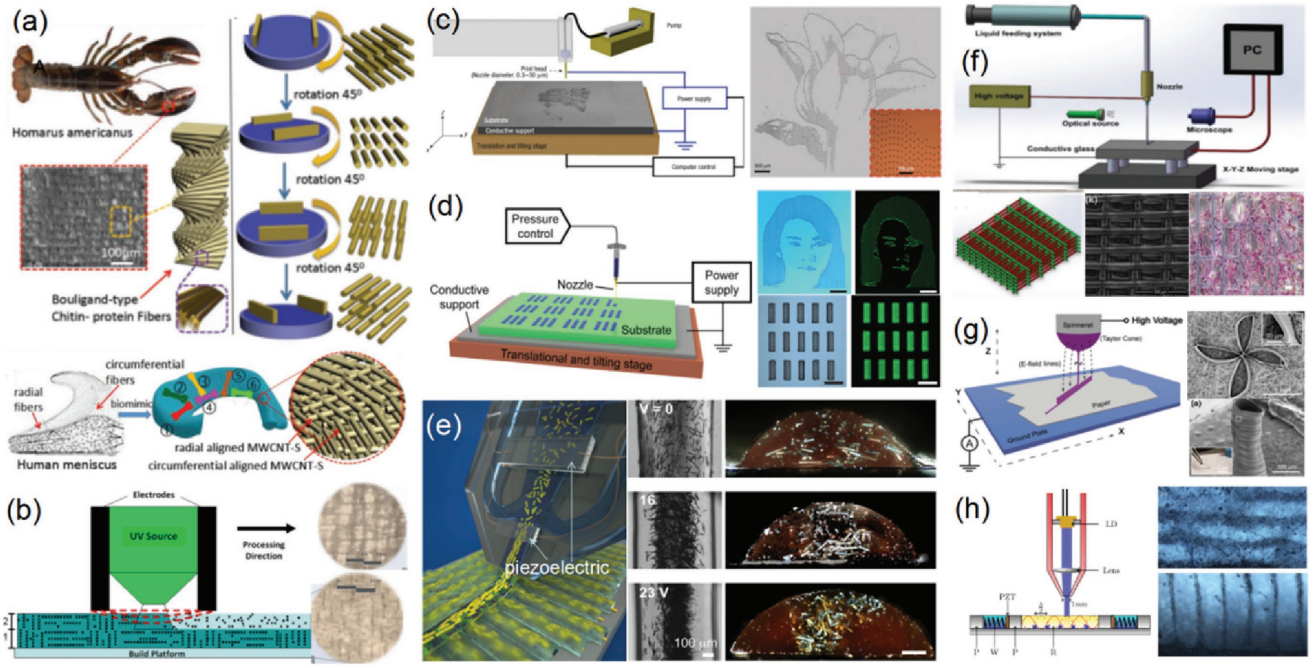

Figure 6. Electric field and acoustic-wave-assisted 3D-printing technology. a) Biomimetic architectures with Bouligand-type MWCNT-S and artificial meniscus created by electrically assisted 3D printing. Reproduced with permission.[112] Copyright 2017, Wiley-VCH. b) Depiction of the field-aided laminar composite process and microscopic images show the alignment of alumina microparticles. Reproduced with permission.[113] Copyright 2014, Springer. c) Image of a flower with printed dots (≈8 μm diameters) fabricated by E-jet printer with substrate/electrode combination mounts on a five-axis stage. Reproduced with permission.[114] Copyright 2007, Nature Publishing Group. d) E-jet printing of various TBADN:DPAVBi patterns with optical and fluorescence microscopy images (from left to right). Reproduced with permission.[115] Copyright 2015, Royal Society of Chemistry. e) Schematic of a microfluidic print nozzle with a coupled piezoelectric actuator and the printed structures. Reproduced with permission.[116] Copyright 2016, Elsevier. f) E-jet printing of 2D and 3D PLGA patterns and cells cultured on scaffolds after 3 d. Reproduced with permission.[117] Copyright 2017, Royal Society of Chemistry. g) Schematic setup of the 3D electrospinning process and a close-up schematic of stacked fibers. Reproduced with permission.[118] Copyright 2015, ACS Publications. h) Ultrasonic manipulation device and optical microscopy images of printed parts reinforced with ultrasonically aligned glass microfibers. Reproduced with permission.[119] Copyright 2016, IOP Publishing.

E-jet printing has been previously utilized to obtain fine patterns of electrodes,[114] and graphene analogs.[121] There are also many bioinspired structures fabricated by the E-jet 3D-printing process. Coordinating the operation of the power supply (electrohydrodynamic phenomena) with the translation stages enables direct-write E-jet printing of inks in arbitrary bioinspired geometries (Figure 6c).[114] An image of a flower is printed with inks that consist of surfactant-stabilized single-walled carbon nanotubes in water. The critical dimension of 1 μm was demonstrated for potential applications including printed electronics and graphic arts. Another E-jet printing method was developed to fabricate small molecule organic light-emitting diode (OLED) pixels with high resolution of 5 μm. The graphic image and optical/fluorescence microscopy images of a woman face demonstrate the versatility of the E-jet printing method (Figure 6d).[115] The E-jet printing technology was also used to fabricate bioinspired and biocompatible scaffolds with enhanced mechanical property (Figure 6f).[117] The results showed that the E-jet printed scaffolds could guide and improve cell growth, potentially enhancing the wound healing performance. A near-field electrospinning technology was developed to directly fabricate 3D structures such as walls, hollow cylinders, and logos on paper substrates by using polyvinylidene fluoride (PVDF) fibers (Figure 6g).[118] This technique has the potential to advance the existing electrospinning technologies to construct 3D structures for biomedical, microelectronics, and MEMS/NMES applications.

Besides electric field, the ultrasound-wave-assisted 3D printing has also been developed. Two propagating plane waves were used to generate a standing wave where the glass fibers will be aligned in photocurable resin (Figure 6h)[119], which leads to anisotropic mechanical properties in the printed objects.[122] Another acoustically excited microfluidic print nozzle was used to tailor the microstructure of printed composite filaments consisting of SiC fibers, solid $BaTiO_3$ spheres, or hollow SiO_2 spheres in an epoxy matrix (Figure 6e).[116] The results demonstrate that the acoustic focusing is a promising technique to control microparticles in fabricating mechanics reinforced composites. As a relatively material agnostic technique for microstructural control, acoustic-assisted 3D printing greatly expands the library of printable fillers and is highly complementary to the existing and emerging 3D-printing technologies.

2.4. Discussion

The 3D-printing materials discussed in this section are shown in **Figure 7**a; a comparison of their mechanical properties with those of natural materials is shown in Figure 7b,c. It is shown

© 2018 WILEY-VCH Verlag GmbH & Co. KGaA, Weinheim

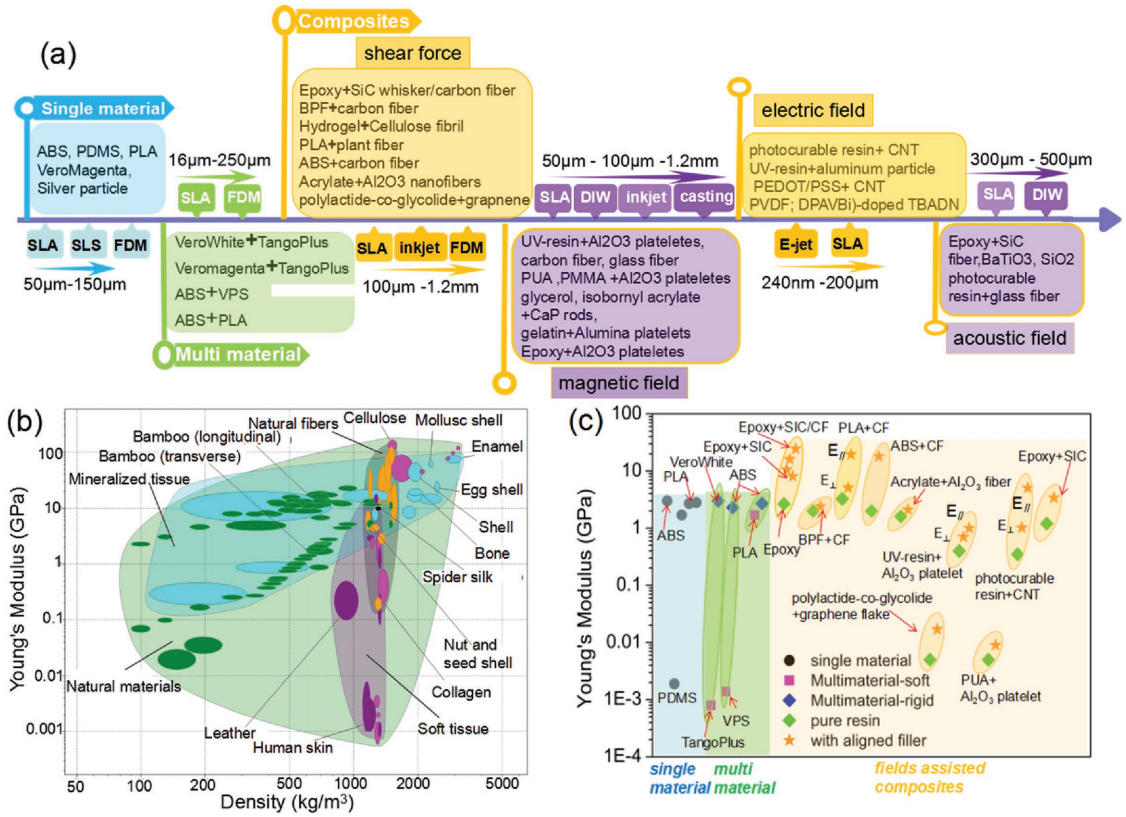

Figure 7. Mechanics reinforced structures by 3D-printing technology. a) Schematic diagram showing the materials and 3D-printing method as well as the resolution used in mechanics reinforced structures. b) Ashby plot showing Young's modulus with density relationships for various natural materials, such as Mollusc shell, bone, and enamel show large amplification in mechanical properties (figure created by the authors using CES Edupack 2017 (Granta Design Limited, 2017)). c) The Young's modulus of bioinspired structures by 3D printing using single material, multimaterials, and composites (CF for carbon fiber).

that the mechanical properties of 3D-printed materials need to be further improved compared with nature. For the single material printing, the future study lies in the shape-guided bioinspired design and the extension of materials from polymers to ceramic and metals (Figure 7a). For the multimaterials printing, the improvement of interface bonding between different kinds of materials and the improvement of printing resolution are important for the fabrication of mechanics reinforced structures. The use of electric and magnetic fields is limited by the fillers with specific electrical or magnetic properties (Figure 7a), hence, how to expand the types of fillers is still a challenge for electric- and magnetic-field-assisted 3D printing. Shear force and acoustic-field-assisted alignment are not limited by materials; however, the alignment pattern is usually limited to be straight or vertical. How to get more complex alignment such as spiral curves that are shown in nature is still a challenge. In order to achieve the optimal property enhancement in the polymer-based composites, the control of the rheological behavior of the mixture is very important. Current magnetically and electrically assisted 3D-printing processes are limited in terms of the relatively low concentration of particles (≈15 vol%) in order to keep the composites sufficiently fluid for spreading and extrusion. High particle volume fractions inevitably increase the viscosity level beyond these upper limits. Alternative approaches have been pursued to obtain complex composite architectures with higher volume fraction of fillers and thus enhanced mechanical performance.[123] Another issue is how to achieve the homogeneous distribution of fillers to enhance the interfacial interaction between the polymer matrix and fillers. The importance of such issues is clearly shown by the widespread research activities in this field and by the numerous attempts to modify the mixtures to achieve better performance of composite materials. These methods can be combined with 3D printing to generate homogeneous distribution of highly bonded fillers with polymer matrix.

3. Bioinspired Shape-Changing Structures by 3D Printing

Most adaptive or responsive systems in engineering world today still operate based on complex sensors and traditional forms of actuations. That is, sensors detect environment change stimuli and accordingly send electrical signals to control actuators to response. In these systems, sensing and actuation are energy intensive and highly reliant on failure-prone and expensive mechanisms[10]. In contrast to human-made responsive systems, nature offers many examples of climate-responsive systems that change their shapes in a metabolism-independent way.[124] In other words, the natural systems dynamically

© 2018 WILEY-VCH Verlag GmbH & Co. KGaA, Weinheim

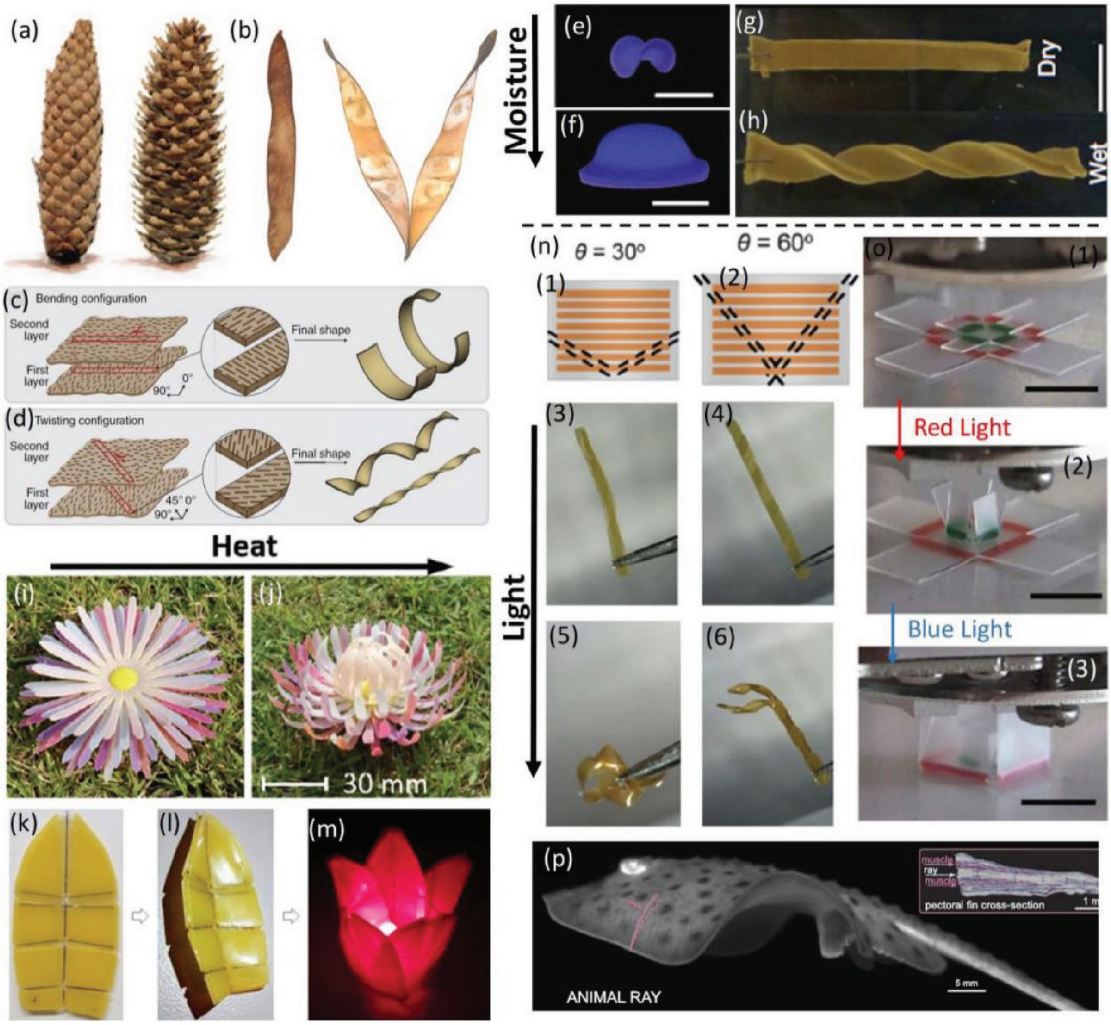

Figure 8. Bioinspired shape-changing structures. a,b) Shape-changing structures in nature: a) pine cones. Reproduced with permission.[10] Copyright 2015, Mary Ann Liebert, Inc. b) Bauhinia pods. Reproduced with permission.[11] Copyright 2011, American Association for the Advancement Science. c,d) Bilayer structures with orthogonally aligned fibers that result in bending and twisting. Reproduced with permission.[102] Copyright 2016, Nature Publishing Group. e–h) Moisture-induced shape-changing structures. e,f) Reproduced with permission.[134] Copyright 2016, Wiley-VCH. g,h) Reproduced with permission.[45] Copyright 2013, Nature Publishing Group. i,j) Reproduced with permission.[135] Copyright 2017, American Association for the Advancement Science. k–m) Reproduced with permission.[136] Copyright 2015, The American Society of Mechanical Engineers. n–p) Light-induced shape-changing structures. n) Reproduced with permission.[137] Copyright 2017, Wiley-VCH. o) Reproduced with permission.[139] Copyright 2017, American Association for the Advancement Science. p) Artificial animal ray: reproduced with permission.[138] Copyright 2016, American Association for the Advancement Science.

change shape without the need of an active metabolism and their behaviors entirely reply on inherent materials and structures. For example, plants, such as pine cones or Bauhinia pods (**Figure 8**a,b), exhibit shape changes in their seed dispersal units upon moisture. This mechanism ensures seeds are dispersed only when the environment is sufficiently hydrated with water. Many attempts have been made to mimic the shape-changing properties in nature.[125,126] Among all the available methods, 3D printing has attracted much interest due to its flexibility in controlling the material distribution in structures.[1,127–129] Tibbits used a term *4D printing* to describe a class of 3D-printing technologies applied to build shape-changing structures.[130] Readers interested in the state of the art of 4D printing can refer to some excellent reviews.[131–133] In this section, we mainly discuss major challenges in 3D-printing bioinspired shape-changing structures and some recent progresses in mitigating these challenges.

The basic principle of shape changing in a wide variety of plants can be attributed to the anisotropic swelling properties of cell walls comprising directionally aligned stiff cellulose microfibrils embedded in a hygroscopic matrix (refer to Figure 8c,d). Upon exposure to water, the composite structures swell preferentially in the direction perpendicular to the microfibrils.[124] Stacking two layers of such structures with orthogonal fiber directions can lead to differential swelling between the top and bottom layers upon water, which further induces bending or twisting movements due to the resulting anisotropic contraction along two orthogonal directions.

© 2018 WILEY-VCH Verlag GmbH & Co. KGaA, Weinheim

Inspired by these structures, a classical design paradigm of shape-changing structures is to arrange responsive shape-changing materials in an anisotropic architecture. This structure exhibits a shrinkage/expansion behavior or even bending and twisting driven by controlled patterning when exposed to stimuli, including moisture, heat, light, etc. In this section, 3D-printing technologies and related materials used to generate shape-changing anisotropy for shape-changing behaviors are discussed.

3.1. Basic Responsive Shape-Changing Materials

According to the environmental source that is used to stimulate 3D-printed shape-changing structures, materials that have been employed can be classified as moisture-induced, heat-induced, and light-induced deformable materials.

Moisture-Induced Deformable Materials: Examples of moisture-induced deformable materials are hydrogels (Figure 8e,f) and hydrogel composites (Figure 8g,h). Hydrogel, such as poly(*N*-isopropyl acrylamide) gel, is a water-swollen and cross-linked polymeric network.[140] It is typically produced by thermally or UV-light-initiated radical polymerization of one or more monomers. Hydrogels can be shaped into complex geometry by stereolithography[134,141–143] or extrusion-based 3D-printing technologies (e.g., direct ink writing[93]). Furthermore, hydrogels can be mixed with cellulose fibers and ceramic platelets to achieve differential stiffness and consequently generate differential swelling properties in the material.[45,93]

Heat-Induced Deformable Materials: Of many available heat-induced deformable materials, shape-memory polymer (SMP) is mostly studied[135,144–146] as shown in Figure 8i,j. Through a thermomechanical training process, temporary shapes can be defined in SMP at a lower temperature and the structure is thus capable of recovering to its original shape upon heating. Compared to hydrogel-based structures, SMP structures have higher modulus and faster response rates. This material can be synthesized as a photocurable liquid resin from commercially available materials and hence has been mainly fabricated by the photo-polymerization-based 3D-printing processes including inkjet printing and laser/projection-based SLA. Besides SMP, some materials exhibiting spontaneous shrinking behaviors upon heat have been applied to build shape-changing structures, including prestrained polymers[147–150] and ceramic green parts.[102]

Light-Induced Deformable Materials: Light-induced shape-changing materials respond to light exposure by generating a volumetric change. In some of these materials, this volumetric change is caused by chemical reactions, such as photo-polymerization or photoisomerization. Examples include photocurable resin and azobenzene. Photocurable resin undergoes volume shrinkage upon illumination due to cross-linking between monomers and cross-linkers[151] while azobenzene exhibits volume expansion under UV light due to a trans-to-cis conversion with different functional group orientations in 3D space[137] (see Figure 8n–o). In some other materials, a light-induced volume change is induced by the heat caused by the light exposure.[139] For example, light-absorbing ink printed on a heat-induced shape-changing material (e.g., Shrinky-Dinks films) converts light energy to localized heat, which in turn causes shrinkage of the structure, as shown in Figure 8o. Besides, contractile biological materials, such as muscle cells, can also be used as light-induced shape-changing materials, which output a contraction force in exposure to light[138,152,153] (Figure 8p).

3.2. Multimaterial 3D Printing for Anisotropy

One approach to achieve shape-changing anisotropy is to combine a responsive shape-changing material with a passive matrix material in a *Bauhinia*-inspired helical architecture using existing multimaterial 3D-printing processes (e.g., polyjet[144,145] or SLA[146]). The structure can be controlled to bend or twist by varying prescribed shape, size, orientations, and volume fractions of the helical strips (refer to **Figure 9**a–d). Basic shape-changing materials available for these multimaterial 3D-printing techniques include SMP[144,145] and hydrogel.[154] Elastomers are typically used as the passive matrix in these structures. More interestingly, incorporating more than one shape-changing material with different responsive properties enables sequential shape changes of a single structure. For example, when multiple SMPs with different thermomechanical properties were incorporated,[146] time-dependent sequential shape changes can be accomplished by providing the required triggering temperatures, as shown in Figure 9e–g.

Some shape-changing structures comprising multiple materials cannot be processed in a single step by the existing 3D-printing processes instead they have been constructed via a multiple-step fabrication process. For example, prestrained polymer-sheet-based structures[136,139,155,156] are fabricated by first cutting a prestrained polymer sheet (e.g., Shrinky-Dinks films[149]) into a 2D shape, and then printing a specific pattern of a stiff material or light absorbing ink onto the surface. The stiff material was used to define a passive region that is insensitive to heat with respect to the other regions, while the light absorbing ink induced a localized heat gradient upon exposed light. Muscle-cell-based structures were built by manually seeding light-induced contractile cells onto a 3D-printed elastomer skeleton to form a biohybrid shape-changing robot triggered by light stimuli (Figure 8p).[138,152,153]

3.3. Field-Assisted 3D Printing for Anisotropy

Compared to multimaterial 3D printing, field-assisted 3D-printing processes can be more efficient in inducing shape-changing anisotropy since the frequent transitions between different materials can be avoided. These techniques typically exploit an external force, such as shear force[93] or magnetic force,[45,102] to align microscale fibers in polymer matrix to induce a desired macroscopic anisotropy.

Shear-induced alignment has been successfully used in a direct ink writing process to attain localized swelling anisotropy in swellable shape-changing structures, as depicted in Figure 9h–j.[10,93] The alignment of stiff cellulose fibrils in hydrogels was controlled by the prescribed printing paths

© 2018 WILEY-VCH Verlag GmbH & Co. KGaA, Weinheim

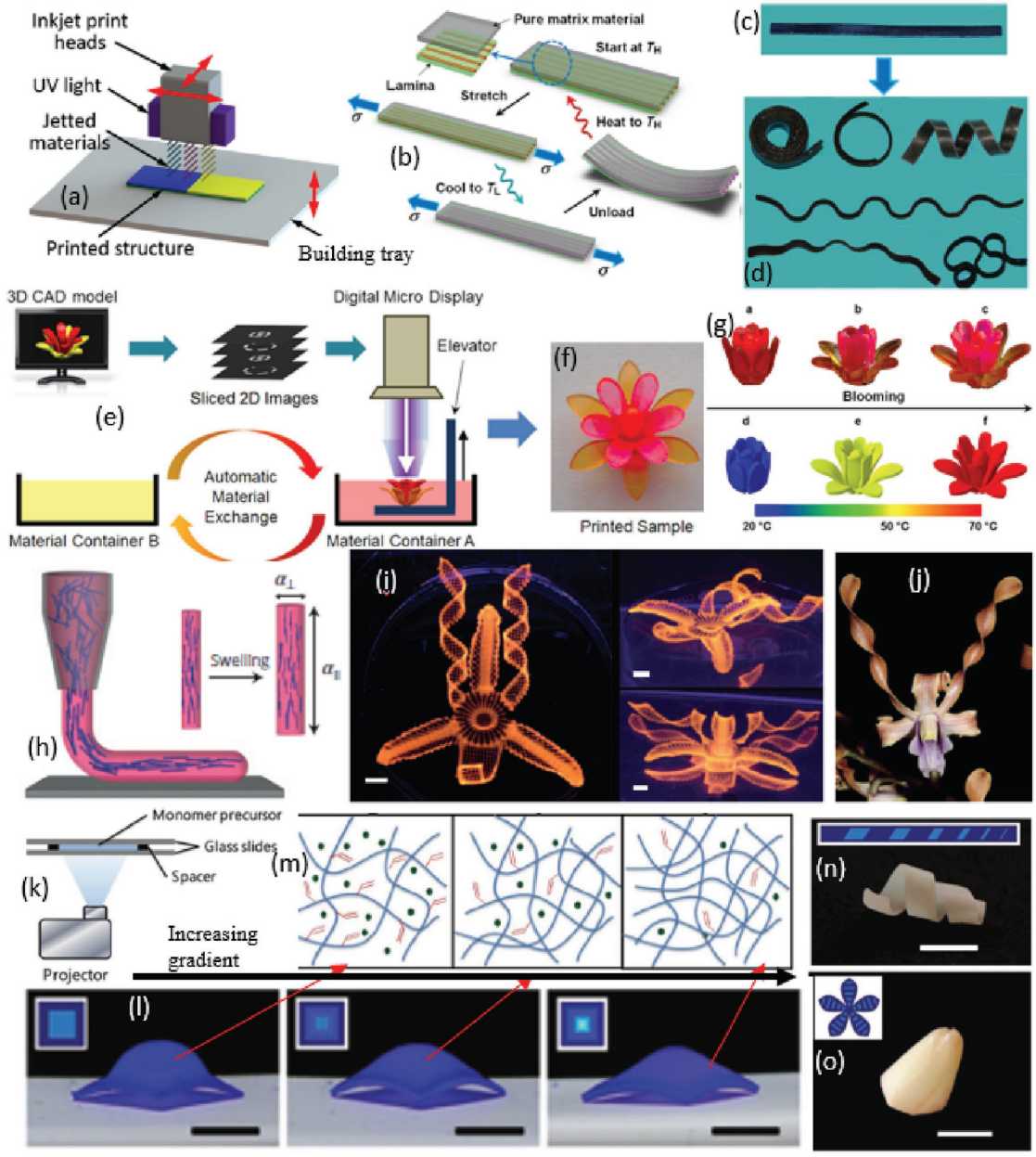

Figure 9. 3D-printing technologies to achieve shape-changing anisotropy. a–d) Polyjet multimaterial 3D printing for SMP. a) Reproduced with permission.[135] Copyright 2017, American Association for the Advancement Science. b–d) Reproduced with permission.[144] Copyright 2013, American Institute of Physics. e–g) Multimaterial DLP for SMP. Reproduced with permission.[146] Copyright 2016, Nature Publishing Group. h–j) Shear-induced fiber alignment by direct ink writing. Reproduced with permission.[93] Copyright 2016, Nature Publishing Group. k–o) Cross-link density gradient achieved by controlling light exposure. Reproduced with permission.[134] Copyright 2016, Wiley-VCH.

and the extent of the alignment can be adjusted by the nozzle diameter and the printing speed. After being cured by UV light, a 3D-printed structure was immersed in deionized water to initiate the swelling-related shape changes. Compared to the traditional subtractive manufacturing processes used to fabricate fiber-based hydrogel composites,[157] the 3D-printing technique offers more flexibility in controlling the local alignment of fibers during the fabrication process, which enables more complex shape-changing behaviors of the structures. The magnetic-field-assisted 3D printing has also been used to control the alignment of inorganic particles within polymer. By applying external magnetic fields, Al_2O_3 platelets coated with superparamagnetic iron oxide nanoparticles can be oriented into programmable shape-changing microstructures in a swellable/shrinkable polymeric matrix.[45,102] The orientations of fillers were preserved after the matrix was cured. The structures not only exhibit a differential shrinking property during heat treatment, but also exhibit a differential swelling property in water when hydrogel is used as the matrix.

© 2018 WILEY-VCH Verlag GmbH & Co. KGaA, Weinheim

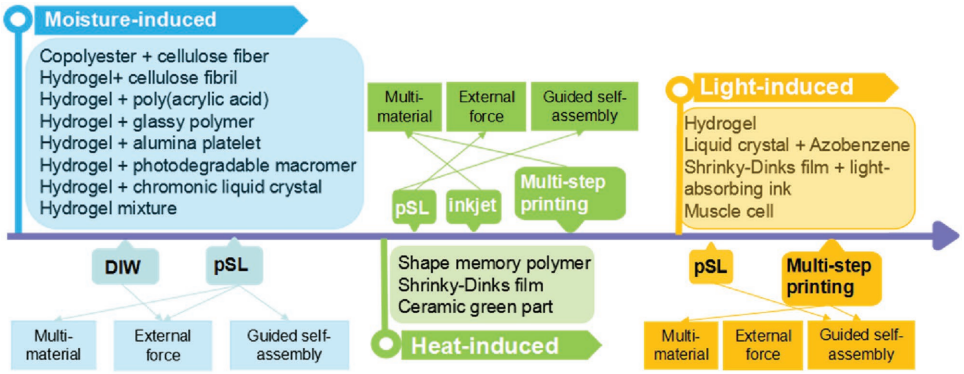

Figure 10. Schematic diagram showing the materials and 3D-printing method used in the reviewed bioinspired shape-changing structures.

3.4. Guided Molecular Self-Assembly-Based 3D Printing for Anisotropy

In addition to multiple materials and fiber/polymer composites, some efforts have been made to gain anisotropic shape changes in a single material through guided self-assembly techniques at the molecular level. These techniques achieve anisotropic molecular densities and orientations through controlling operation conditions of 3D-printing processes, which contribute to the macroscopic shape-changing behaviors of the resultant structures. Examples of the guided molecular self-assembly techniques include tuning cross-linking density of polymerization[134,135,142,151,158] and aligning liquid crystal,[137,159] etc.

A cross-linking density gradient in polymers can be achieved by tuning the process parameters during the fabrication process, such as the light dose exposure in SLA(as shown in Figure 9k–o) or the heating temperature and moving speed of the nozzle in FDM.[158] This gradient gives rise to an anisotropic swelling property in response to moisture in moisture-induced deformable materials, such as hydrogel,[134,142] and an anisotropic shrinkage rate in response to heat in heat-induced polymer materials.[135,147,148,151,158] The shrinkage is constrained by the building platform during the fabrication process, yielding a strain gradient within the 3D-printed structures. Heating the final structures releases the built-in strain and accordingly results in desired shape-changing behaviors. In contrast to cross-linked polymers, chromonic liquid-crystal polymer is a material whose anisotropy can be induced by aligning the material's molecular direction.[137,159] A chromonic liquid-crystal molecule features an anisotropic rod-like structure, whose direction can be aligned by a rubbing plate. When incorporated with a basic shape-changing material (e.g., azobenzene[137]), this material introduces the desired shape-changing anisotropy through a directed molecular alignment, which is in analogy to stiff fibers in fiber–polymer composites.

3.5. Discussion

In summary, shape-changing structures can be achieved via 3D-printing responsive and deformable materials in a bioinspired architecture with anisotropic material properties. The responsive and deformable materials exhibit simple shape changes, such as shrinkage or expansion, upon exposure to external stimuli including moisture, heat, or light. More complex shape-changing behaviors including bending and twisting can be achieved by anisotropically encoding different basic shape-changing materials in 3D-printed structure. According to the scale at which a shape-changing anisotropy is introduced, the fabrication techniques can be classified as multimaterial 3D printing, field-assisted 3D printing, and guided-molecular self-assembly-based 3D printing. Despite the recent advances in 3D printing of shape-changing structures, challenges still exist that need to be addressed. First, the material selection for 3D-printed shape-changing structures is still limited: mainly a few categories of polymers are currently available, which significantly restrict the potential applications of shape-changing structures (**Figure 10**). Moreover, the stimuli used to trigger shape-changing behaviors are still based on laboratory environments and might not be broadly applicable in real world. Meanwhile, the shape-changing behaviors triggered by these stimuli may have big variations and cannot be reliably and accurately controlled. This makes the shape-changing structures particularly difficult to be applied in an actual human-centered system. In the future, more material selections need to be explored and incorporated into shape-changing structures to achieve better physical properties, such as mechanical rigidity, biodegradability, chemical, or thermal resistance, etc. Better simulation and design methods also need to be developed to address the robustness and accuracy of shape-changing structures.[150] Real-world environment should be investigated to identify accessible stimuli in order to reliably trigger shape-changing behaviors. Finally, how such shape-changing behaviors can be well controlled and integrated in an actual human system requires further study.

4. 3D Printing of Bioinspired Interface Structures

Besides mechanical property as shown in the mechanics reinforced and shape-changing structures, nature provides inspirations on other material properties such as interface, optical, and electrical properties as well. Using 3D-printing technology, the bioinspired interfaces including hydrodynamic surface, superhydrophobic surface, and microfluidic structure are discussed in this section.

© 2018 WILEY-VCH Verlag GmbH & Co. KGaA, Weinheim

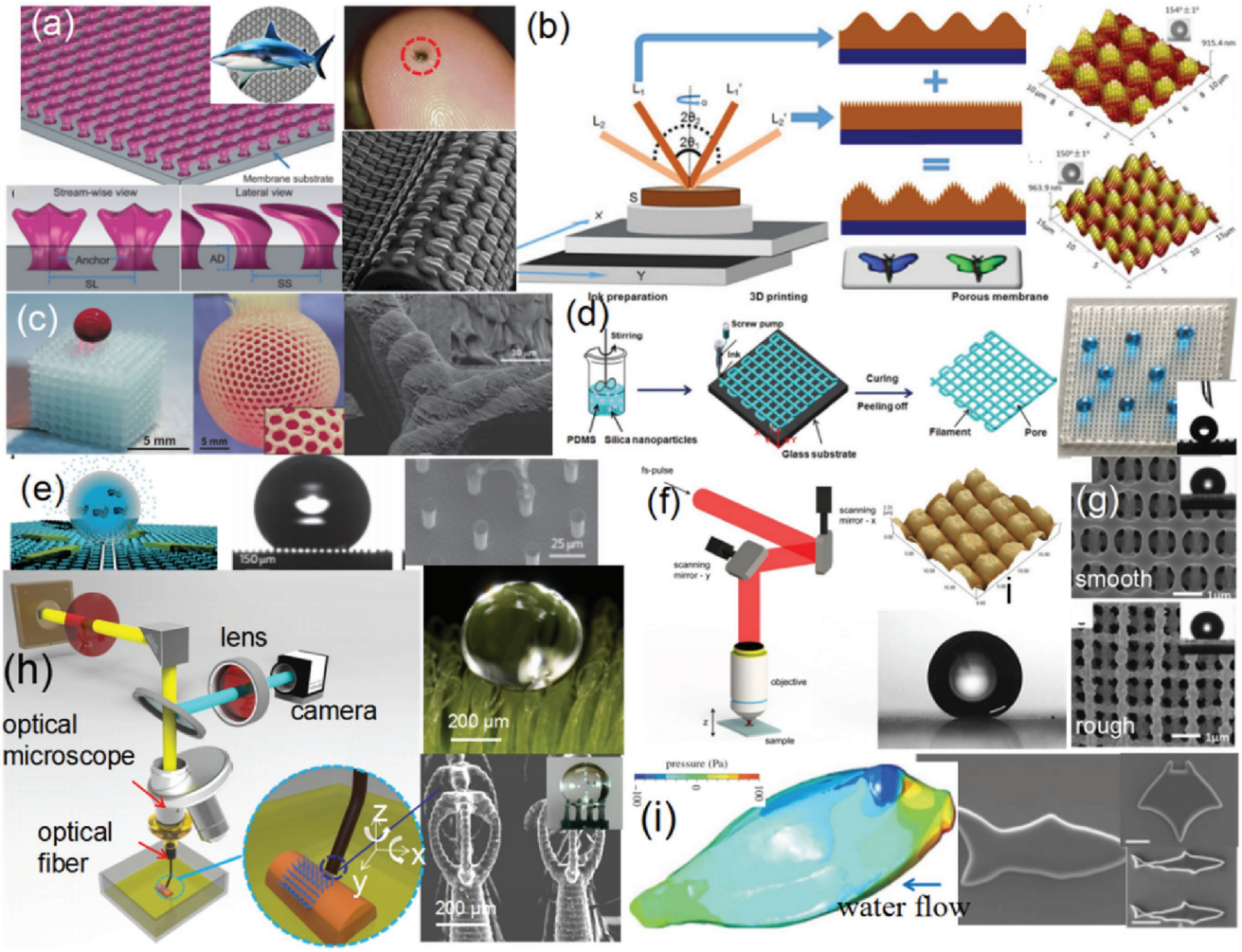

Figure 11. Bioinspired 3D-printing hydrodynamic surface structures. a) Shark denticles were enlarged from the micro-CT model and then synthesized on a membrane substrate. Reproduced with permission.[12] Copyright 2015, IOP Publishing. b) Schematic of angle varied multiple exposures of two-beam laser interference lithography process and the fabricated superhydrophobic hierarchical surfaces. Reproduced with permission.[163] Copyright 2017, Wiley-VCH. c) SEM images of iBalland dyed water on poly(PFMA)-iLattice and filled poly(PFMA)-iBall. Reproduced with permission.[164] Copyright 2013, Royal Society of Chemistry. d) Schematic of the 3D printing of a superhydrophobic porous membrane using nanosilica-filled PDMS ink. Reproduced with permission.[165] Copyright 2017, Royal Society of Chemistry. e) Superhydrophobic arrays fabricated by electron-beam lithography and the evaporation process of water droplet. Reproduced with permission.[166] Copyright 2011, Nature Publishing Group. f) Schematic diagram of the experimental setup for femtosecond (fs)-laser processing of superhydrophobic surface. Reproduced with permission.[167] Copyright 2011, Elsevier. g) Wetting behaviors of fluorosilane-treated epoxy-POSS diamond structures. Reproduced with permission.[168] Copyright 2012, Wiley-VCH. h) Bioinspired superhydrophobic eggbeater structure by 3D printing. Reproduced with permission.[169] Copyright 2017, Wiley-VCH. i) Simulation graph shows pressure on the box fish carapace surface and 3D printing of artificial microfish. Reproduced with permission.[161] Copyright 2017, The Royal Society Publishing.[162] Copyright 2015, Wiley-VCH.

4.1. Bioinspired 3D-Printed Hydrodynamic Surface

Fish scales not only provide protection, but also reduce frictional fluid drag during swimming.[13] For example, shark skin is covered by placoid scales with unique external profiles that resemble tiny hydrofoils[12,14]; however, such shapes are difficult to fabricate by using the traditional manufacturing technologies. The 3D-printed shark skin using micro-computed-tomography (micro-CT) imaging shows increased swimming speed (6.6%) and 25.2% increment with taggered-overlapped pattern with reduced static drag (up to 8.7%) compared with smooth surface (**Figure 11**a).[12] This is because the leading edge vortex with greater vorticity being generated by the 3D-printed shark skin than the smooth surface.[14,160] In another study, models of trunkfish and boxfish were 3D printed to reveal how their unique body shapes contribute to high maneuverability (Figure 11i).[161] Computational fluid dynamics simulation of pressure distribution shows that the 3D-printed boxy shape generates strong destabilizing moments produced by pressure waves. An artificial microfish was fabricated using the micro-SLA process for the drug delivery controlled by the magnetic field (Figure 11i).[162] Platinum (Pt) nanoparticles were coated on the fish head for chemically mediated propulsion, and iron oxide nanoparticles are added on the fish tale for magnetic guidance. This strategy can be readily extended to a fully integrated microswimmer

© 2018 WILEY-VCH Verlag GmbH & Co. KGaA, Weinheim

system as a powerful platform for applications including drug delivery, personal therapeutics, and environmental conservation.

4.2. Bioinspired 3D Printing of Superhydrophobic Surface

In nature, many kinds of plants and animals possess hydrophobic or superhydrophobic surfaces that are attributed to complex micro- and nanostructures on the surfaces. 3D printing presents a new way to study the bioinspired hydrophobic surface by replicating the complex structures. Inspired by Salvinia Molesta leaves, superhydrophobic eggbeater structures were fabricated by the immersed surface accumulation 3D-printing process and the potential applications in microdroplet manipulation and oil/water separation were demonstrated (Figure 11h).[169,170] Artificial hairs with eggbeater heads were also reproduced (100 times smaller scaling down) by 3D laser lithography.[16] Although the micropatterned surface is not superhydrophobic (contact angle ≈122°), it shows air retention behavior and could be potentially used for drag force reduction. The initiator-integrated 3D printing was developed to modify microlattices from superhydrophilic to superhydrophobic (Figure 11c).[164] A perfect sphere-shaped water droplet formed on the poly(PFMA)-grafted lattice and droplets permeated into the poly(PEGMA)-grafted lattice. The 3D-printed superhydrophobic membrane made by hydrophobic nanosilica-filled polydimethylsiloxane ink exhibits excellent mechanical stability and enhanced lifetime usage (Figure 11d).[165] It also shows high oil water separation efficiency (99.6%) under a high flux of 23 700 L m^{-2} h^{-1}, which could be optimized via computer program to adjust the pore size.

Inspired by butterfly wings, hierarchical superhydrophobic structure was fabricated by the two beam laser interference lithography technology (Figure 11b).[163] In addition, 3D diamond structure was fabricated by the 3D holographic lithography (Figure 11g) and micropillars decorated with regular arrays of silver nanodots were fabricated by the electron-beam lithography (Figure 11e).[166] The 3D-printed hierarchical surfaces were treated with fluoroalkylsilane to add chemical hydrophobicity. The 3D-printed diamond structure shows superhydrophobic property after treated with a thin layer of low surface energy material (Figure 11g).[168] Combined structural color and self-cleaning properties were achieved to mimic the multifunctions of butterfly wings. The micropillars surface also shows superhydrophobic property with high contact angles and low friction forces. Laser microstructuring with 70 ps pulses and 532 nm Nd:YAG was used to produce square-shaped pillar patterns with superhydrophobic property (contact angle of 157°) (Figure 11f).[167] The surface structuring method presents to be an interesting option to control the wetting property of polymeric surfaces.

4.3. Bioinspired 3D Printing of Microfluid Structure

Complex vascular network in tissue engineering plays a critical role in supplying cells with oxygen and nutrients as well as removing CO_2 and cellular waste.[19] Recapitulating this complexity in vitro has become a fundamental challenge for the fabrication of living tissues (**Figure 12**a).[171] Traditional fabrication technologies lack the capability of building complex vascular architecture and usually require separate approaches to create vessels in each size range.[19] With the help of 3D printing, it is possible to fabricate vessels with various length scales in one step. The early study focused on mimicking the shape complexity of vasculature that pervades in animal and human body. The architecture of mouse liver vasculature derived from a μ-CT angiography and magnetic resonance imaging scan was fabricated by a multiphoton variant of SLA using photocurable resin, (Figure 12k),[181] in which channels consisting of microsized fluidic tubes were fabricated. The high resolution of the multiphoton SLA process enables the fabricated branch channels with 18 μm luminal diameter and 5 μm thickness (Figure 12b).[172] Another way to fabricate bifurcating fluidic networks is based on using the inkjet printing process to deposit alginate into a supporting bath of calcium chloride (Figure 12 c).[173] The calcium chloride bath serves as an ionic cross-linker for the deposited alginate and the buoyant force exerted on the alginate droplets supports the formation of complex overhangs and spanning regions. To make more complex branches, a freeform reversible embedding of suspended hydrogels (FRESH) was used to produce physiologically relevant structures including a branching arterial tree and a 3D-scanned embryonic chick heart with internal trabeculae (Figure 12d).[174] This 3D-printing technology is based on the alginate and fibrinogen cross-linking by infusing the gelation slurry with calcium chloride and thrombin, respectively. As a key intermediate step between plastic matrices and living tissues, more complex branching networks were printed within a pluronic hydrogel (Figure 12e).[175] The blood vessels were then fabricated by the removal of temporary sacrificial materials. Complex vascular 3D networks with branching architectures were fabricated in epoxy matrices (Figure 12f) ,[176] which encompass many key features of native vasculature; however, they were not created in biomaterials and were lack of functions.

To fully mimic the biological environment, bifurcating channels vary in diameter from 1 mm to 200 μm are fabricated by converting a 3D-printed thermoplastic material into a gelatin network template by using an intermediate alginate hydrogel. The channels are fully 3D, hierarchical, and customizable due to the CAD-based model design. The results show good cell seeding with the presence of tight junctions between channel endothelial cells, as well as high cell viability and spreading in the bulk hydrogel (Figure 12g).[177] Another 3D-printing process is to use direct extrusion of hydrogel microparticles within a supporting slurry to build 3D structures (Figure 12h).[178] Photoreactive polyvinyl alcohol was cross-linked after printing and the fully cross-linked structures were recovered from the Carbopol slurry by immersing the 3D-printed structures in stirred water. The results show thinner lines are generated with the increment of speed and the spheroids of MCF10A cells written in the granular gel are viable. Sacrificial agarose templating was used to fabricate mesoscale branching networks. These agarose fibers could be readily removed under light vacuum to get channels 0.25–1 mm in diameter (Figure 12i). Improved oxygen and nutrient transport in gels within the channels result in higher viability and alkaline expression of MC3T3 cells than in block gels.[179] A further improvement was made by the microscale continuous optical printing of 3D blood vessel models (Figure 12j). The 3D-printed vessels (4 × 5 mm and 6 μm thick) grew into tissue after in vitro cultivation and were then implanted into mice through wounds in the skin. The implanted

© 2018 WILEY-VCH Verlag GmbH & Co. KGaA, Weinheim

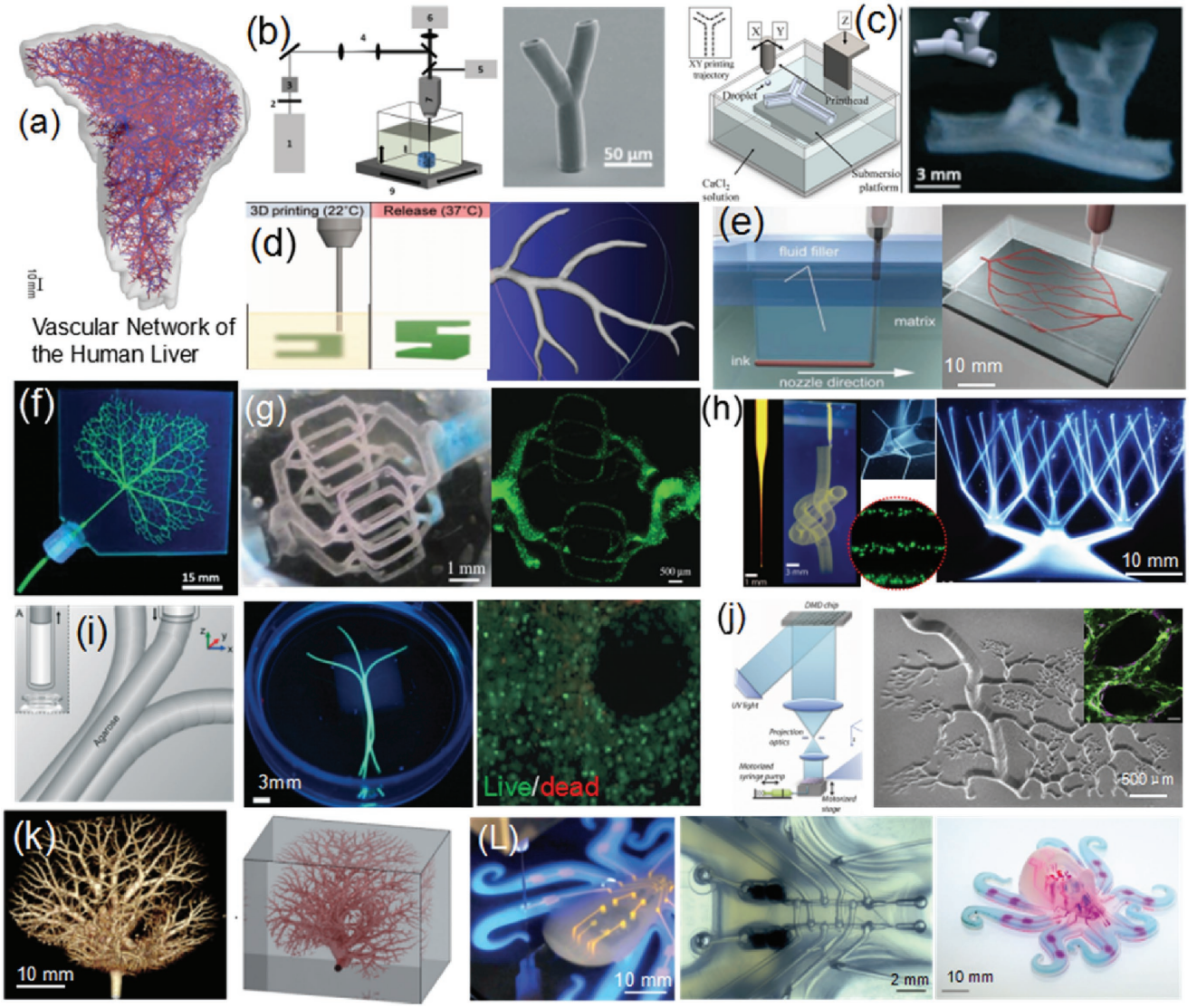

Figure 12. Bioinspired 3D printing of microfluidic structures. a) Vascular networks in human liver. Reproduced with permission.[171] Copyright 2015, PLoS Publishing. b) A multiphoton variant of SLA was used to create exceptionally high resolution bifurcating fluidic channels. Reproduced with permission.[172] Copyright 2012, Multidisciplinary Digital Publishing Institute. c) Inkjet deposition of alginate into a calcium chloride bath allowed horizontal (left) and horizontal/vertical (right) branching freestanding fluidic channels. Reproduced with permission.[173] Copyright 2015, Wiley-VCH. d) FRESH printing was used to deposit alginate into a gelatin slurry to form the architecture of the human right coronary arterial tree. Reproduced with permission.[174] Copyright 2015, American Association for the Advancement of Science. e) Schematics of omnidirectional printing of 3D microvascular networks within a hydrogel reservoir. Reproduced with permission.[175] Copyright 2011, Wiley-VCH. f) 3D-printed network to mimic the leaf venation pattern of an English ivy plant. Reproduced with permission.[176] Copyright 2010, Royal Society of Chemistry. g) 3D printing of a hydrogel channel and cell in the channel. Reproduced with permission.[177] Copyright 2017, The Royal Society Publishing. h) 3D-printed hierarchically branched tubular networks. Reproduced with permission.[178] Copyright 2015, American Association for the Advancement of Science. i) Photographs of the bioprinted templates (green) enclosed in GelMA hydrogels and viability and differentiation of MC3T3 cells. Reproduced with permission.[179] Copyright 2014, Royal Society of Chemistry. j) 3D-printed bioinspired vascular networks and endothelial network formation after one-week culture of the prevascularized tissue construct in vitro. Reproduced with permission.[180] Copyright 2017, Elsevier. k) 3D-printed vascular architecture in hydrogel by merging current anatomical mapping technologies with 3D printing. Reproduced with permission.[181] Copyright 2014, PLoS Publishing. l) 3D-printed fully soft, autonomous robot assembly with microfluidic soft controller. Reproduced with permission.[182] Copyright 2016, Nature Publishing Group.

vessels had successfully merged with the existing blood vessel network and were circulating blood. The limitation is that they are not yet capable of transporting nutrients or waste.[180]

Besides the mimicry of blood vessels to transport nutrition, a microfluidic logic circuit was recently developed for the 3D printing of octopus robot. The octobot is powered by a chemical reaction that transforms hydrogen peroxide into a large amount of gas. The gas controlled by an electronic oscillator flows into the octobot's arms (through microfluidic channels) and inflates them like a balloon (Figure 12L).[182] The 3D-printed soft robots have advantages over hard robots for their flexibility and capability of safely interacting with humans. This research

© 2018 WILEY-VCH Verlag GmbH & Co. KGaA, Weinheim

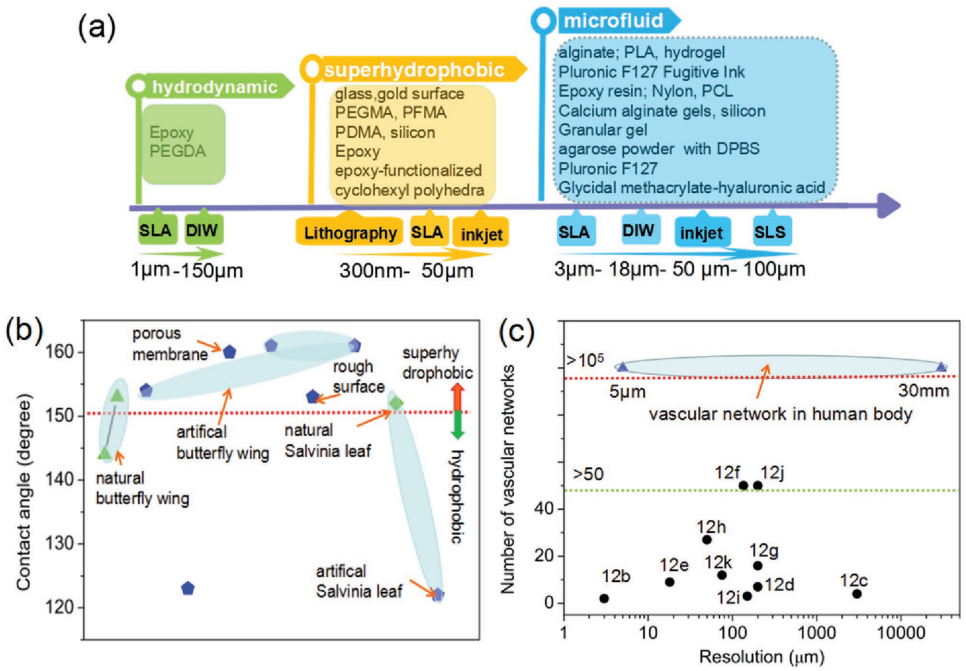

Figure 13. a) Schematic diagram showing the 3D-printing methods and materials as well as the printing resolutions used in hydrodynamic, superhydrophobic, and microfluid structures. b) Comparison of contact angle of natural and 3D-printing structures. c) Comparison of number of vascular networks and resolution of 3D-printed microfluidic devices with the human body.

enables the programmable assembly of multimaterials and provides the foundation for autonomous soft robots fabrication.

4.4. Discussion

The 3D-printing materials and processes that were used to fabricate the aforementioned bioinspired interface structures are listed in **Figure 13**a, and the comparisons of 3D-printed structures with related natural structures are shown in Figure 13b,c. For the bioinspired 3D printing of superhydrophobic surface, the challenge lies in the fabrication of complex multiscale structures that may have microscale, mesoscale, and macroscale features. In addition, potential applications of superhydrophobic surfaces including drag force reduction, droplet manipulation, and oil/water separation need to be further studied. For the bioinspired 3D-printing microfluid devices, recent study has demonstrated the development of 3D-printed vascular networks to achieve basic functions. However, there is still a long way to go for the engineered tissues with vascular networks to recapitulate the functions of the native counterparts (Figure 13c). The design of materials (biomaterials) and architectures (multiscales) that are mechanically strong and biologically compatible is important to enable the engineered organs to be fully functional within body.

5. 3D Printing of Bioinspired Optical Devices

The natural optical structures are composed of a myriad of scales ranging from nanoscale to macroscale. They have evolved to display, produce, reflect, absorb, and manipulate light,[183] which provide us inspirations for designing functional optical devices and systems for various applications.[184] For instance, the brilliant iridescent colors of butterfly's wings are generated by multiscale photonic structures that can minimize internal reflections of light and at the same time maximize the emitted light intensity (**Figure 14**a).[185–187] Magnetophotonic crystals that could reflect iridescent visible light can be reproduced from *Morpho* butterfly wings using reduction fabrication process.[38,188] Additionally, the complex compound eyes have been evolved to get better capability of detecting edges and forming images[189] (Figure 14b). Such an eye design gives an inspiration for the design and fabrication of an artificial receptor matrix containing a microlens array and a pinhole array in the focal plane.[190] Inspired by microscale hemisphere arrays of brittle stars, biomimetic porous lens arrays with tunable light transmission were designed for the desired optical properties[191] (Figure 14c). Using the three-beam interference lithography, the fabricated porous lens arrays can control the transportation of light-absorbing liquid in the channels between lenses.[192,193] Similarly, inspired by the hierarchical nanostructures of fireflies[184] (Figure 14d), the organic OLEDs with highly efficient light extraction and wide-angle illumination were developed.[194,195] Therefore, understanding the natural optical structures and replicating their mechanisms in engineered optical structures and systems have become increasingly important. Recent advances in 3D-printing technology and optical materials have the potential to enable the fabrication of nano/microscale optical structures with complex shapes for designed optical systems.[193,196]

5.1. Material Development for 3D-Printing Optics

The material selection of complex optical systems mainly depends on the application requirements.[196] Specifically, the

© 2018 WILEY-VCH Verlag GmbH & Co. KGaA, Weinheim

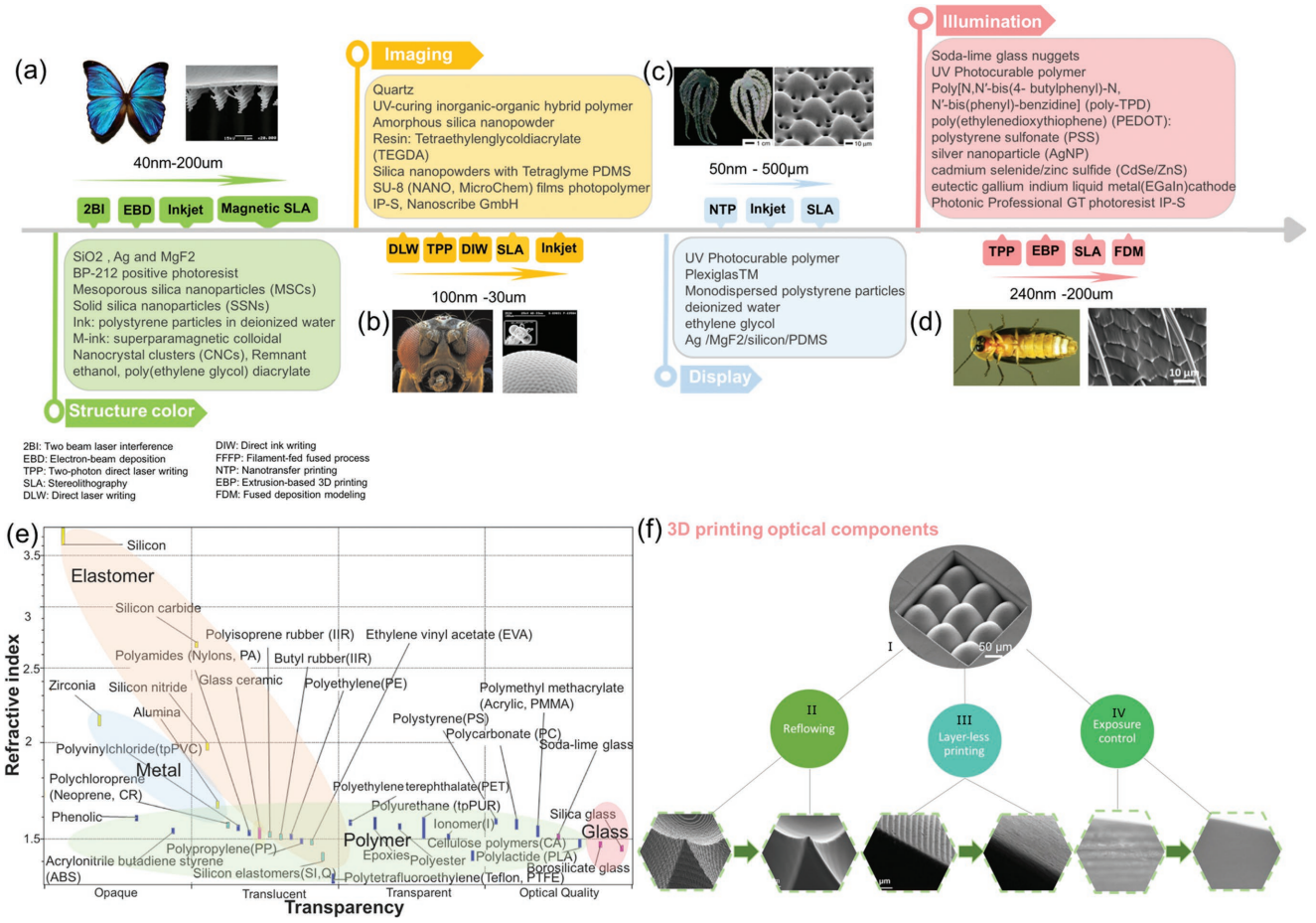

Figure 14. 3D printing of bioinspired optical devices. a) The iridescence of the *Morpho rhetenor* butterfly comes from a microscopic array. Reproduced with permission.[183] Copyright 2012, Royal Society of Chemistry. b) Natural apposition compound eye. Head of the fruit fly "*Drosophila melanogaster*" and scanning electron microscopy (SEM) image of the head and eye section of the moth "*Ephestia kuehniella*." Reproduced with permission.[184] Copyright 2015, CRC Press. c) Light-sensitive species *Ophiocoma wendtii* changes color markedly from day (left) to night (right) and SEM of the peripheral layer of a DAP from *O. wendtii*. Reproduced with permission.[191] Copyright 2001, Macmillan. d) An optical image of a male firefly (*Pyrocoelia rufa*) and asymmetric microstructures on the lantern cuticle of a male firefly. Reproduced with permission.[195] Copyright 2012, Sherpa RoMEO. e) Ashby plot for material selection with different requirements of refractive index and transparency. f) Current 3D-printing processes to achieve smooth surface quality. I) Reproduced with permission.[197] Copyright 2017, SPIE. II) Reflowing: Reproduced with permission.[197] Copyright 2017, SPIE. III) Layerless printing: Reproduced with permission.[198] Copyright 2015, American Association for the Advancement of Science. IV) Exposure control: Reproduced with permission.[199] Copyright 2012, Elsevier.

optical properties mainly include refractive index, abbe value, reflectivity, and transparency. Generally, most biological multifunctional optical structures are transmissive to light and the transmission effect varies over the spectral region from UV to infrared (IR). Based on these requirements, the optical materials mainly consist of glass, optical crystal, plastics, and semiconductor materials (Figure 14e). Recently optical plastics are becoming readily available but the shape complexity of optical devices is still limited by the traditional molding process. By taking advantages of 3D printing, the fabrication of optical components with complex bionic 3D geometric shapes can become reality. For example, polycarbonates, acrylics, and polystyrenes will be cross-linked and solidified with sufficient energy under high temperature or light exposure using 3D-printing methods.[190,196,200] Even optical crystal and semiconductor materials have been successfully fabricated by various 3D-printing processes.[194,195]

Compared with polymers, glass plays a critical role in optical applications because of its high transmission as well as strong mechanical properties. However, glass is notoriously difficult to shape, which requires high-temperature melting for fabricating macroscopic objects or hazardous chemicals for microscopic features.[201] Nowadays, a lot of researchers put efforts on developing 3D printing of glass and two categories of novel processes have been developed including direct printing and indirect printing. In the direct printing, the silicon glass is directly accumulated to form 3D geometric shape under high temperature by using direct spark, high-speed electron beam and laser (**Figure 15**b).[201–206] For example, the filament-fed laser-heated process was developed to fabricate transparent glass (Figure 15a).[202,203] The FDM process can also be modified to print transparent or even colored glass using heating elements with a temperature of 1010 °C (Figure 15c).[201,204] However, these processes are limited by the nonperfect surface

© 2018 WILEY-VCH Verlag GmbH & Co. KGaA, Weinheim

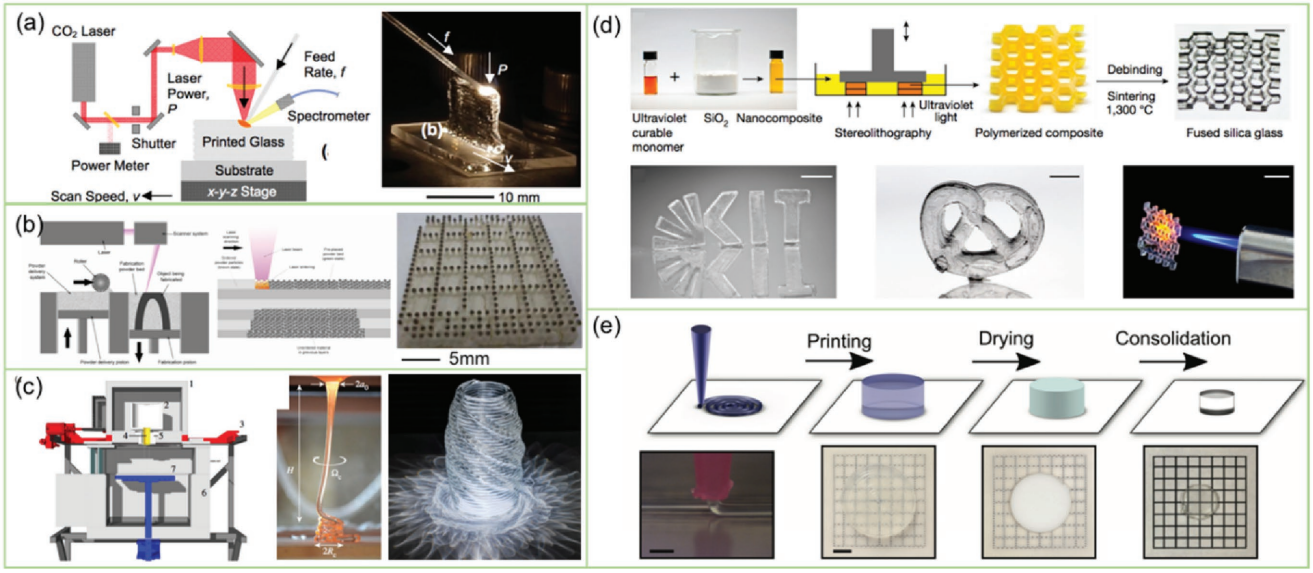

Figure 15. Design and fabrication of transparent glass by 3D printing. a) The illustration and physical model of filament-fed fused quartz process. Reproduced with permission.[202] Copyright 2016, SPIE. b) The layout of selective laser melting process for glass fabrication. Reproduced with permission.[205] Copyright 2014, Elsevier. c) The schematic view of molten glass sewing machine and caustic patterns created by illumination from an overhead LED. Reproduced with permission.[204] Copyright 2016, Royal Society. d) 3D printing of fused silica glass using a stereolithography system with mixture of ultraviolet-curable polymer and amorphous silica nanopowder. Reproduced with permission.[208] Copyright 2017, Macmillan. e) Direct ink writing of glass and the silica powder is fastened at high temperature to generate a transparent 3D-printed glass part. Reproduced with permission.[209] Copyright 2017, Wiley-VCH.

quality and insufficient heating for precise optical applications. To address this problem, in the indirect printing, the green part is first created using binder/ silicon particles composites by 3D printing and then postprocessed to remove the polymer binder and sinter the silicon particles[207–209] (Figure 15e). Currently, shrinkage behavior (27.88%) in the postprocessing step shows significant influence on 3D-printed structures due to the debinding and sintering process to remove the apparent porosity and to increase bulk density (Figure 15d).[208] The 3D-printed glass shows the same transparency in the ultraviolet, visible, and infrared parts of spectrum as commercial fused silica glass. Due to the advance in multimaterial fabrication, the gradient-composition glass structures with tunable optical and mechanical properties can also be fabricated using the inkjet-based 3D-printing method.[209] Overall, these 3D-printing processes enable the mold-free formation of transparent glass structures, which can widen the optical applications in future.

5.2. Recent Process Developments in 3D-Printing Optics

To create prototype of optical lenses and devices, traditional fabrication methods are limited by their high cost, time-consuming, and difficulties in modifying designs. Besides, the postprocessing steps such as sanding, polishing, bead blasting, or vapor smoothing may change the structural details or the overall shape, especially for microscale complex optical structures.[184,197] 3D printing may provide breakthroughs for the fabrication of smooth optical surfaces (Figure 14f). For example, a postcuring method was developed by curing the residual material on the surface to eliminate the layer staircase effects.[197] Similarly, smooth surface quality can be achieved using dual exposures by curing the residual resin between neighboring layers.[199,210,211] Furthermore, 3D objects can be directly printed without the layer staircase effect by the continuous liquid interface projection (CLIP) method, which could lead to other novel 3D-printing processes for optics.[198] The fabrication of microlens using 3D printing could be difficult since the required quality and error control are difficult to achieve in the printing process. To address the problem, research on adjusting the light intensity of each pixel in a mask image to accurately control the height of cured material has been developed.[212] The quality of the 3D-printed microlens can be monitored by a feedback control system during the printing process.[212,213]

5.3. 3D-Printed Bioinspired Optical Structures

Biological solutions in nature present inspiration and design principles for the construction of multifunctional artificial optical devices and systems with multiscale structures. The fabrication of such bioinspired optical structures can be enabled by the multiscale 3D-printing processes. In the following sections, recent 3D-printing methods that were developed in different size scales for building various bioinspired optical structures are discussed.

5.3.1. Macroscale Biomimetic Optical Structures

Inspired by the illumination function of firefly, researchers developed semiconducting quantum-dot-based light-emitting diodes (QD-LEDs) that exhibit pure and tunable color emission

© 2018 WILEY-VCH Verlag GmbH & Co. KGaA, Weinheim

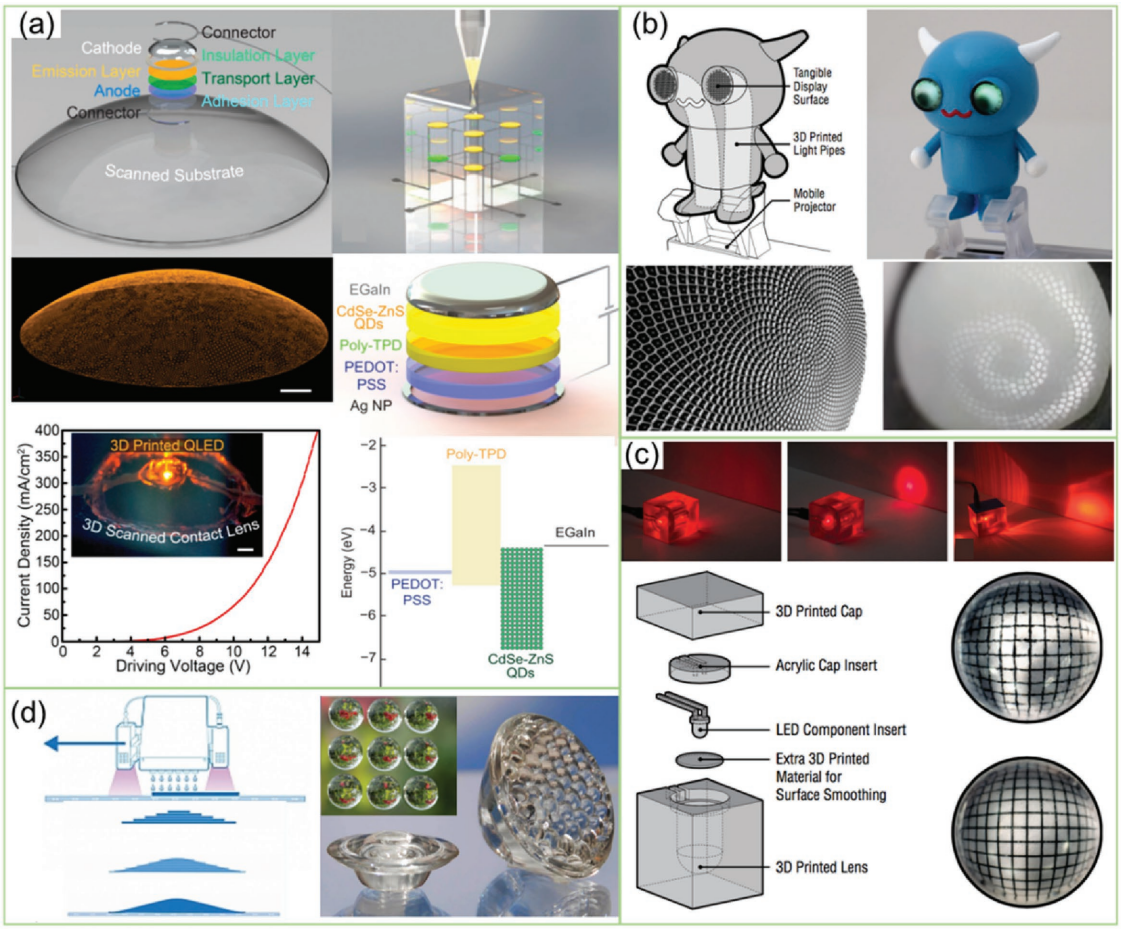

Figure 16. Design and fabrication of biological macroscale optical structures by 3D printing. a) Bionic QD-LED design and 3D-printed QD-LEDs on a 3D-scanned curvilinear substrate. Reproduced with permission.[214] Copyright 2014, American Chemical Society. b) 3D-printed artificial display eye of interaction character. Reproduced with permission.[215] Copyright 2013, ACM. c) Design and 3D-printed optical elements including concave and convex lens and beamsplitter. Reproduced with permission.[200] Copyright 2012, ACM. d) Optical lens array with smooth surface fabricated by new developed 3D-printing method. Reproduced with permission.[216] Copyright 2013, Luxexcel.

properties by using the multimaterial extrusion-based 3D-printing process (**Figure 16**a).[214] Benefits from the multimaterial 3D-printing process include fabricating electrodes, semiconductors, and polymers in the same process for desired functionalities. The printed OD-LEDs in different spectrum ranging from UV to IR show better brightness compared with the traditional commercial LED. Furthermore, multidimensional electronic arrays of interconnected QD-LEDS were printed onto curvilinear surface contact lens by incorporating the 3D scanning of surface topology. Inspired by the functions of eyes such as light detection, shape distinguishing, and image focusing,[189] researchers from Disney designed the optical devices comprised of a bundle of optical fibers for the projection of images with designed shapes (Figure 16b). A fiber-arranged algorithm inspired by classic Fibonacci spirals of sunflower is applied to avoid image distortion.[215] Based on the design of artificial eyes, the touching sensor and interactive characters are further developed. Other optical components including plano-concave lens, plano-convex lens, and beamsplitter can also be fabricated by the same inkjet process as shown in Figure 16c.[200] These designed optical components are fabricated by the layer-based commercial 3D printer (Objet Eden260V) using transparent photopolymers (plexiglas) with a translucent support material. However, the surface quality, material transparency, and fabrication resolution still need to be improved for practical applications. To fabricate smooth optical structures, Luxexcel group invented a novel 3D-printing process based on the inkjet printing method to prototype and manufacture functional optics (Figure 16d). By controlling the interval time between droplet jetting and UV light exposure, each droplet of UV-curable polymer can flow to smooth surface along the printed structure rather than a single spherical shape.[216] Transparent prisms or lenses and freeform shapes with full color 3D graphics and textures can be printed with good surface quality using such technology. Macroscale biologically designed optical components fabricated by 3D printing will play an important role in future interactive device especially if the optical and structural components can be printed in the same process rather than being assembled together manually.

© 2018 WILEY-VCH Verlag GmbH & Co. KGaA, Weinheim

5.3.2. Micro- and Nanoscale Biomimetic Optical Structures

Micro- and nanoscale features exist in most of the functional optical systems in nature such as fly eyes and butterfly wings. Currently, these optical structures are fabricated using microjet fabrication, ultraviolet molding, photoresist, hot embossing, and electron-beam lithography.[217,218] Most of these fabrication methods have limited capability in meeting the requirements of biomimetic optical designs. In comparison, 3D printing provides a potential method to address the fabrication challenge. For example, inspired by the fly eyes in nature, a microscale artificial compound eye that is distortion-free with wide field view was developed by the high-speed voxel-modulation laser scanning (HVLS) (**Figure 17**a).[217] Compared with the laser direct writing process with single voxel, HVLS is proposed to improve fabrication efficiency dramatically by selecting appropriate voxel dimension based on the fabrication part size. The 3D-printed hexagonal-shaped artificial eye structures achieved fully fill factor, large numerical aperture, and high uniform optical distribution in all directions, which significantly reduce the image distortion compared with the traditional single lens. Similarly, by mimicking the eagle eyes, a microscale camera was designed and constructed by directly printing multiple bionic objectives lens onto a complementary metal-oxide semiconductor (CMOS) image sensor.[216] A full field view of 70° with angular resolution up to two cycles per degree in the center of the image can be achieved by this artificial optical system, which consists of four such printed doublet lenses with different focal lengths (Figure 17b).[218] Similar micro- and nanoscale optics with complex artificial eye lens were fabricated by the femtosecond two-photon direct laser writing process. The 3D-printed multilens achieves high optical performance with the field view of 80°. Even triplet objective lens can be fabricated on the optical fiber or CMOS image sensor, which may have wide applications in cell biology, autonomous vision, and illumination

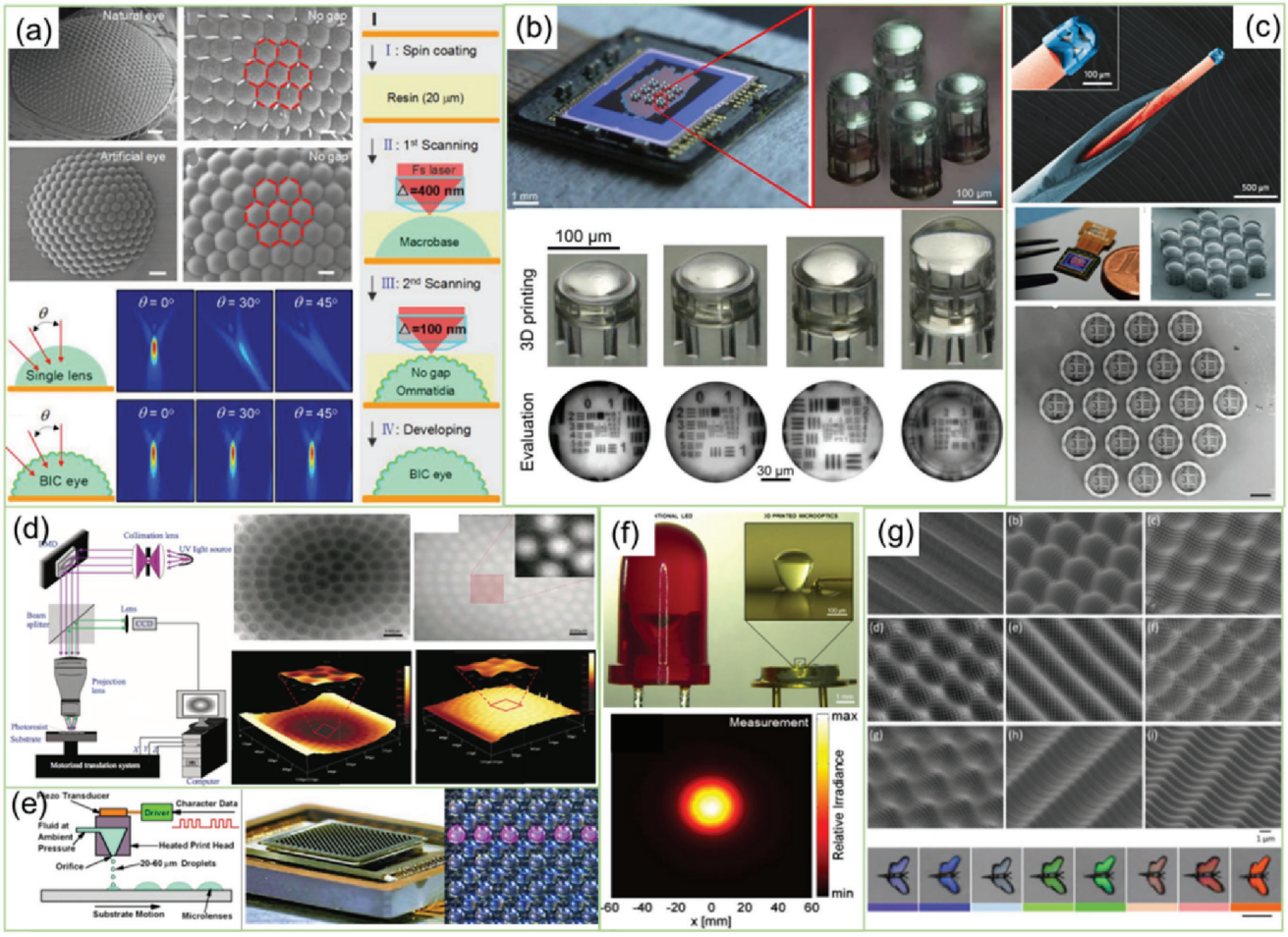

Figure 17. Design and fabrication of biological micro- and nanoscale optical structures by 3D printing. a) High-quality 3D artificial compound eyes printed by voxel-modulation femtosecond laser writing. Reproduced with permission.[217] Copyright 2014, Wiley-VCH. b) 3D-printed eagle eye: compound microlens system for foveated imaging. Reproduced with permission.[218] Copyright 2017, American Association for the Advancement of Science. c) Colored SEM image of a triplet lens objective attached to an optical fiber inserted into the hollow needle of a syringe. Natural compound eye and high-quality BIC eye prepared by the high-speed voxel-modulation laser scanning method. Reproduced with permission.[219] Copyright 2016, Macmillan. d) Curved microlens array fabricated by DMD-based digital maskless lithography. Reproduced with permission.[220] Copyright 2017, IOP. e) Microlens array in smart-pixel array module. Reproduced with permission.[221] Copyright 2001, Optical Society of America. f) Ultracompact on-chip LED collimation optics by 3D femtosecond direct laser writing. Reproduced with permission.[222] Copyright 2016, Optical Society of America. g) Angle-multiplexed optical printing of biomimetic butterfly hierarchical 3D textures. Reproduced with permission.[163] Copyright 2017, Wiley-VCH.

© 2018 WILEY-VCH Verlag GmbH & Co. KGaA, Weinheim

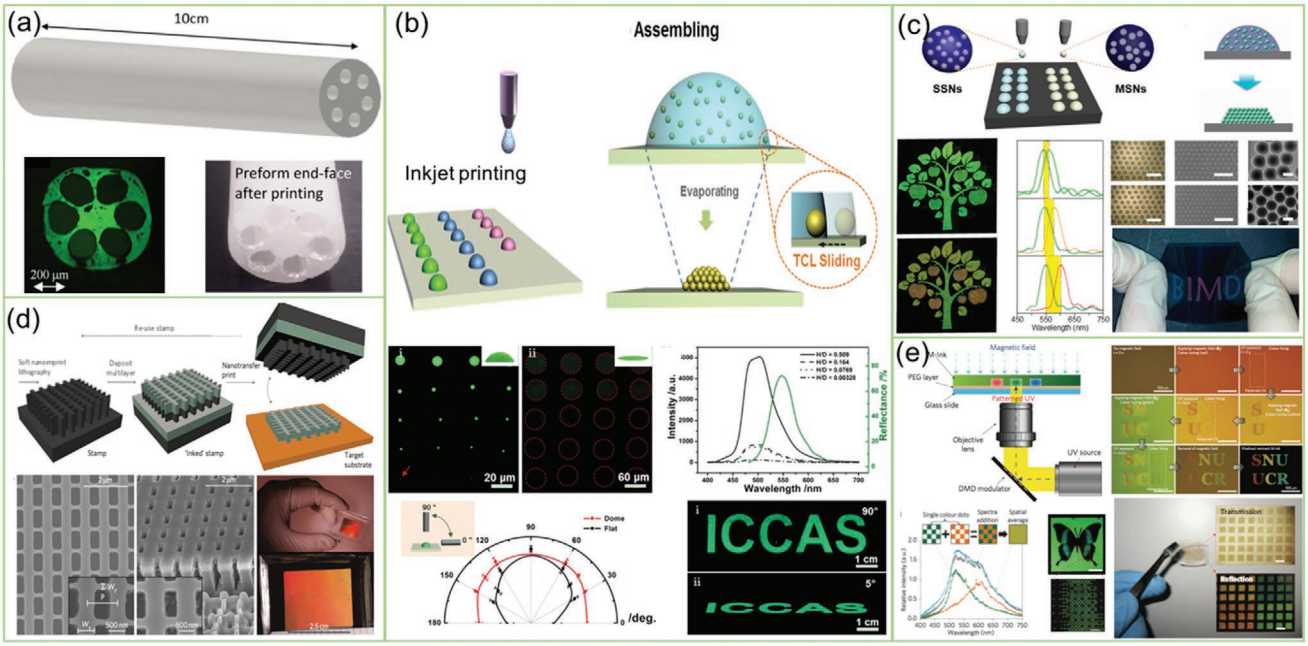

Figure 18. 3D-printed bioinspired multiscale optical structures. a) 3D optical fiber with multiscale features by printed FDM process. Reproduced with permission.[225] Copyright 2015, Optical Society of America. b) Wide viewing angle display was constructed by patterned photonic crystal domes which is fabricated by inkjet printing with three-phase contact line sliding. Reproduced with permission.[226] Copyright 2013, Wiley-VCH. c) Bioinspired vapor-responsive colloidal photonic crystal patterns by inkjet printing. Reproduced with permission.[223] Copyright 2014, American Chemical Society. d) Nanotransfer-printed large-area flexible 3D optical negative index metamaterial inspired by multiscale structures of butterfly wings. Reproduced with permission.[227] Copyright 2011, Macmillan. e) High-resolution multiple structural color inspired by creatures in nature was printed by lithography under magnetic field using single material with photonic crystal. Reproduced with permission.[228] Copyright 2009, Macmillan.

systems (Figure 17c).[219] Microlens array can be printed by the DMD-based digital maskless stereolithography and the shape of microlens can be controlled precisely by double gray-scale masks[220] (Figure 17d). Adjusting the shape of liquid droplet with piezo transducer, several hundred micrometer diameter microdevices can be fabricated by the inkjet printing method[221] (Figure 17e). Dielectric concentrator with dimension smaller than 200 μm can be directly manufactured on an LED chip. Based on it, the light output can be increased by a factor of 6.2 in collimation direction with 50% reduction of half-angle emission (Figure 17f).[222] Based on the optical performance of bionic lens, nonconventional triangular illumination patterns were designed and printed to manipulate high-quality miniature illumination. Inspired by the hierarchical structures of butterfly, hierarchical patterns in a large-scale area were fabricated by the two-beam interference lithography process with angle-multiplexed exposures and scanning. The developed fabrication process has a capability to build complex 3D hierarchical textured surfaces with the height dimension ranging from 0.9 μm down to 40 nm by precisely controlling the exposure rate. Several natural phenomena including iridescence, directionality of reflectivity, and polarization at different colors have been demonstrated with such 3D-printed biomimetic optical structures (Figure 17g).[163]

5.3.3. Multiscale Biomimetic Optical Structures

Multiscale 3D-printing technology provides a potential solution to the needs of reproducing bioinspired multiscale optical structures. Several processes were developed to achieve multiscale fabrication with two development trends. Combining multiple manufacturing processes was developed as an intuitive way to fabricated objects with features ranging from macroscale to nanoscale.[224] To simplify the fabrication process, multiscale structures were also fabricated by a single 3D-printing process. For example, optical fiber inspired by lotus root with a macroscale solid core surrounded by microscale air holes is fabricated by FDM process using transparent thermosetting polymer (**Figure 18**a).[225] Patterned photonic crystal (PC) domes with angle-independent photonic bandgaps were fabricated by the inkjet printing process. As the solvent evaporates, all particles move inward and assemble into high H/D PC domes on an octadecyltrichlorosilane-treated substrate by the three-phase contact line sliding process (Figure 18b). Using this method the PC domes can be arranged with designed pattern, which can enhance brightness 40 times compared with the traditional method. The molecules viewing angle can also be waded from 0° to 180°.[226] Multicolor shifting properties were also achieved by multiscale colloidal photonic crystals patterns fabricated by the inkjet printing process with mesoporous colloidal nanoparticle ink. The original color and vapor-responsive color shifting extent can be precisely controlled by adjusting the size and mesoporous proportion of nanoparticles (Figure 18c).[223] This fabrication method provides a great promise for developing advanced optical components such as dynamic display and multifunctional sensor array. Inspired by the structured color from periodic nanostructures in nature, multiscale large-area negative index metamaterials with 3D multilayer formats

© 2018 WILEY-VCH Verlag GmbH & Co. KGaA, Weinheim

were fabricated by the transfer printing process (Figure 18d).[227] This structure exhibits a strong, negative index of refraction in the near-infrared spectral range. Artificial high-resolution patterning of multiple structural colors can also be fabricated by the highly efficient maskless lithography process. The color can be tunable by magnetically changing the periodicity of the nanostructure fixed by photochemically immobilizing those structures in a polymer network (Figure 18e).[228] Overall, the combination of optical materials with smart materials using 3D printing and other advanced manufacturing methods will play an important role in the realization of multiscale bionic optical devices in future.

5.4. Discussion

Nature provides incredible inspirations for the design and manufacturing of optical structures with diverse applications. Some studied examples include structural color of butterfly for display, compound eye for imaging system, and firefly for illumination.[185,190,194] Compared with the traditional fabrication methods, 3D-printing technology provides benefits in fabricating multiscale and multimaterials bioinspired optical structures. Currently, even though defects such as the layer staircase effects and limited material options exist in most 3D-printing processes, further development of 3D-printing technology in order to fabricate bioinspired optical structures is still attractive due to its unique capability on shape and material control. Furthermore, some multiscale 3D-printing methods such as CLIP,[198] multimaterial inkjet printing,[223,226] feedback-controlled micro-stereolithography,[213] and 3D femtosecond directly laser writing[217,219,222] have been developed to enhance the capability of 3D-printing processes to fabricate more complicated bioinspired optical structures. In addition to the further development of 3D-printing technology, the hybrid fabrication processes by integrating 3D printing with other traditional fabrication technologies can be explored as a promising direction to build bioinspired optical structures for applications such as intelligent soft sensors, medical devices, and microoptical imaging systems.

6. 3D Printing of Bioinspired Electrical Devices

Living organism is structurally isolated from environment by some coverings such as a shell, a skin, or a membrane. This covering not only protects the organism from the threats but also helps it adapt to the environment. For instance, human skin with an integrated, stretchable network of sensors that are linked to brain is an irreplaceable organ. It allows body to effortlessly distinguish between pressure, pain, warm, and cold stimuli. Recreating the properties of this covering by using electronic devices has profound effect on medicine, intelligent robot, and prosthetics.[229–231] In order to build mechanically compliant and multifunctional biomimetic devices, new materials and fabrication methods are constantly being developed to address the challenges.[232,233] Among them, 3D printing has noticeable advantages on fabricating complex geometry and integrating multiple materials.[234] The section will review some recent 3D-printing developments for realizing efficient electronic devices to sense and generate biomimetic signals.

6.1. Composites and Printing Requirements

Typical 3D-printing materials for bioinspired electrical devices comprise fillers, binders, solvents, and additives.[233,235] The selection of these composites is ultimately depends on the design requirements of electronic devices and the type of 3D-printing processes to be used. The fillers are a key in 3D-printing materials, which could be organic, metallic, ceramic, or combinations of thereof.[236–239] The binder helps the homogeneous dispersion of fillers as well as binding the fillers together. Solvent provides good solubility, favorable viscosity, surface tension, and homogeneity. Additives in the form of surfactants, stabilizers, adhesion improvers, humectants, and penetration promoters are included in the 3D-printing materials to impart desired rheological, wetting, healing, or stretching properties to enable a specific 3D-printing process. Apart from these, elastomer such as silicone and PDMS is also widely used as the base or package materials for electrical devices.[240]

The 3D-printing techniques for these multifunctional composites comprise primarily inkjet printing, fused deposited modeling, stereolithography-based printing, and direct laser writing.[235,241–244] The inkjet printing process relies on localized and controlled ink dispensing onto the substrate, which can fabricate electronic sensor with a wide variety of materials including metal, organic, ceramic, and colloid. However, limited by the nozzle size, the resolution of this method is usually larger than 30 μm.[238] The stereolithography-based 3D printing and the direct laser writing processes are widely used for much smaller resolution that could go down to 200 nm.[242] However, the polymerization property of the used materials and the small part size that can be printed limit the applications of these fabrication methods. Therefore, the selection of 3D-printing techniques largely depends on the type of materials and the scale of electronic device, which are discussed in more detail in the following sections.

6.2. Filler Materials

As a key in 3D-printing materials, various fillers have been investigated for the fabrication of biomimetic electrical device to mimic the organism's sensory receptor. These fillers include conductive, piezoelectric, and materials with other properties.

6.2.1. Conductive Materials

The sensory receptors in skin detect a wide range of sensations, including static pressure and strain, vibration, temperature, and humidity. Conductive materials such as ionic salt, metal particle, liquid metal, and carbons are widely used to mimic the performance of these receptors due to their resistance and capacity changes under certain stimuli. **Figure 19** shows some 3D-printed biomimetic electrical devices with conductive materials and the

© 2018 WILEY-VCH Verlag GmbH & Co. KGaA, Weinheim

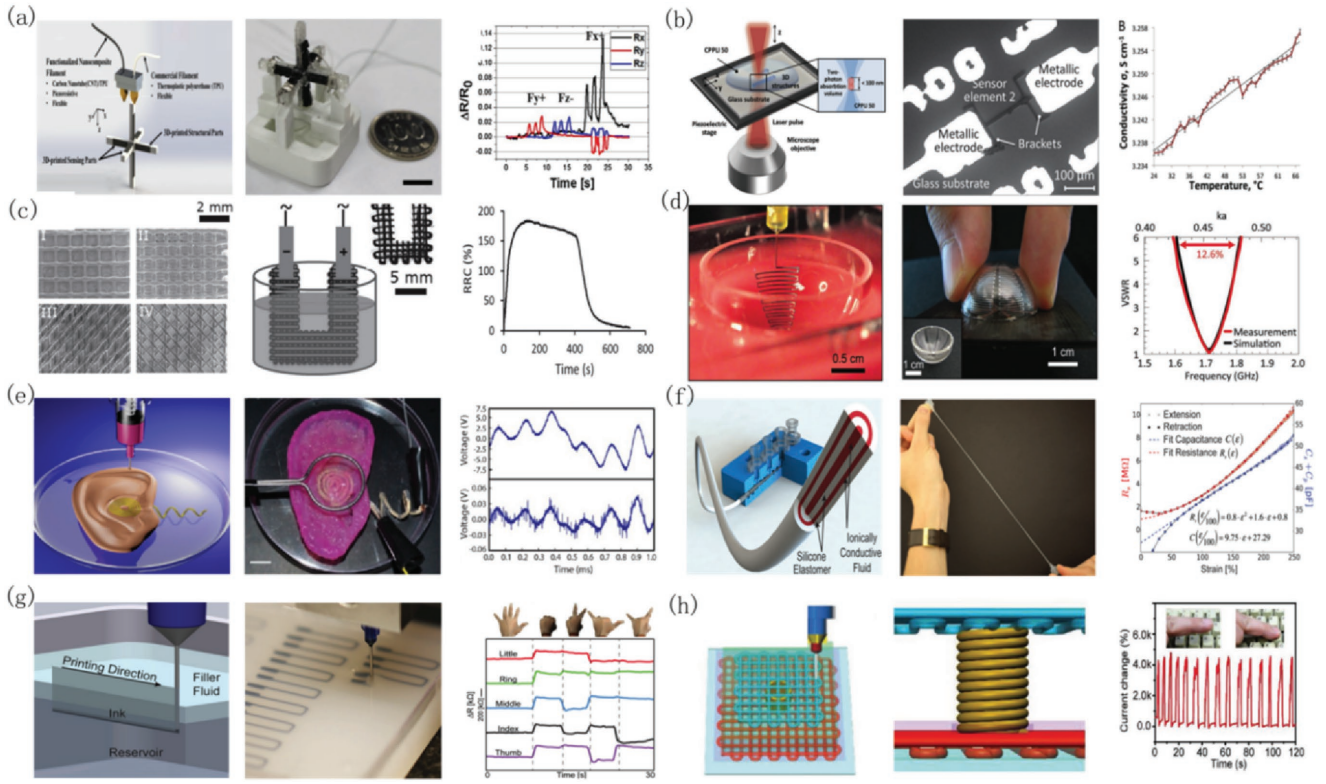

Figure 19. 3D printing of bioinspired electrical devices. a) Schematic of printing process (left). Optical image of tactile sensor with 10 mm scale bar (middle). Relative resistance change responds to pressure in different directions (right). Reproduced with permission.[254] Copyright 2017, Elsevier. b) Schematic of printing process (left). HRSEM image of sensor element (middle). Conductivity change in response to temperature (right). Reproduced with permission.[242] Copyright 2015, Wiley-VCH. c) SEM images of sensor printed in four layers with different patterns (left). Schematic showing liquid sensitivity testing of liquid sensor (middle). A typical liquid sensitivity test graph showing the increase and decrease of the RRC of a liquid sensor while immersion/drying cycles (right). Reproduced with permission.[257] Copyright 2016, Wiley-VCH. d) Optical image of an antenna being printed onto the interior surface of a glass substrate embedded in a PDMS mold (left), and optical images of this antenna before (inset) and after connecting to the feedlines (middle). Measured and simulated voltage standing wave ratio versus frequency response (right). Reproduced with permission.[256] Copyright 2011, Wiley-VCH. e) Illustration of the 3D-printed bionic ear (left). Electrical characterization of the bionic ear (middle). Transmitted (top) and received (bottom) audio signals of bionic ears (right). Reproduced with permission.[255] Copyright 2013, American Chemical Society. f) Schematic of printing process (left), linear sensors strained to 150% strain (middle), and model predictions, sensor resistance, and total capacitance of the sensor up to 250% strain (right). Reproduced with permission.[252] Copyright 2015, Wiley-VCH. g) Schematic of printing process (left), optical image of sensors with hairpin corner shape (middle), and electrical resistance change as a function of time for strain sensors within the glove at five different hand positions (right). Reproduced with permission.[253] Copyright 2014, Wiley-VCH. h) Schematic of printing process (left), optical image of helicoidal sensor (middle), and current change signals in response to dynamic loading and unloading cycles in pressing (right). Reproduced with permission.[236] Copyright 2017, Wiley-VCH.

corresponding relative resistance and capacity change.[245–253] A novel carbon nanotube/thermoplastic polyurethane filament was developed and used to manufacture 3D electronics using the fused deposition modeling process (Figure 19a).[254] The developed electronic sensors display a change in resistance under external force. Conductive hydrogel with lithium chloride was applied in a transparent resistive strain sensor. The 3D-printing process was performed by an extrusion-based 3D printer. A UV curing was used to solidify the extruded ink and prevent its extensive spreading. The capability of corresponding sensor was sensitive enough to detect inadvertent finger motions.[235] Liquid–polymer composites with ionic salt were fabricated by the direct laser writing lithography process to measure the temperature and relative humidity through the change of conductivity (resistance). Higher temperatures lead to higher mobility and result in the increase of conductivity. Conductivity also varies with different humidity levels between 3% and 50% at a constant temperature of 23 °C (Figure 19b).[242] Metal particle such as silver nanoparticle also plays an important role in biomimetic electrical device. 3D tactile sensors made with silver/silicone inks were built using the inkjet printing process. The resistance of the device decreases 12-fold and the signal intensity increases with different finger pressures (Figure 19h).[236] These response signals prove the detection of differentiating human movements by 3D-printed sensors. Besides, 3D-printed antennas with metal particles have shown great potentials to transmit and receive signals, which can be used to mimic the auditory sense and olfaction (Figure 19d,e).[255,256]

6.2.2. Piezoelectric Materials

The fast adapting receptors of organism that can respond to dynamic force and vibrations are very important for texture

© 2018 WILEY-VCH Verlag GmbH & Co. KGaA, Weinheim

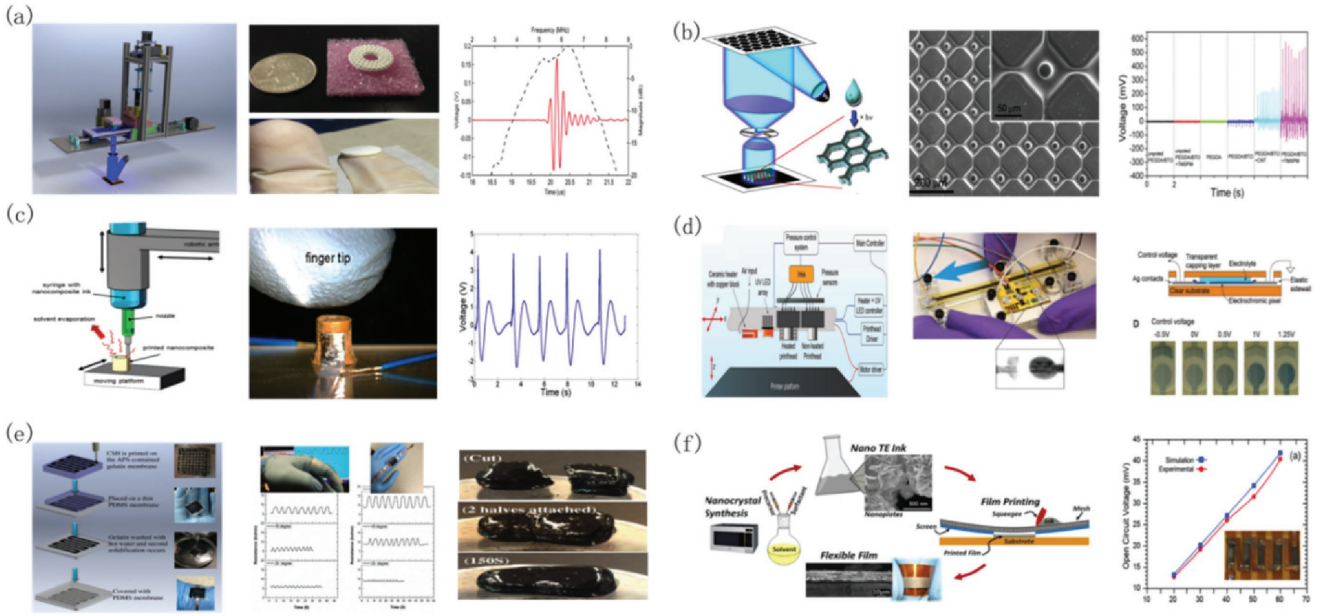

Figure 20. a) Schematic of printing process (left), optical image of the printed piezoelectric ceramic (middle), and output voltage and normalized spectrum (right). Reproduced with permission.[237] Copyright 2016, Elsevier. b) Schematic of printing process (left), optical image showing the printed 3D piezoelectric composite (middle), and voltage response of composite with cycling load (right). Reproduced with permission.[241] Copyright 2014, American Chemical Society. c) Schematic of printing process (left), optical image showing the printed piezoelectric sensor (middle), and voltage output upon consecutive finger taps (right). Reproduced with permission.[260] Copyright 2017, American Chemical Society. d) Schematic of printing process (left), optical image of autonomous sensory system (middle), and pixel change when the strain sensor is extended (right). Reproduced with permission.[238] Copyright 2017, Wiley-VCH. e) Schematic of printing process (left), resistance variation of the hydrogel strip (middle), and the hydrogel was cut into two halves and then brought together again (right). Reproduced with permission.[261] Copyright 2017, Wiley-VCH. f) Schematic illustration of screen printing of thermoelectric films on flexible substrate and sintered flexible films (left). Experimental and calculated open circuit voltage versus temperature differences (right). Reproduced with permission.[262] Copyright 2016, Nature Publishing Group.

discrimination and slip detection.[229] Piezoelectric has the ability to convert vibration, compressive/tensile stresses to the electric signal, which is well suited to mimic the performance of fast adapting receptors.[237,241] Piezoelectric polymers have mechanical flexibility, small active elements, and biocompatibility. Hence, they are suitable to be used to build biomimetic systems. Various poly(vinylidene fluoride) patterns designed for piezoelectric and pyroelectric responses were printed using the FDM process.[258,259] In addition, PVDF/$BaTiO_3$ nanoparticle composite was printed by the inkjet 3D-printing process to generate complex-shaped, flexible, and lightweight piezoelectric devices (**Figure 20**c).[260] These devices with PVDF can generate responses to dynamically varying forces and vibrations. Kim et al. embedded piezoelectric ceramic powder that was covalently grafted with linker molecule in a PEGDA matrix and used the stereolithography process to build piezoelectric devices. Using controlled exposure light, the carbon–carbon double bonds in photoinitiator are cross-linked to form the piezoelectric nanoparticles and polymer network. Compared to other composites, this 3D-printed device is flexible and provides a high piezoelectric constant (d_{33}) at 39 pC N^{-1} (Figure 20b).[241] In a further study, Chen et al. demonstrate a method to fabricate the piezoelectric ceramic using the mask-image-projection-based stereolithography technology. The high viscosity slurry was made by $BaTiO_3$ nanoparticle and photocurable resin. A piezoelectric array for self-focused ultrasonic transducer was obtained after post-processing to realize the energy focusing and ultrasonic sensing. The 3D-printed piezoelectric devices exhibit a piezoelectric constant and a relative permittivity of 160 pC N^{-1} and 1350, respectively (Figure 20a).[237]

6.2.3. Other Materials

Some creatures have the ability to change their shape and color to adapt to the environment and respond to threats. Insects such as Golden tortoise beetle change the transparency of its exoskeleton by special sensing and actuation mechanisms responding to the diverse stress. To mimic this behavior, an autonomous sensory system with PEDOT:PSS solvent inks was printed by an inkjet-based UV curing method. The transparency of PEDOT:PSS varies with the applied potential (Figure 20d).[238] Besides, additive manufacturing processes of thermoelectric materials and self-healing materials have also been studied (Figure 20e,f).[261,262] Such materials have the potential to mimic temperature sensory and human skin.

6.3. Discussions

Figure 21a shows the 3D-printing processes and related materials that can be used to fabricate biomimetic electrical devices. Biomimetic electrical devices can benefit from 3D-printing technology due to its capability of fabricating complex geometry

© 2018 WILEY-VCH Verlag GmbH & Co. KGaA, Weinheim

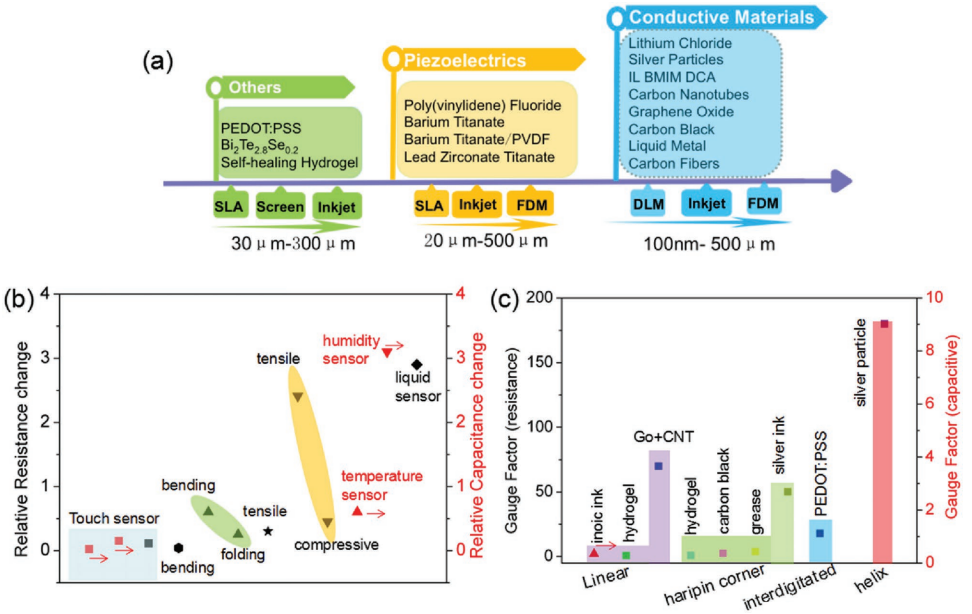

Figure 21. a) Representative filler materials that can be used for biomimetic device, b) some functions of printed device with conductive materials and the corresponding relative resistance and capacity change, and c) gauge factor with different materials and geometry.

to deliver customized shapes that maybe tailored to an individual's body. In addition to human skin, 3D printing may also enable the intimate integration of electronic devices with other substrates. The custom 3D tactile sensors on any freeform surface have great potential toward bionic skin applications.[236] Biomimetic electrical devices can also benefit from 3D printing due to its capability of integrating multiple materials by embedding multilayer electronic circuits within complex 3D structures. In addition to multimaterial printing, liquid-metal-based passive/active components and silicon-integrated circuits embedded within 3D-printed objects can also be used to expand the devices' capability to deliver various actuations, sensing, and signal processing.

The ability of 3D printing in fabricating complex geometry not only enables the variations of sizes and shapes, but also improves the performance of the 3D-printed biomimetic devices. For example, inspired by insect olfaction, 3D electrical antennas are fabricated by conformal printing of silver inks onto convex and concave hemispherical surfaces in the form of conductive meander lines. 3D antenna displays significant bandwidth improvements relative to their linear and planar counterparts.[255] Other examples include strain gauges that are widely used for sensory receptors in animals' skin. A fundamental parameter of the strain gauge is its sensitivity to strain, expressed quantitatively as the gauge factor (GF).[263] GF is the ratio of the fractional change in electrical resistance ($\Delta R/R_0$) or capacitance ($\Delta C/C_0$) to the fractional change in strain ε. Figure 21b,c shows the relative resistance and capacitance change of different sensors and gauge factors with different materials and geometries, respectively. The results indicate that complex geometry by 3D printing such as interdigitated structure, continuous hairpin corners, and helix has great potential to improve the gauge factor and sensitivity of the electrical dev ices.[235,236,252,253,264–268] Nowadays, although a large number of 3D-printed materials have been used to mimic human organs, most researches are still focused on the piezoresistance and piezoelectric properties. Other properties including self-healing and actuation are both fundamentally important in nature and increasingly important in various engineering applications. We can expect major changes in 3D-printed biomimetic electrical devices to address such needs in the future. Thin-film transistors, sensors, and actuators are widely used in biomimetic systems. Those electronic components with diverse materials and multilayers structures will also require the further development of more multimaterial and multifunctional 3D-printing processes as well as the combination of 3D printing with other fabrication technologies.

7. Conclusions and Outlook

Nature has developed high-performance materials and structures over millions of years' evolution; they present valuable sources of inspiration for engineering material systems. Biomimicry by learning from nature's concepts and design principles is driving a paradigm shift in modern engineering science and technology development. To address the fabrication challenges presented by biomimicry study, additive manufacturing (3D printing) could be a powerful tool for building hypothetical models in order to understand the biological function and its interaction with the environmental constraints in nature and in engineering systems. The recent developments on bioinspired 3D-printing technology have demonstrated the potential of fabricating more sustainable materials and structures inspired by nature.

Despite significant progresses in the fabrication of bioinspired materials and structures as well as the related applications, there are still many challenges that need to be addressed.

© 2018 WILEY-VCH Verlag GmbH & Co. KGaA, Weinheim

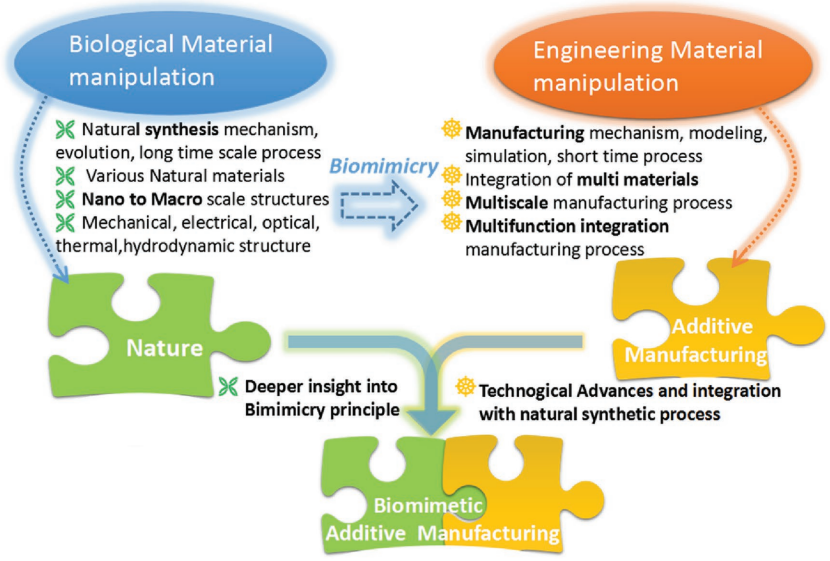

Figure 22. Integration of additive manufacturing and biomimicry promises to enable breakthroughs in engineering technology development in the coming decades.

(1) The synthesis mechanisms of nature need to be further studied for the design of bioinspired structures that can be used in engineering systems. For the purpose, 3D printing together with other technologies needs to be developed to reveal the underlying mechanisms behind the exciting properties and phenomena that are observed in nature. Nature creates organism in relatively large time scale, for example, the bone growth will take years. In contrast, 3D printing is a man-made synthetic manufacturing process, and the production life cycle involving 3D printing is measured in hours or days. It is important to understand the mechanism of the material forming (growing) process in nature and identify the main reasons of the necessity of long time scale, which may inspire us to find a substitutive way to mimic the natural growing process but with shorter time scale. In this way, 3D printing can best duplicate the natural creation process and meet the production time scale in engineering context. Improving our understanding of these materials and structures may provide further insight into techniques for replicating these natural materials synthetically instead of simply duplicating biological structures[34] (**Figure 22**).

(2) Structural materials in nature, unlike most synthetic materials, tend to use a mixture of various kinds of materials (e.g., proteins, polysaccharides, calcites, aragonites, and collagen fibers) rather than using a single material. The properties of the individual constituents are often meager, but they form high-performance hybrids under ambient conditions with low energy requirements.[34] These resulting materials are lightweight, yet display impressive combinations of mechanical, electrical, and other physical properties.[269] However, the materials used in bioinspired 3D printing are usually restricted to polymers, certain ceramics, and metals. These materials have limitations such as low tensile strength and low temperature resistance. The study to broaden the kinds of materials that can be 3D printed as well as to develop novel composites is a critical task in the future. In addition, it is very challenging for current 3D-printing technology to process materials in different categories due to the incompatible forming conditions. For example, the formation of inorganic materials (minerals, e.g., hydroxyapatite (HAP)) requires high-temperature sintering, under which the biopolymers can hardly survive. In contrast, nature assembles these materials under the same condition by growing the mineral crystals, biopolymers, and cells. Such crystal growing process in natural conditions may provide implications for us to design new 3D-printing process to handle multiple materials from different categories in the same built to best mimic the nature designs. New material deposition mechanisms may also enable multimaterial 3D printing with higher resolution and faster speed.

(3) All biological structures are multiscale (from nano to macro) and multifunctional (e.g., biological, mechanical, optical, electrical, etc.). Multiscale structures of biological materials in nature play important roles in achieving functional integration.[3,270] For example, the nanostructures on butterfly wings provide colors as well as superhydrophobicity with self-cleaning properties.[185,271] Gecko feet with nanostructures not only demonstrate striking attachment and detachment with high maneuverability and efficiency, but also possess self-cleaning, self-repairing, and wear-resistant properties.[3,272] While recent bioinspired 3D-printing technologies struggle to reproduce a single function of nature structures, the reproduction of these multiscale and multifunctional biological structures with impressive efficiency is still way beyond current manufacturing processes. This presents an ongoing challenge for multidisciplinary research involving material scientists and process engineers as well as optical, mechanical, electrical, and biomedical engineers.

(4) Design is the direct input of 3D-printing process and therefore plays an important role in nature-inspired engineering. Creatures in nature have high geometry complexity, hierarchical complexity, and functional complexity, which brings challenges to the engineering design process due to limited computational power. Topology-based multiscale rational design with repetitive features has the potential to address the complexity challenges involved in natural creation process. On the other hand, the nature developed organisms over many length scales and each of them defines the unique properties of the organism in a synergic way. It is desired to establish a holistic multiscale modeling and simulation framework to understand the mechanism and the relationship of structure and property. However, most of the current research only focuses on the study at single length scale which cannot provide high-fidelity understanding and prediction of the property and performance of bioinspired synthetic creations. The major challenge is still rooted from the dilemma of highly complex physiochemical phenomena among the multiscale structural interaction and the limited computational resources. The data-driven approach

© 2018 WILEY-VCH Verlag GmbH & Co. KGaA, Weinheim

may provide an effective pathway to understand the mechanism of the natural development process by learning the relation between the material structural organization, the material properties, and the related functionalities. This will not only guide the downstream nature-inspired design process, but also may reveal new materials and fabrication processes that do not exist in nature yet be more effective than natural design.

(5) Nature designs creatures in an efficient and elegant way. It would be a wise idea to take advantage of the power of nature and to integrate natural creation as part of the 3D-printing process. Attempts have been made in bioprinting and composite 3D printing. For example, cells can be assembled into an anatomical structure by 3D printing, after which the nature will take over by fusing the cells into tissues with required biofunctionality as well as improved structural integrity and geometric fidelity, the endothelialized vascular engineered by 3D printing is a good example. Another example is the freeze-casting-based inkjet 3D-printing process for ceramic and composite fabrication of multiscale architectures.[273,274] This process is inspired by the formation of sea ice where the growth of ice crystals in seawater expels colloids and traps them in a complex porous network. In this 3D-printing process, the macroscale structure is manipulated by the inkjet printing process while the microscale structure is taken care by nature, i.e., the spontaneous ice crystal growth will form the morphology and geometry of the microstructures of the fabricated ceramic or composite object. An artificial bone by printing HAP particle with multiscale structure would be a good example for such cases.

(6) 3D-printing technology needs to be further improved in the future in order to fabricate complex biological structures. One potential direction is to develop new multiscale 3D-printing technology by integrating different 3D-printing processes developed for different size scales to address the multiscale challenge required by the bioinspired structure fabrication.[170] Another promising direction is to integrate the 3D-printing process with traditional fabrication technology. For example, the field-assisted 3D printing as discussed in Section 2.3 proves to be an effective way of building anisotropic biomimetic reinforced structures. Robotic placement of components and complementary techniques, such as micromachining, dispensing of functional inks, and embedding of wires, could also be combined with 3D-printing processes. Such integration could provide increased control of multiple materials, geometric scales, and functionalities in 3D-printed structures.[55,275] As another example, 3D printing incorporated with freeze–drying has been reported for the fabrication of graphene aerogel with excellent mechanical and electrical properties.[273] However, the research on such hybrid manufacturing processes is impossible without cross-fertilization between the different disciplines including biology, chemistry, physics, materials science, etc. Natural creation process itself can be regarded as an additive manufacturing process, for example, nature starts with a single cell and ends with a living organism by gradually adding materials by growing or taking from environment. Such process can inspire new additive manufacturing technologies, which hypothetically can create objects closer to natural structures in a more effective and efficient way.

Overall, understanding natural structures and replicate them by 3D printing for various engineering applications will lead us to drive the biomimicry field forward. At the same time, the fabrication challenges presented by biomimicry will lead to more novel biomimetic additive manufacturing processes. The future study on bioinspired 3D printing will fall in the category of multifunctional, multiscale, multimaterial, and multidimensional (4D printing) fabrication. The development of biomimetic additive manufacturing technology will further lead to breakthroughs in constructing next-generation functional materials and structures for future engineering systems.

Acknowledgements

The preparation of this review was supported by the National Science Foundation (NSF) (Grant Nos. CMMI 1335476 and CMMI 1663663) and USC's Alfred E. Mann Institute.

Conflict of Interest

The authors declare no conflict of interest.

Keywords

3D printing, bioinspired mechanics reinforced structure, bioinspired optics, bioinspired shape-changing structures, wearable sensors

Received: November 8, 2017
Revised: January 25, 2018
Published online: June 19, 2018

[1] U. G. Wegst, H. Bai, E. Saiz, A. P. Tomsia, R. O. Ritchie, *Nat. Mater.* **2015**, *14*, 23.
[2] N. Huebsch, D. J. Mooney, *Nature* **2009**, *462*, 426.
[3] K. Liu, L. Jiang, *Nano Today* **2011**, *6*, 155.
[4] Y. Mengüç, S. Y. Yang, S. Kim, J. A. Rogers, M. Sitti, *Adv. Funct. Mater.* **2012**, *22*, 1246.
[5] J. Sun, B. Bhushan, *RSC Adv.* **2012**, *2*, 7617.
[6] E. A. Zimmermann, B. Gludovatz, E. Schaible, N. K. Dave, W. Yang, M. A. Meyers, R. O. Ritchie, *Nat. Commun.* **2013**, *4*, 2634.
[7] J. J. Martin, B. E. Fiore, R. M. Erb, *Nat. Commun.* **2015**, *6*, 8641.
[8] C. S. Tiwary, S. Kishore, S. Sarkar, D. R. Mahapatra, P. M. Ajayan, K. Chattopadhyay, *Sci. Adv.* **2015**, *1*, e1400052.
[9] N. M. Pugno, S. W. Cranford, M. J. Buehler, *Small* **2013**, *9*, 2747.
[10] D. Correa, A. Papadopoulou, C. Guberan, N. Jhaveri, S. Reichert, A. Menges, S. Tibbits, *3D Print. Addit. Manuf.* **2015**, *2*, 106.
[11] S. Armon, E. Efrati, R. Kupferman, E. Sharon, *Science* **2011**, *333*, 1726.
[12] L. Wen, J. C. Weaver, P. J. Thornycroft, G. V. Lauder, *Bioinspiration Biomimetics* **2015**, *10*, 066010.
[13] G. D. Bixler, B. Bhushan, *Adv. Funct. Mater.* **2013**, *23*, 4507.
[14] L. Wen, J. C. Weaver, G. V. Lauder, *J. Exp. Biol.* **2014**, *217*, 1656.

 © 2018 WILEY-VCH Verlag GmbH & Co. KGaA, Weinheim

[15] W. Barthlott, T. Schimmel, S. Wiersch, K. Koch, M. Brede, M. Barczewski, S. Walheim, A. Weis, A. Kaltenmaier, A. Leder, *Adv. Mater.* **2010**, *22*, 2325.
[16] O. Tricinci, T. Terencio, B. Mazzolai, N. M. Pugno, F. Greco, V. Mattoli, *ACS Appl. Mater. Interfaces* **2015**, *7*, 25560.
[17] C. Zeiger, I. C. R. da Silva, M. Mail, M. N. Kavalenka, W. Barthlott, H. Hölscher, *Bioinspiration Biomimetics* **2016**, *11*, 056003.
[18] D. J. Babu, M. Mail, W. Barthlott, J. J. Schneider, *Adv. Mater. Interfaces* **2017**, *4*, 1700273.
[19] I. S. Kinstlinger, J. S. Miller, *Lab Chip* **2016**, *16*, 2025.
[20] P. Blinder, P. S. Tsai, J. P. Kaufhold, P. M. Knutsen, H. Suhl, D. Kleinfeld, *Nat. Neurosci.* **2013**, *16*, 889.
[21] D. B. Kolesky, R. L. Truby, A. Gladman, T. A. Busbee, K. A. Homan, J. A. Lewis, *Adv. Mater.* **2014**, *26*, 3124.
[22] H. Li, X. Gong, Q. Ni, J. Zhao, H. Zhang, T. Wang, W. Yu, *Appl. Phys. Lett.* **2014**, *105*, 143705.
[23] Z. Sun, T. Liao, L. Sheng, J. H. Kim, S. X. Dou, J. Bell, *Mater. Today Chem.* **2016**, *1*, 84.
[24] F. Colonnier, A. Manecy, R. Juston, H. Mallot, R. Leitel, D. Floreano, S. Viollet, *Bioinspiration Biomimetics* **2015**, *10*, 026002.
[25] H. Duan, Y. Deng, X. Wang, F. Liu, *IEEE Aerosp. Electron. Syst. Mag.* **2013**, *28*, 36.
[26] K. I. Jang, H. U. Chung, S. Xu, C. H. Lee, H. Luan, J. Jeong, H. Cheng, G. T. Kim, S. Y. Han, J. W. Lee, *Nat. Commun.* **2015**, *6*, 6566.
[27] Z. Wang, F. Jiang, Y. Zhang, Y. You, Z. Wang, Z. Guan, *ACS Nano* **2014**, *9*, 271.
[28] Z. Lei, Q. Wang, S. Sun, W. Zhu, P. Wu, *Adv. Mater.* **2017**, *29*.
[29] H. H. Chou, A. Nguyen, A. Chortos, J. W. To, C. Lu, J. Mei, T. Kurosawa, W. G. Bae, J. B. H. Tok, Z. Bao, *Nat. Commun.* **2015**, *6*, 8011.
[30] B. Wang, W. Yang, J. McKittrick, M. A. Meyers, *Prog. Mater Sci.* **2016**, *76*, 229.
[31] S. E. Naleway, M. M. Porter, J. McKittrick, M. A. Meyers, *Adv. Mater.* **2015**, *27*, 5455.
[32] J. Aizenberg, P. Fratzl, *Adv. Funct. Mater.* **2013**, *23*, 4398.
[33] N. Zhao, Z. Wang, C. Cai, H. Shen, F. Liang, D. Wang, C. Wang, T. Zhu, J. Guo, Y. Wang, *Adv. Mater.* **2014**, *26*, 6994.
[34] C. Zhang, D. A. Mcadams, J. C. Grunlan, *Adv. Mater.* **2016**, *28*, 6292.
[35] Q. Zhang, X. Yang, P. Li, G. Huang, S. Feng, C. Shen, B. Han, X. Zhang, F. Jin, F. Xu, *Prog. Mater. Sci.* **2015**, *74*, 332.
[36] S. V. Murphy, A. Atala, *Nat. Biotechnol.* **2014**, *32*, 773.
[37] Y. M. Song, Y. Xie, V. Malyarchuk, J. Xiao, I. Jung, K. J. Choi, Z. Liu, H. Park, C. Lu, R. H. Kim, *Nature* **2013**, *497*, 95.
[38] Q. Li, Q. Zeng, L. Shi, X. Zhang, K.-Q. Zhang, *J. Mater. Chem. C* **2016**, *4*, 1752.
[39] K. Fu, D. Moreno, M. Yang, K. L. Wood, *J. Mech. Des.* **2014**, *136*, 111102.
[40] B. Su, Y. Tian, L. Jiang, *J. Am. Chem. Soc* **2016**, *138*, 1727.
[41] L. Pu, R. Saraf, V. Maheshwari, *Sci. Rep.* **2017**, *7*, 5834.
[42] F. Bouville, E. Maire, S. Meille, B. Van de Moortèle, A. J. Stevenson, S. Deville, *Nat. Mater.* **2014**, *13*, 508.
[43] Q. Cheng, L. Jiang, Z. Tang, *Acc. Chem. Res.* **2014**, *47*, 1256.
[44] M. D. T. Zongsong Gan, Min Gu, *Sci. Adv.* **2016**, e1600084.
[45] R. M. Erb, J. S. Sander, R. Grisch, A. R. Studart, *Nat. Commun.* **2013**, *4*, 1712.
[46] S. H. Huang, P. Liu, A. Mokasdar, L. Hou, *Int. J. Adv. Manuf. Technol.* **2013**, *67*, 1191.
[47] W. Gao, Y. Zhang, D. Ramanujan, K. Ramani, Y. Chen, C. B. Williams, C. C. Wang, Y. C. Shin, S. Zhang, P. D. Zavattieri, *Comput.-Added Des.* **2015**, *69*, 65.
[48] B. P. Conner, G. P. Manogharan, A. N. Martof, L. M. Rodomsky, C. M. Rodomsky, D. C. Jordan, J. W. Limperos, *Addit. Manuf.* **2014**, *1*, 64.
[49] W. E. Frazier, *J. Mater. Eng. Perform.* **2014**, *23*, 1917.
[50] S. M. Thompson, L. Bian, N. Shamsaei, A. Yadollahi, *Addit. Manuf.* **2015**, *8*, 36.
[51] S. Mellor, L. Hao, D. Zhang, *Int. J. Prod. Econ.* **2014**, *149*, 194.
[52] N. Guo, M. C. Leu, *Front. Mech. Eng.* **2013**, *8*, 215.
[53] M. Vaezi, H. Seitz, S. Yang, *Int. J. Adv. Manuf. Technol.* **2013**, *67*, 1721.
[54] G. Mitteramskogler, R. Gmeiner, R. Felzmann, S. Gruber, C. Hofstetter, J. Stampfl, J. Ebert, W. Wachter, J. Laubersheimer, *Addit. Manuf.* **2014**, *1*, 110.
[55] A. Zhakeyev, P. Wang, L. Zhang, W. Shu, H. Wang, J. Xuan, *Adv. Sci.* **2017**, *4*, 1700187.
[56] J. Y. Lee, W. S. Tan, J. An, C. K. Chua, C. Y. Tang, A. G. Fane, T. H. Chong, *J. Membr. Sci.* **2016**, *499*, 480.
[57] M. Gebler, A. J. S. Uiterkamp, C. Visser, *Energy Policy* **2014**, *74*, 158.
[58] H. Ghariblu, S. Rahmati, *J. Manuf. Sci. Eng.* **2014**, *136*, 041004.
[59] A. T. Gaynor, N. A. Meisel, C. B. Williams, J. K. Guest, *J. Manuf. Sci. Eng.* **2014**, *136*, 061015.
[60] E. Sallica-Leva, R. Caram, A. Jardini, J. Fogagnolo, *J. Mech. Behav. Biomed. Mater.* **2016**, *54*, 149.
[61] M. Jamshidinia, M. M. Atabaki, M. Zahiri, S. Kelly, A. Sadek, R. Kovacevic, *J. Mater. Process. Technol.* **2015**, *226*, 264.
[62] W. Yang, I. H. Chen, B. Gludovatz, E. A. Zimmermann, R. O. Ritchie, M. A. Meyers, *Adv. Mater.* **2013**, *25*, 31.
[63] S. Rudykh, C. Ortiz, M. C. Boyce, *Soft Matter* **2015**, *11*, 2547.
[64] P. Liu, D. Zhu, J. Wang, T. Q. Bui, *J. Bionic Eng.* **2017**, *14*, 356.
[65] V. R. Sherman, H. Quan, W. Yang, R. O. Ritchie, M. A. Meyers, *J. Mech. Behav. Biomed. Mater.* **2017**, *73*, 1.
[66] R. Martini, F. Barthelat, *J. Mech. Phys. Solids* **2016**, *92*, 195.
[67] P. Liu, D. Zhu, Y. Yao, J. Wang, T. Q. Bui, *Mater. Des.* **2016**, *99*, 201.
[68] R. Martini, Y. Balit, F. Barthelat, *Acta Biomater.* **2017**, *55*, 360.
[69] M. M. Porter, N. Ravikumar, F. Barthelat, R. Martini, *J. Mech. Behav. Biomed. Mater.* **2017**, *73*, 114.
[70] G. X. Gu, I. Su, S. Sharma, J. L. Voros, Z. Qin, M. J. Buehler, *J. Biomech. Eng.* **2016**, *138*, 021006.
[71] Z. Gan, M. D. Turner, M. Gu, *Sci. Adv.* **2016**, *2*, e1600084.
[72] J. Song, S. Reichert, I. Kallai, D. Gazit, M. Wund, M. C. Boyce, C. Ortiz, *J. Struct. Biol.* **2010**, *171*, 318.
[73] Z. Qin, G. S. Jung, M. J. Kang, M. J. Buehler, *Sci. Adv.* **2017**, *3*, e1601536.
[74] M. S. Saleh, C. Hu, R. Panat, *Sci. Adv.* **2017**, *3*, e1601986.
[75] Z. Qin, B. G. Compton, J. A. Lewis, M. J. Buehler, *Nat. Commun.* **2015**, *6*, 7038.
[76] I. Malik, M. Mirkhalaf, F. Barthelat, *J. Mech. Phys. Solids* **2017**, *102*, 224.
[77] J. Duro-Royo, K. Zolotovsky, L. Mogas-Soldevila, S. Varshney, N. Oxman, M. C. Boyce, C. Ortiz, *Comut.-Added Des.* **2015**, *60*, 14.
[78] S. Rudykh, M. C. Boyce, *Adv. Eng. Mater.* **2014**, *16*, 1311.
[79] R. Ghosh, H. Ebrahimi, A. Vaziri, *Europhus. Lett.* **2016**, *113*, 34003.
[80] A. Browning, C. Ortiz, M. C. Boyce, *J. Mech. Behav. Biomed. Mater.* **2013**, *19*, 75.
[81] L. S. Dimas, G. H. Bratzel, I. Eylon, M. J. Buehler, *Adv. Funct. Mater.* **2013**, *23*, 4629.
[82] P. Tran, T. D. Ngo, A. Ghazlan, D. Hui, *Composites, Part B* **2017**, *108*, 210.
[83] G. X. Gu, F. Libonati, S. Wettermark, M. J. Buehler, *J. Mech. Behav. Biomed. Mater.* **2017**, *76*, 135.
[84] G. X. Gu, M. Takaffoli, A. J. Hsieh, M. J. Buehler, *Extreme Mech. Lett.* **2016**, *9*, 317.
[85] G. X. Gu, M. Takaffoli, M. J. Buehler, *Adv. Mater.* **2017**, *29*, 1700060.
[86] S. Frølich, J. C. Weaver, M. N. Dean, H. Birkedal, *Adv. Eng. Mater.* **2017**, *19*, e201600848.

© 2018 WILEY-VCH Verlag GmbH & Co. KGaA, Weinheim

[87] R. Ghosh, H. Ebrahimi, A. Vaziri, *Appl. Phys. Lett.* **2014**, *105*, 233701.
[88] R. Mirzaeifar, L. S. Dimas, Z. Qin, M. J. Buehler, *ACS Biomater. Sci. Eng.* **2015**, *1*, 295.
[89] S. Kamat, H. Kessler, R. Ballarini, M. Nassirou, A. H. Heuer, *Acta Mater.* **2004**, *52*, 2395.
[90] B. G. Compton, J. A. Lewis, *Adv. Mater.* **2014**, *26*, 5930.
[91] J. Taboas, R. Maddox, P. Krebsbach, S. Hollister, *Biomaterials* **2003**, *24*, 181.
[92] J. P. Lewicki, J. N. Rodriguez, C. Zhu, M. A. Worsley, A. S. Wu, Y. Kanarska, J. D. Horn, E. B. Duoss, J. M. Ortega, W. Elmer, *Sci. Rep.* **2017**, *7*, 43401.
[93] A. S. Gladman, E. A. Matsumoto, R. G. Nuzzo, L. Mahadevan, J. A. Lewis, *Nat. Mater.* **2016**, *15*, 413.
[94] R. Matsuzaki, M. Ueda, M. Namiki, T.-K. Jeong, H. Asahara, K. Horiguchi, T. Nakamura, A. Todoroki, Y. Hirano, *Sci. Rep.* **2016**, *6*, 23058.
[95] H. L. Tekinalp, V. Kunc, G. M. Velez-Garcia, C. E. Duty, L. J. Love, A. K. Naskar, C. A. Blue, S. Ozcan, *Compos. Sci. Technol.* **2014**, *105*, 144.
[96] D. E. Yunus, W. Shi, S. Sohrabi, Y. Liu, *Nanotechnology* **2016**, *27*, 495302.
[97] A. E. Jakus, E. B. Secor, A. L. Rutz, S. W. Jordan, M. C. Hersam, R. N. Shah, *ACS Nano* **2015**, *9*, 4636.
[98] Z. Quan, A. Wu, M. Keefe, X. Qin, J. Yu, J. Suhr, J.-H. Byun, B.-S. Kim, T.-W. Chou, *Mater. Today* **2015**, *18*, 503.
[99] D. Kokkinis, M. Schaffner, A. R. Studart, *Nat. Commun.* **2015**, *6*, 8643.
[100] H. Le Ferrand, F. Bouville, T. P. Niebel, A. R. Studart, *Nat. Mater.* **2015**, *14*, 1172.
[101] J. J. Martin, M. S. Riederer, M. D. Krebs, R. M. Erb, *Soft Matter* **2015**, *11*, 400.
[102] F. L. Bargardi, H. Le Ferrand, R. Libanori, A. R. Studart, *Nat. Commun.* **2016**, *7*, 13912.
[103] J. J. Martin, A. Caunter, A. Dendulk, S. Goodrich, R. Pembroke, D. Shores, R. M. Erb, *Proc. SPIE* **2017**, *10194*, 101941l.
[104] L. Lu, P. Guo, Y. Pan, *J. Manuf. Sci. Eng.* **2017**, *139*, 071008.
[105] H. Song, J. Spencer, A. Jander, J. Nielsen, J. Stasiak, V. Kasperchik, P. Dhagat, *J. Appl. Phys.* **2014**, *115*, 17E308.
[106] J. Sander, R. Erb, L. Li, A. Gurijala, Y.-M. Chiang, *Nat. Energy* **2016**, *1*, 16099.
[107] J. Billaud, F. Bouville, T. Magrini, C. Villevieille, A. R. Studart, *Nat. Energy* **2016**, *1*, 16097.
[108] M. M. Porter, M. Yeh, J. Strawson, T. Goehring, S. Lujan, P. Siripasopsotorn, M. A. Meyers, J. McKittrick, *Mater. Sci. Eng., A* **2012**, *556*, 741.
[109] M. M. Porter, L. Meraz, A. Calderon, H. Choi, A. Chouhan, L. Wang, M. A. Meyers, J. McKittrick, *Compos. Struct.* **2015**, *119*, 174.
[110] R. M. Erb, R. Libanori, N. Rothfuchs, A. R. Studart, *Science* **2012**, *335*, 199.
[111] T. P. Niebel, F. J. Heiligtag, J. Kind, M. Zanini, A. Lauria, M. Niederberger, A. R. Studart, *RSC Adv.* **2014**, *4*, 62483.
[112] Y. Yang, Z. Chen, X. Song, Z. Zhang, J. Zhang, K. K. Shung, Q. Zhou, Y. Chen, *Adv. Mater.* **2017**, *29*, 1605750.
[113] L. R. Holmes, J. C. Riddick, *JOM* **2014**, *66*, 270.
[114] J.-U. Park, M. Hardy, S. J. Kang, K. Barton, K. Adair, D. kishore Mukhopadhyay, C. Y. Lee, M. S. Strano, A. G. Alleyne, J. G. Georgiadis, *Nat. Mater.* **2007**, *6*, 782.
[115] K. Kim, G. Kim, B. R. Lee, S. Ji, S.-Y. Kim, B. W. An, M. H. Song, J.-U. Park, *Nanoscale* **2015**, *7*, 13410.
[116] R. R. Collino, T. R. Ray, R. C. Fleming, J. D. Cornell, B. G. Compton, M. R. Begley, *Extreme Mech. Lett.* **2016**, *8*, 96.
[117] T. Liu, R. Huang, J. Zhong, Y. Yang, Z. Tan, W. Tan, *J. Mater. Chem. B* **2017**, *5*, 3728.
[118] G. Luo, K. S. Teh, Y. Liu, X. Zang, Z. Wen, L. Lin, *ACS Appl. Mater. Interfaces* **2015**, *7*, 27765.
[119] T. M. Llewellyn-Jones, B. W. Drinkwater, R. S. Trask, *Smart Mater. Struct.* **2016**, *25*, 02LT01.
[120] D. Van den Ende, S. Van Kempen, X. Wu, W. Groen, C. Randall, S. Van der Zwaag, *J. Appl. Phys.* **2012**, *111*, 124107.
[121] B. W. An, K. Kim, M. Kim, S. Y. Kim, S. H. Hur, J. U. Park, *Small* **2015**, *11*, 2263.
[122] M.-S. Scholz, B. Drinkwater, R. Trask, *Ultrasonics* **2014**, *54*, 1015.
[123] A. R. Studart, *Chem. Soc. Rev.* **2016**, *45*, 359.
[124] I. Burgert, P. Fratzl, *Philos. Trans. R. Soc., A* **2009**, *367*, 1541.
[125] K. Oliver, A. Seddon, R. S. Trask, *J. Mater. Sci.* **2016**, *51*, 10663.
[126] A. R. Studart, *Angew. Chem., Int. Ed.* **2015**, *54*, 3400.
[127] G. V. Franks, C. Tallon, A. R. Studart, M. L. Sesso, S. Leo, *J. Am. Ceram. Soc.* **2017**, *100*, 458.
[128] Y. Zhang, F. Zhang, Z. Yan, Q. Ma, X. Li, Y. Huang, J. A. Rogers, *Nat. Rev. Mater.* **2017**, *2*, 17019.
[129] S. J. Jeon, A. W. Hauser, R. C. Hayward, *Acc. Chem. Res.* **2017**, *50*, 161.
[130] S. Tibbits, *Archit. Des.* **2014**, *84*, 116.
[131] Y. C. Li, Y. S. Zhang, A. Akpek, S. R. Shin, A. Khademhosseini, *Biofabrication* **2016**, *9*, 012001.
[132] F. Momeni, X. Liu, J. Ni, *Mater. Des.* **2017**, *122*, 42.
[133] Z. X. Khoo, J. E. M. Teoh, Y. Liu, C. K. Chua, S. Yang, J. An, K. F. Leong, W. Y. Yeong, *Virtual Phys. Prototyping* **2015**, *10*, 103.
[134] L. Huang, R. Jiang, J. Wu, J. Song, H. Bai, B. Li, Q. Zhao, T. Xie, *Adv. Mater.* **2017**, *29*.
[135] Z. Ding, C. Yuan, X. Peng, T. Wang, H. J. Qi, M. L. Dunn, *Sci. Adv.* **2017**, *3*, e1602890.
[136] T. H. Kwok, C. C. Wang, D. Deng, Y. Zhang, Y. Chen, *J. Mech. Des.* **2015**, *137*, 111413.
[137] S. J. Aßhoff, F. Lancia, S. Iamsaard, B. Matt, T. Kudernac, S. P. Fletcher, N. Katsonis, *Angew. Chem., Int. Ed.* **2017**, *56*, 3261.
[138] S. J. Park, M. Gazzola, K. S. Park, S. Park, V. Di Santo, E. L. Blevins, J. U. Lind, P. H. Campbell, S. Dauth, A. K. Capulli, *Science* **2016**, *353*, 158.
[139] Y. Liu, B. Shaw, M. D. Dickey, J. Genzer, *Sci. Adv.* **2017**, *3*, e1602417.
[140] E. M. Ahmed, *J. Adv. Res.* **2015**, *6*, 105.
[141] Z. J. Wang, C. N. Zhu, W. Hong, Z. L. Wu, Q. Zheng, *J. Mater. Chem. B* **2016**, *4*, 7075.
[142] E. Käpylä, S. M. Delgado, A. M. Kasko, *ACS Appl. Mater. Interfaces* **2016**, *8*, 17885.
[143] S. J. Jeon, R. C. Hayward, *Adv. Mater.* **2017**, *29*.
[144] Q. Ge, H. J. Qi, M. L. Dunn, *Appl. Phys. Lett.* **2013**, *103*, 131901.
[145] Q. Ge, C. K. Dunn, H. J. Qi, M. L. Dunn, *Smart Mater. Struct.* **2014**, *23*, 094007.
[146] Q. Ge, A. H. Sakhaei, H. Lee, C. K. Dunn, N. X. Fang, M. L. Dunn, *Sci. Rep.* **2016**, *6*, 31110.
[147] C. N. Bowman, C. J. Kloxin, *AIChE J.* **2008**, *54*, 2775.
[148] D. Liu, D. J. Broer, *Langmuir* **2014**, *30*, 13499.
[149] Y. Liu, J. K. Boyles, J. Genzer, M. D. Dickey, *Soft Matter* **2012**, *8*, 1764.
[150] D. Deng, Y. Yang, Y. Chen, X. Lan, J. Tice, *Smart Mater. Struct.* **2017**, *26*, 085040.
[151] Z. Zhao, J. Wu, X. Mu, H. Chen, H. J. Qi, D. Fang, *Sci. Adv.* **2017**, *3*, e1602326.
[152] V. Chan, K. Park, M. B. Collens, H. Kong, T. A. Saif, R. Bashir, *Sci. Rep.* **2012**, *2*, 857.
[153] J. Kim, J. Park, S. Yang, J. Baek, B. Kim, S. H. Lee, E.-S. Yoon, K. Chun, S. Park, *Lab Chip* **2007**, *7*, 1504.
[154] A. Sidorenko, T. Krupenkin, A. Taylor, P. Fratzl, J. Aizenberg, *Science* **2007**, *315*, 487.
[155] D. Deng, Y. Chen, *J. Mech. Des.* **2015**, *137*, 021701.
[156] D. Deng, T. H. Kwok, Y. Chen, *J. Mech. Des.* **2017**, *139*, 081702.
[157] Q. Zhang, D. Yan, K. Zhang, G. Hu, *Sci. Rep.* **2015**, *5*, 8936.

© 2018 WILEY-VCH Verlag GmbH & Co. KGaA, Weinheim

[158] R. S. Kularatne, H. Kim, M. Ammanamanchi, H. N. Hayenga, T. H. Ware, *Chem. Mater.* **2016**, *28*, 8489.
[159] C. K. McGinn, L. I. Laderman, N. Zimmermann, H.-S. Kitzerow, P. J. Collings, *Phys. Rev. E: Stat., Nonlinear, Soft Matter Phys.* **2013**, *88*, 062513.
[160] A. Lang, P. Motta, P. Hidalgo, M. Westcott, *Bioinspiration Biomimetics* **2008**, *3*, 046005.
[161] S. Van Wassenbergh, K. van Manen, T. A. Marcroft, M. E. Alfaro, E. J. Stamhuis, *J. R. Soc. Int.* **2015**, *12*, 20141146.
[162] W. Zhu, J. Li, Y. J. Leong, I. Rozen, X. Qu, R. Dong, Z. Wu, W. Gao, P. H. Chung, J. Wang, C. Chen, *Adv. Mater.* **2015**, *27*, 4411.
[163] M. I. Abid, L. Wang, Q. D. Chen, X. W. Wang, S. Juodkazis, H. B. Sun, *Laser Photonics Rev.* **2017**, *11*, 1600187.
[164] X. Wang, X. Cai, Q. Guo, T. Zhang, B. Kobe, J. Yang, *Chem. Commun.* **2013**, *49*, 10064.
[165] J. Lv, Z. Gong, Z. He, J. Yang, Y. Chen, C. Tang, Y. Liu, M. Fan, W. M. Lau, *J. Mater. Chem. A* **2017**, *5*, 12435.
[166] F. De Angelis, F. Gentile, F. Mecarini, G. Das, M. Moretti, P. Candeloro, M. Coluccio, G. Cojoc, A. Accardo, C. Liberale, *Nat. Photonics* **2011**, *5*, 682.
[167] M. R. Cardoso, V. Tribuzi, D. T. Balogh, L. Misoguti, C. R. Mendonça, *Appl. Surf. Sci.* **2011**, *257*, 3281.
[168] J. Li, G. Liang, X. Zhu, S. Yang, *Adv. Funct. Mater.* **2012**, *22*, 2980.
[169] Y. Yang, X. Li, X. Zheng, Z. Chen, Q. Zhou, Y. Chen, *Adv. Mater.* **2018**, *30*, 1704912.
[170] X. Li, Y. Chen, *J. Manuf. Process.* **2017**.
[171] L. O. Schwen, A. Schenk, C. Kreutz, J. Timmer, M. M. B. Rodríguez, L. Kuepfer, T. Preusser, *PLoS One* **2015**, *10*, e0133653.
[172] W. Meyer, S. Engelhardt, E. Novosel, B. Elling, M. Wegener, H. Krüger, *J. Funct. Biomater.* **2012**, *3*, 257.
[173] K. Christensen, C. Xu, W. Chai, Z. Zhang, J. Fu, Y. Huang, *Biotechnol. Bioeng.* **2015**, *112*, 1047.
[174] T. J. Hinton, Q. Jallerat, R. N. Palchesko, J. H. Park, M. S. Grodzicki, H.-J. Shue, M. H. Ramadan, A. R. Hudson, A. W. Feinberg, *Sci. Adv.* **2015**, *1*, e1500758.
[175] W. Wu, A. DeConinck, J. A. Lewis, *Adv. Mater.* **2011**, *23*, H178.
[176] W. Wu, C. J. Hansen, A. M. Aragón, P. H. Geubelle, S. R. White, J. A. Lewis, *Soft Matter* **2010**, *6*, 739.
[177] A. W. Justin, R. A. Brooks, A. E. Markaki, *J. R. Soc. Int.* **2016**, *13*, 20160768.
[178] T. Bhattacharjee, S. M. Zehnder, K. G. Rowe, S. Jain, R. M. Nixon, W. G. Sawyer, T. E. Angelini, *Sci. Adv.* **2015**, *1*, e1500655.
[179] L. E. Bertassoni, M. Cecconi, V. Manoharan, M. Nikkhah, J. Hjortnaes, A. L. Cristino, G. Barabaschi, D. Demarchi, M. R. Dokmeci, Y. Yang, *Lab Chip* **2014**, *14*, 2202.
[180] W. Zhu, X. Qu, J. Zhu, X. Ma, S. Patel, J. Liu, P. Wang, C. S. E. Lai, M. Gou, Y. Xu, *Biomater.* **2017**, *124*, 106.
[181] J. S. Miller, *PLoS Biol.* **2014**, *12*, e1001882.
[182] M. Wehner, R. L. Truby, D. J. Fitzgerald, B. Mosadegh, G. M. Whitesides, J. A. Lewis, R. J. Wood, *Nature* **2016**, *536*, 451.
[183] A. E. Rawlings, J. P. Bramble, S. S. Staniland, *Soft Matter* **2012**, *8*, 6675.
[184] V. Greanya, *Bioinspired Photonics: Optical Structures and Systems Inspired by Nature*, CRC Press, Boca Raton, FL **2015**.
[185] M. H. Bartl, *Proc. Natl. Acad. Sci. USA* **2014**, *111*, 15602.
[186] V. Saranathan, C. O. Osuji, S. G. Mochrie, H. Noh, S. Narayanan, A. Sandy, E. R. Dufresne, R. O. Prum, *Proc. Natl. Acad. Sci. USA* **2010**, *107*, 11676.
[187] R. Martín-Palma, C. Pantano, A. Lakhtakia, *Appl. Phys. Lett.* **2008**, *93*, 083901.
[188] W. Peng, S. Zhu, W. Wang, W. Zhang, J. Gu, X. Hu, D. Zhang, Z. Chen, *Adv. Funct. Mater.* **2012**, *22*, 2072.
[189] J. Duparré, F. Wippermann, *Bioinspiration Biomimetics* **2006**, *1*, 1.
[190] D. Radtke, J. Duparré, U. D. Zeitner, A. Tünnermann, *Opt. Express* **2007**, *15*, 3067.
[191] J. Aizenberg, A. Tkachenko, S. Weiner, L. Addadi, G. Hendler, *Nature* **2001**, *412*, 819.
[192] S. Yang, J. Aizenberg, *Mater. Today* **2005**, *8*, 40.
[193] S. Yang, G. Chen, M. Megens, C. K. Ullal, Y. J. Han, R. Rapaport, E. L. Thomas, J. Aizenberg, *Adv. Mater.* **2005**, *17*, 435.
[194] J. J. Kim, Y. Lee, H. G. Kim, K. J. Choi, H. S. Kweon, S. Park, K. H. Jeong, *Proc. Natl. Acad. Sci. USA* **2012**, *109*, 18674.
[195] J. J. Kim, J. Lee, S. P. Yang, H. G. Kim, H. S. Kweon, S. Yoo, K. H. Jeong, *Nano Lett.* **2016**, *16*, 2994.
[196] F. Liu, B. Dong, X. Liu, *Bio-Inspired Photonic Structures: Prototypes, Fabrications and Devices Optical Devices in Communication and Computation*, InTech, Rijeka, Croatia **2012**.
[197] N. Chidambaram, R. Kirchner, R. Fallica, L. Yu, M. Altana, H. Schift, *Adv. Mater. Technol.* **2017**, *2*, 1700018.
[198] J. R. Tumbleston, D. Shirvanyants, N. Ermoshkin, R. Janusziewicz, A. R. Johnson, D. Kelly, K. Chen, R. Pinschmidt, J. P. Rolland, A. Ermoshkin, *Science* **2015**, *347*, 1349.
[199] Y. Pan, X. Zhao, C. Zhou, Y. Chen, *J. Manuf. Process.* **2012**, *14*, 460.
[200] K. Willis, E. Brockmeyer, S. Hudson, I. Poupyrev, in *Proc. 25th Annual ACM Symposium on User Interface Software Technology–UIST'12* (Eds: R. Miller, H. Benko, C. Latulipe), ACM, New York **2012**, pp. 589–598.
[201] J. Klein, M. Stern, G. Franchin, M. Kayser, C. Inamura, S. Dave, J. C. Weaver, P. Houk, P. Colombo, M. Yang, *3D Print. Addit. Manuf.* **2015**, *2*, 92.
[202] J. Luo, L. J. Gilbert, D. A. Bristow, R. G. Landers, J. T. Goldstein, A. M. Urbas, E. C. Kinzel, *Proc. SPIE* **2016**, *9378*, 93780Y.
[203] J. Luo, L. J. Gilbert, C. Qu, R. G. Landers, D. A. Bristow, E. C. Kinzel, *J. Manuf. Sci. Eng.* **2017**, *139*, 061006.
[204] P. T. Brun, C. Inamura, D. Lizardo, G. Franchin, M. Stern, P. Houk, N. Oxman, *Philos. Trans. R. Soc., A* **2017**, *375*, 20160156.
[205] M. Fateri, A. Gebhardt, S. Thuemmler, L. Thurn, *Phys. Procedia* **2014**, *56*, 357.
[206] S. Pauly, L. Löber, R. Petters, M. Stoica, S. Scudino, U. Kühn, J. Eckert, *Mater. Today* **2013**, *16*, 37.
[207] G. Marchelli, R. Prabhakar, D. Storti, M. Ganter, *Rapid Prototyping J.* **2011**, *17*, 187.
[208] F. Kotz, K. Arnold, W. Bauer, D. Schild, N. Keller, K. Sachsenheimer, T. M. Nargang, C. Richter, D. Helmer, B. E. Rapp, *Nature* **2017**, *544*, 337.
[209] D. T. Nguyen, C. Meyers, T. D. Yee, N. A. Dudukovic, J. F. Destino, C. Zhu, E. B. Duoss, T. F. Baumann, T. Suratwala, J. E. Smay, *Adv. Mater.* **2017**, *29*, 1701181.
[210] Y. Pan, Y. Chen, *J. Micro. Nano-Manuf.* **2015**, *3*, 031001.
[211] Y. Pan, Y. Chen, *Addit. Manuf.* **2016**, *12*, 321.
[212] A. S. Jariwala, *Modeling and Process Planning for Exposure Controlled Projection Lithography*, Georgia Institute of Technology, Atlanta, GA **2013**.
[213] A. S. Jariwala, R. E. Schwerzel, D. W. Rosen, *Solid Freeform Fabr. Symp. Proc.* **2011**, 99
[214] Y. L. Kong, I. A. Tamargo, H. Kim, B. N. Johnson, M. K. Gupta, T. W. Koh, H. A. Chin, D. A. Steingart, B. P. Rand, M. C. McAlpine, *Nano Lett.* **2014**, *14*, 7017.
[215] E. Brockmeyer, I. Poupyrev, S. Hudson, in *Proc. 26th Annual ACM Symposium on User Interface Software and Technology* (Eds: S. Izadi, A. Quigley, I. Poupyrev, T. Igarashi), ACM, New York **2013**.
[216] J. Biskop, R. van de Vrie, *US20150093552A1* **2013**.
[217] D. Wu, J. N. Wang, L. G. Niu, X. L. Zhang, S. Z. Wu, Q. D. Chen, L. P. Lee, H. B. Sun, *Adv. Opt. Mater.* **2014**, *2*, 751.
[218] S. Thiele, K. Arzenbacher, T. Gissibl, H. Giessen, A. M. Herkommer, *Sci. Adv.* **2017**, *3*, e1602655.
[219] T. Gissibl, S. Thiele, A. Herkommer, H. Giessen, *Nat. Photonics* **2016**, *10*, 554.
[220] N. Luo, Z. Zhang, *J. Micromech. Microeng.* **2017**, *27*, 035015.
[221] W. R. Cox, T. Chen, D. J. Hayes, *Opt. Photonics News* **2001**, *12*, 32.

© 2018 WILEY-VCH Verlag GmbH & Co. KGaA, Weinheim

[222] S. Thiele, T. Gissibl, H. Giessen, A. M. Herkommer, *Opt. Lett.* **2016**, *41*, 3029.
[223] L. Bai, Z. Xie, W. Wang, C. Yuan, Y. Zhao, Z. Mu, Q. Zhong, Z. Gu, *ACS Nano* **2014**, *8*, 11094.
[224] J. W. Choi, M. Yamashita, J. Sakakibara, Y. Kaji, T. Oshika, R. B. Wicker, *Biomed. Microdevices* **2010**, *12*, 875.
[225] K. Cook, J. Canning, S. Leon-Saval, Z. Reid, M. A. Hossain, J.-E. Comatti, Y. Luo, G. D. Peng, *Opt. Lett.* **2015**, *40*, 3966.
[226] M. Kuang, J. Wang, B. Bao, F. Li, L. Wang, L. Jiang, Y. Song, *Adv. Opt. Mater.* **2014**, *2*, 34.
[227] D. Chanda, K. Shigeta, S. Gupta, T. Cain, A. Carlson, A. Mihi, A. J. Baca, G. R. Bogart, P. Braun, J. A. Rogers, *Nat. Nanotechnol.* **2011**, *6*, 402.
[228] H. Kim, J. Ge, J. Kim, S. e. Choi, H. Lee, H. Lee, W. Park, Y. Yin, S. Kwon, *Nat. Photonics* **2009**, *3*, 534.
[229] A. Chortos, J. Liu, Z. Bao, *Nat. Mater.* **2016**, *15*, 937.
[230] M. L. Hammock, A. Chortos, B. C. K. Tee, J. B. H. Tok, Z. Bao, *Adv. Mater.* **2013**, *25*, 5997.
[231] Y. Yang, B. Zhu, D. Yin, J. Wei, Z. Wang, R. Xiong, J. Shi, Z. Liu, Q. Lei, *Nano Energy* **2015**, *17*, 1.
[232] R. D. Farahani, M. Dubé, D. Therriault, *Adv. Mater.* **2016**, *28*, 5794.
[233] J. Kim, R. Kumar, A. J. Bandodkar, J. Wang, *Adv. Electron. Mater.* **2016**.
[234] Y. Yang, Z. Chen, X. Song, B. Zhu, T. Hsiai, P.-I. Wu, R. Xiong, J. Shi, Y. Chen, Q. Zhou, *Nano Energy* **2016**, *22*, 414.
[235] K. Tian, J. Bae, S. E. Bakarich, C. Yang, R. D. Gately, G. M. Spinks, Z. Suo, J. J. Vlassak, *Adv. Mater.* **2017**, *29*, 1604827.
[236] S. Z. Guo, K. Qiu, F. Meng, S. H. Park, M. C. McAlpine, *Adv. Mater.* **2017**, *29*, 1701218.
[237] Z. Chen, X. Song, L. Lei, X. Chen, C. Fei, C. T. Chiu, X. Qian, T. Ma, Y. Yang, K. Shung, *Nano Energy* **2016**, *27*, 78.
[238] S. Sundaram, Z. Jiang, P. S. Amorn, D. S. Kim, M. A. Baldo, W. Matusik, *Adv. Mater. Technol.* **2017**, *2*, 1600257.
[239] X. Song, Z. Chen, L. Lei, K. Shung, Q. Zhou, *Rapid Prototyping J.* **2017**, *23*, 44.
[240] Y. Z. Ji, Z. Wang, B. Wang, Y. Chen, T. Zhang, L. Q. Chen, X. Song, L. Chen, *Adv. Eng. Mater.* **2017**, *19*, 1600803.
[241] K. Kim, W. Zhu, X. Qu, C. Aaronson, W. R. McCall, S. Chen, D. J. Sirbuly, *ACS Nano* **2014**, *8*, 9799.
[242] N. A. Bakhtina, U. Loeffelmann, N. MacKinnon, J. G. Korvink, *Adv. Funct. Mater.* **2015**, *25*, 1683.
[243] L. He, X. Song, *JOM* **2018**, *70*, 407.
[244] X. Song, Y. Chen, T. W. Lee, S. Wu, L. Cheng, *J. Manuf. Process.* **2015**, *20*, 456.
[245] S. J. Leigh, R. J. Bradley, C. P. Purssell, D. R. Billson, D. A. Hutchins, *PLoS One* **2012**, *7*, e49365.
[246] S. R. Shin, R. Farzad, A. Tamayol, V. Manoharan, P. Mostafalu, Y. S. Zhang, M. Akbari, S. M. Jung, D. Kim, M. Comotto, *Adv. Mater.* **2016**, *28*, 3280.
[247] R. Barras, I. Cunha, D. Gaspar, E. Fortunato, R. Martins, L. Pereira, *Flexible Printed Electron.* **2017**, *2*, 014006.
[248] C. Gaspar, J. Olkkonen, S. Passoja, M. Smolander, *Sensors* **2017**, *17*, 1464.
[249] Z. Lei, Q. Wang, P. Wu, *Mater. Horiz.* **2017**, *4*, 694.
[250] M. G. Mohammed, R. Kramer, *Adv. Mater.* **2017**, *29*, 1604965.
[251] M. Schmitz, M. Khalilbeigi, M. Balwierz, R. Lissermann, M. Mühlhäuser, J. Steimle, in *Proc. 28th Annual ACM Symposium on User Interface Software & Technology* (Ed: S. Follmer), ACM, New York **2015**, pp. 253–258.
[252] A. Frutiger, J. T. Muth, D. M. Vogt, Y. Mengüç, A. Campo, A. D. Valentine, C. J. Walsh, J. A. Lewis, *Adv. Mater.* **2015**, *27*, 2440.
[253] J. T. Muth, D. M. Vogt, R. L. Truby, Y. Mengüç, D. B. Kolesky, R. J. Wood, J. A. Lewis, *Adv. Mater.* **2014**, *26*, 6307.
[254] K. Kim, J. Park, J. H. Suh, M. Kim, Y. Jeong, I. Park, *Sens. Actuators, A* **2017**, *263*, 493.
[255] M. S. Mannoor, Z. Jiang, T. James, Y. L. Kong, K. A. Malatesta, W. O. Soboyejo, N. Verma, D. H. Gracias, M. C. McAlpine, *Nano Lett.* **2013**, *13*, 2634.
[256] J. J. Adams, E. B. Duoss, T. F. Malkowski, M. J. Motala, B. Y. Ahn, R. G. Nuzzo, J. T. Bernhard, J. A. Lewis, *Adv. Mater.* **2011**, *23*, 1335.
[257] K. Chizari, M. A. Daoud, A. R. Ravindran, D. Therriault, *Small* **2016**, *12*, 6076.
[258] H. Kim, F. Torres, Y. Wu, D. Villagran, Y. Lin, T.-L. B. Tseng, *Smart Mater. Struct.* **2017**.
[259] C. Lee, J. A. Tarbutton, *Smart Mater. Struct.* **2014**, *23*, 095044.
[260] S. Bodkhe, G. Turcot, F. P. Gosselin, D. Therriault, *ACS Appl. Mater. Interfaces* **2017**, *9*, 20833.
[261] M. A. Darabi, A. Khosrozadeh, R. Mbeleck, Y. Liu, Q. Chang, J. Jiang, J. Cai, Q. Wang, G. Luo, M. Xing, *Adv. Mater.* **2017**, *29*, 1700533.
[262] T. Varghese, C. Hollar, J. Richardson, N. Kempf, C. Han, P. Gamarachchi, D. Estrada, R. J. Mehta, Y. Zhang, *Sci. Rep.* **2016**, *6*, 33135.
[263] N. Lu, C. Lu, S. Yang, J. Rogers, *Adv. Funct. Mater.* **2012**, *22*, 4044.
[264] S. Liu, L. Li, *ACS Appl. Mater. Interfaces* **2017**, *9*, 26429.
[265] J. Y. Kim, S. Ji, S. Jung, B. H. Ryu, H. S. Kim, S. S. Lee, Y. Choi, S. Jeong, *Nanoscale* **2017**, *9*, 11035.
[266] J. U. Lind, T. A. Busbee, A. D. Valentine, F. S. Pasqualini, H. Yuan, M. Yadid, S. J. Park, A. Kotikian, A. P. Nesmith, P. H. Campbell, *Nat. Mater.* **2016**, *16*, 303.
[267] S. K. Das, J. R. Baptist, R. Sahasrabuddhe, W. H. Lee, D. O. Popa, *Proc. SPIE* **2016**, *9859*, 985905.
[268] S. Agarwala, G. L. Goh, Y. L. Yap, G. D. Goh, H. Yu, W. Y. Yeong, T. Tran, *Sens. Actuators, A* **2017**, *263*, 593.
[269] E. Munch, M. E. Launey, D. H. Alsem, E. Saiz, A. P. Tomsia, R. O. Ritchie, *Science* **2008**, *322*, 1516.
[270] K. Liu, L. Jiang, *ACS Nano* **2011**, *5*, 6786.
[271] Y. Zheng, X. Gao, L. Jiang, *Soft Matter* **2007**, *3*, 178.
[272] S. Sethi, L. Ge, L. Ci, P. M. Ajayan, A. Dhinojwala, *Nano Lett.* **2008**, *8*, 822.
[273] Q. Zhang, F. Zhang, S. P. Medarametla, H. Li, C. Zhou, D. Lin, *Small* **2016**, *12*, 1702.
[274] P. L. Yan, E. Brown, Q. Su, J. Li, J. Wang, C. Xu, C. Zhou, D. Lin, *Small* **2017**, *13*, 1701756.
[275] E. MacDonald, R. Wicker, *Science* **2016**, *353*, aaf2093.

 © 2018 WILEY-VCH Verlag GmbH & Co. KGaA, Weinheim